JACOBS
UNIVERSITY

Itinerant Spin Dynamics in Structures of Reduced Dimensionality

A dissertation presented
by

Paul Thomas Wenk

in partial fulfillment of the requirements
for the degree of
Doctor of Philosophy
in the subject of

Physics

Thesis Committee:
Prof. Dr. Stefan Kettemann [thesis advisor] (Jacobs University Bremen, Germany & Pohang University of Science and Technology, South Korea)
Prof. Dr. Georges Bouzerar (Institut Néel, France & Jacobs University Bremen, Germany)
Prof. Dr. Ulrich Kleinekathöfer (Jacobs University Bremen, Germany)

Date of Defense: August, 29 2011

Jacobs University Bremen
School of Engineering and Science

This updated version (V2) of the thesis contains corrections of typos and spelling errors.
Regensburg, 15.02.18

Itinerant Spin Dynamics in Structures of Reduced Dimensionality

Abstract

In the present thesis results of the study of spin dynamics and quantum transport in disordered semiconductor quantum wires with spin-orbit coupling are presented. Starting from basic spin dynamics we derive the dependence of the weak localization correction to the conductance on the strength and the kind of spin-orbit interaction (linear and cubic Dresselhaus, as well as Rashba coupling), the width of the quantum wires as well as the mobility, temperature and Zeeman term. Furthermore, we exploit the connection found between the microscopic picture given by the Cooperon and the spin diffusion equation to extract the spin relaxation rate which shows the same wire dependencies as the weak localization correction. We also show how the result depends on the smoothness and the direction of the transverse confinement of the quantum wires. In this context we have addressed the question concerning long persisting or even persistent spin states in spintronic devices, presenting the corresponding optimal adjustment of spin orbit couplings of different kind and optimal alignment of the wire direction in semiconductor crystals. Experiments[HSM$^+$06, HSM$^+$07, KKN09, LSK$^+$07, WGZ$^+$06, SGB$^+$09] which report the dimensional reduction of the spin relaxation rate in agreement with previous results were raising new questions, in particular as regarding the crossover from diffusive to ballistic wires, which we answer using modified Cooperon equation. In addition, we focus on the intrinsic spin Hall effect, which is only due to spin-orbit coupling. Having shown the basic features with analytical calculations, we solve the spin Hall conductivity in presence of binary and block-distributed impurities (Anderson model). At this we apply the Kernel Polynomial Method, which allows for a finite size analysis of the metal-insulator transition and the calculation of spin Hall conductivity in large systems compared with those addressable with exact diagonalization.

Contents

Citations to Previously Published Work

Large portions of the chapters have appeared in the following four papers:

1. Wenk P., Kettemann S. et al. Spin Polarized Transport and Spin Relaxation in Quantum Wires. In: NanoScience and Technology. Springer-Verlag Berlin Heidelberg; (2010).
2. Wenk P., Kettemann S. Spin Relaxation in Quantum Wires. In: Sattler K, Francis& Taylor Handbook on Nanophysics.; (2010) p.49.
3. Wenk P., Kettemann S. Dimensional Dependence of Weak Localization Corrections and Spin Relaxation in Quantum Wires with Rashba Spin Orbit Coupling. Phys. Rev. B. **81** 125309 (2010).
4. Wenk P., Kettemann S. Direction Dependence of Spin Relaxation in Confined Two-Dimensional Systems. Phys. Rev. B. **83** 115301 (2011).

Acknowledgments

Completing this doctoral work has been a wonderful experience. It is with pleasure that I acknowledge the advise and support by the people with whom I was working during the time in Hamburg and Bremen.

In particular, I owe my interest in the fascinating world of condensed matter to my thesis advisor Professor Stefan Kettemann. It started all by a small and seemingly simple task concerning ballistic spin transport. During the induction into the field of spintronics his advice helped me to see on the one hand the richness of effects which were often counter-intuitive, and on the other hand, he showed me how to get a feeling for the nature of the complex problem we were working on by application of fundamental rules. He gave me plenty of scope to chose my direction of interest and always encouraged me in many fruitful discussions.

Professor Georges Bouzerar I owe not only the rediscovery of my interest in programming and a boost in my rusty C++ skills from school time but also a better understanding of how to squeeze the essential of a phenomenon into the computer and extract meaningful physics out of it. His questions furthered my insight of the subject matter.

Throughout my years as a PhD student, I was supported for many semesters by the DFG-SFB508 B9 at the Institute for Theoretical Physics in Hamburg and by the DFG CC5120 at the Jacobs University Bremen, through the generosity of my advisor. I thank the Conrad Naber foundation for providing my scholarship for my first year at the Jacobs University Bremen. In addition, I had the opportunity to take part in many interesting and productive conferences (some including even singing) where some were founded by the World Class University program through the Korea Science and Engineering Foundation.

Finally, I also would like to acknowledge the support of my colleagues at the Hamburg and Jacobs University, creating a stimulating environment.

Dedicated to Linda,
my parents
and my brother Daniel.

Stephanie: So, how was your day?
Leonard: Y'know, I'm a physicist - I thought about stuff.
Stephanie: That's it?
Leonard: I wrote some of it down.

From "The Big Bang Theory" episode The Panty Pinata Polarization.

Chapter 1

Introduction

Structure of this thesis

This thesis falls into four parts,

- Fundamentals of spin dynamics and spin relaxation mechanisms (Chapter 1 and 2),
- Spin Dynamics in Quantum Wires:
  - Dimensional dependence of weak localization and weak antilocalization and the relation to spin diffusion (Chapter 3)
  - Direction dependence of spin relaxation and diffusive-ballistic crossover (Chapter 4)
- Spin Hall Effect (Chapter 5)
- Critical Discussion and Future Perspective (Chapter 6)

The field of interest which we are going to present in this PhD thesis is called spintronics. Nowadays it is not only a Gedankenexperiment, the emerging technology of it is already partially in use, e.g. in Magnetoresistive RAMs[AF07] which use the giant magnetoresistance discovered by Albert Fert and Peter Grünberg (*Nobel Prize 2007*)[BBF$^+$88, BGSZ89]. But what is actually spintronics? In a paper from 2004, D'yakonov states that "What most people apparently mean by spintronics is the fabrication of some useful devices using a) creation of a non-equilibrium spin density in a semiconductor, b) manipulation of the spins by external fields, and c) detection of the resulting spin state."[Dya04]. One part of this work will mainly focus on the second point, manipulation of the spin and understanding the limitations of spin propagation. The main objective is to shed light on some interesting effects in the field of spin-dependent electronic transport.

Looking in the literature one realizes that many proposals for two-dimensional (2D) spintronic devices are based on the presence of spin-orbit coupling (SOC) in a 2D electron system (2DES) semiconductor heterostructure. This idea goes back to the spin field-effect transistor proposed by Datta and Das[DD90] which is schematically plotted in Fig. 1.1. The

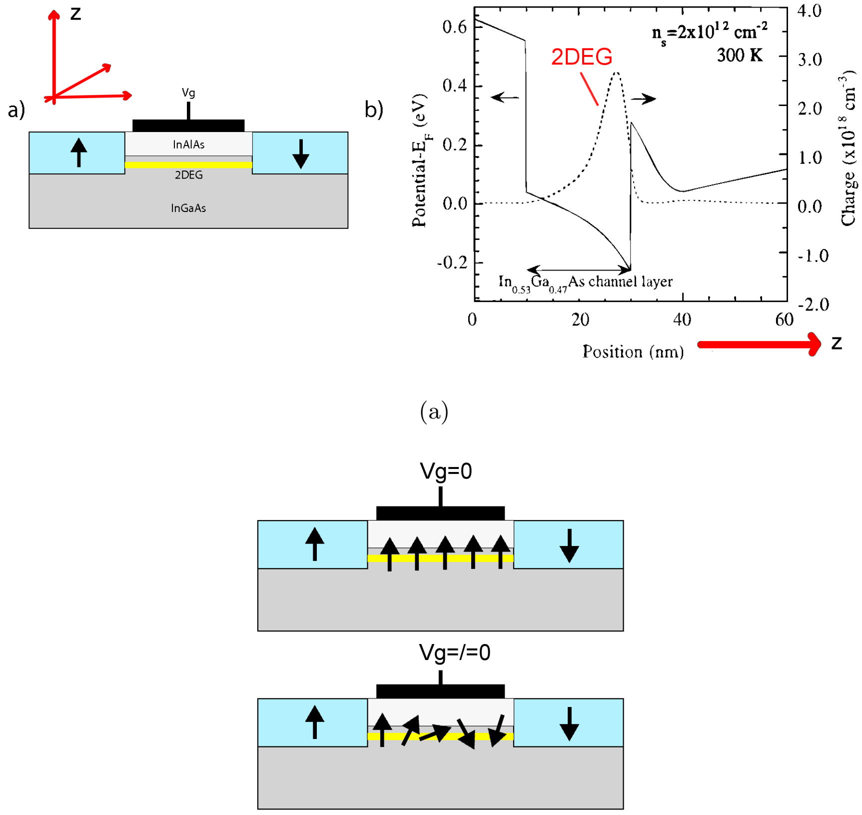

(a)

(b)

Figure 1.1: (a) a) Schematic of Datta-Das spin modulator device in a cross-section. The 2D electron gas (2DEG) has a distance of L from the emitter (↑) to the collector (↓). Normal to this cross-section there is an additional confinement. b) The conduction band which confines the electrons to a 2D system and the electron distribution (dotted) are shown. Taken from Ref. [NATE97]. (b) Manipulation of spin precession due to SOC by gate voltage.

electrons are injected from metallic leads into the 2DES with the spin parallel to the transport direction. In the nonmagnetic region the spin is changed along the distance L due to the coupling of spin degree of freedom and orbital motion of the electron. In this model the electrons are moving ballistically in a quasi one-dimensional channel, due to a second confinement. The result for weak SOC in first order perturbation theory is a modulation of the spin current with a phase-shift

$$\Delta\theta = \frac{2\alpha m_e}{\hbar^2} L, \tag{1.1}$$

with α the strength of SOC and m_e the effective electron mass. This phase-shift $\Delta\theta$ can be manipulated by the confining field E_z via the gate which, in turn, changes the probability to find the spin in the "down" state at the drain. The gate-control makes the spin-FET so promising for spintronic applications. In Sec. 2.3.3 we will review this transport in ballistic wires.

Applying this model in an experiment one is, however, confronted with several problems. Spintronic devices which rely on coherent spin precession of conduction electrons [DD90, ZFD04] require a small spin relaxation rate $1/\tau_s$. But as the electron momentum is randomized due to disorder, the coupling between spin and orbital degree of freedom, the spin-orbit (SO) interaction, is expected to result not only in a spin precession but in randomization of the electron spin. This coupling can lead to counter intuitive effects as the following, described by D'yakonov and Perel'[DP72]: Analyzing the spin transport in e.g. n-type semiconductors at low temperature ($T \lesssim 5$K), one finds that the more the electron is scattered the longer is the lifetime of the initial spin state. Such experiments are often performed in devices where the wire width W is several nanometers wide, so that boundary effects can play an important role: Looking at the extreme situation where W is of the order of Fermi wavelength λ_F, the D'yakonov-Perel' spin relaxation is expected to vanish,[KK00, MFA02] since the backscattering from impurities can in one-dimensional wires only reverse the SO field and thereby the spin precession. Immediately the following question arises: *How many channels can be added without enlarging the spin relaxation rate significantly?* In Ref. [Ket07], which is the starting point for the analysis presented in the first part of the present work, S. Kettemann could show, that $1/\tau_s$ is already strongly reduced in much wider wires: as soon as the wire width W is smaller than bulk spin precession length L_{SO}, which is the length on which the electron spin precesses a full cycle. Since L_{SO} can be several μm and is not changed significantly as the wire width W is reduced, the reduction of spin relaxation can be very useful for applications.

The study of the reduction of the spin relaxation rate in quantum wires for widths exceeding both the elastic mean-free path l_e and λ_F is in addition motivated by the fact that recently it could be observed with optical[HSM+06] as well as with measurements of the change in magnetoconductivity.[DLS+05, LSK+07, SGP+06, WGZ+06, KKN09]

We have a tool to study such dephasing and symmetry-breaking mechanisms in conductors[AAKL82, Ber84, CS86]: It is the quantum interference of electrons in low-dimensional, disordered conductors. We will show in Chapter 3 how this effect results in corrections to the electrical conductivity $\Delta\sigma$, which is known as weak localization (WL) effect. Obviously also here we focus on systems with entanglement of spin and charge by SO interaction. The SO field, which has various forms in the semiconductor, makes the effect richer because it can enhance the conductivity by reversing the effect of WL. This is called weak antilocalization (WAL). We are going to calculate the correction with the Cooperon equation. Due to the fact that the origin of the interference-suppression is the randomization of the spin, more precise, the D'yakonov and Perel' spin relaxation in this work, it seems natural to establish a connection between the spin diffusion picture, e.g derived from the Eilenberger equation by Schwab *et al.*[SDGR06], and the local correction described by using the Cooperon equation, as we are going to show in Sec. 3.3. The link to applications in the field of spintronics is a better insight in what possibilities we have to create long living spin modes which will appear as special cases in our calculation.

As mentioned, the addition of boundaries can change the spin relaxation significantly. The change depends on kind and direction of the wire boundaries. Chapter 4 will focus especially on the latter. The connection between the WL and the spin diffusion will help us to understand both at the same time: The magnetoconductivity and the existence of persistent spin states for a given wire.

Having derived a consistent theory of spin relaxation in quantum wires, one could wonder why there are measurements of the spin lifetime like done by Kunihashi *et al.*[KKN09] in gate-fitted narrow wires from magnetotransport experiments, which show deviations from theory. This happens although all dominant SO coupling (SOC) types, namely linear Rashba and lin. and cubic Dresselhaus SOC, have been included in the theory. The crucial point is: If a part of the SOCs is left out, i.e. the cubic Dresselhaus SOC, one has great accordance between experiment and theory. In Chapter 4 we are going to show how this puzzle is resolved by doing a crossover from the diffusive to the ballistic regime and revealing a suppression of the problematic terms.

Throughout this work we set $\hbar \equiv 1$.

Chapter 2

Spin Dynamics: Overview and Analysis of 2D Systems

2.1 Short Reminder on the Origin of Spin Orbit Coupling

The interaction which makes spintronic devices so interesting is a relativistic effect, the SOC. The intrinsic degree of freedom spin is a direct consequence of the Lorentz invariant formulation of quantum mechanics. Expanding the relativistic Dirac equation in the ratio of the electron velocity and the speed of light up to the order $(v/c)^2$ (the derivation can be found in standard textbooks like Ref. [Sak67]) one gets

$$\left(\frac{p^2}{2m_{e0}} - e\varphi - \frac{p^4}{8m_{e0}^3c^2} - \frac{e}{4m_{e0}^2c^2}\boldsymbol{\sigma}\cdot(\nabla\varphi\times\mathbf{p}) - \frac{e}{8m_{e0}^2c^2}\Delta\varphi\right)\psi = (E - m_{e0}c^2)\psi,$$

with the electrostatic potential φ, and the free electron mass m_{e0}. Our interest concerns the so-called Thomas term $-e/(4m_{e0}^2c^2)\boldsymbol{\sigma}\cdot(\nabla\varphi\times\mathbf{p})$. In atomic physics we assume that the electric field is a central field, $\mathbf{E}(r) = -(d\varphi/dr)\mathbf{e}_r$ which leads to

$$\begin{aligned}
-\frac{e}{4m_{e0}^2c^2}\boldsymbol{\sigma}\cdot(\nabla\varphi\times\mathbf{p}) &= -\frac{e}{4m_{e0}^2c^2}\left(-\frac{1}{r}\frac{d\varphi}{dr}\right)\boldsymbol{\sigma}\cdot(\mathbf{r}\times\mathbf{p}) && (2.1)\\
&= -\frac{e}{2m_{e0}^2c^2}\frac{1}{r}\frac{d\varphi}{dr}\hat{\mathbf{s}}\cdot\mathbf{L} && (2.2)\\
&\equiv \lambda\hat{\mathbf{s}}\cdot\mathbf{L}, && (2.3)
\end{aligned}$$

with $\hat{\mathbf{s}} = \boldsymbol{\sigma}/2$.

Due to the lattice-periodic potential in a crystalline solid this effect can have strong influence

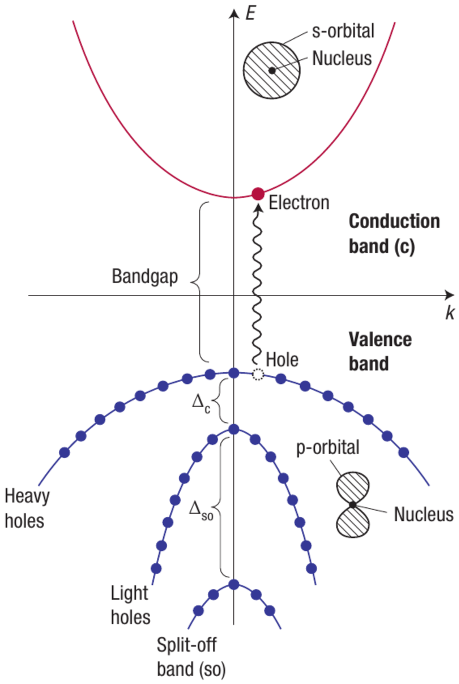

Figure 2.1: Schematic representation of the band structure of GaAs around the Γ point (extracted from Ref. [Bur08]).

on the energy band structure. Using the Kane Model it can be shown that the SOC due to lattice-periodic potential leads to a lifting of degeneracy with a gap $\Delta_{\text{SO}} = 3/(4\lambda)$ (with λ form Eq. (2.3)) between the Γ_{8v} states describing heavy and light holes and Γ_{7v} states, as sketched in Fig. 2.1 where Γ_{7v} is represented as the split-off band.[DR93, Win04a] It is important to notice that in the following we do not focus on the SOC which is due to strong Coulomb potential of the atomic core regions, but on the appearance of SO effect in the conduction band due to an additional external electric field and spatial symmetry breaking as explained in more detail in the next sections. Notice that the effects we present in this work are therefore on a different energy scale: The Pauli splitting Δ_{SO} can be large, 0.34 eV in GaAs, compared to splitting at the conduction band which is on the order of meV in GaAs.

Before we review the spin dynamics of conduction electrons and holes in semiconductors and metals, let us first reconsider the spin dynamics of a localized spin, as governed by the Bloch equations.

2.2 Dynamics of a Localized Spin

A localized spin $\hat{\mathbf{s}}$, like a nuclear spin, or the spin of a magnetic impurity in a solid, precesses in an external magnetic field $\mathbf{B}$ due to the Zeeman interaction with Hamiltonian $H_Z = -\gamma_g \hat{\mathbf{s}}\mathbf{B}$, where γ_g is the corresponding gyromagnetic ratio of the nuclear spin or magnetic impurity spin, respectively, which we will set equal to one unless needed explicitly. This spin dynamics is governed by the Bloch equation of a localized spin,

$$\partial_t \hat{\mathbf{s}} = \gamma_g \hat{\mathbf{s}} \times \mathbf{B}. \tag{2.4}$$

This equation is identical to the Heisenberg equation $\partial_t \hat{\mathbf{s}} = -i[\hat{\mathbf{s}}, H_Z]$ for the quantum mechanical spin operator $\hat{\mathbf{s}}$ of an $S = 1/2$-spin, interacting with the external magnetic field $\mathbf{B}$ due to the Zeeman interaction with Hamiltonian H_Z. The solution of the Bloch equation for a magnetic field pointing in the z-direction is $\hat{s}_z(t) = \hat{s}_z(0)$, while the x- and y- components of the spin are precessing with frequency $\boldsymbol{\omega}_0 = \gamma_g \mathbf{B}$ around the z-axis, $\hat{s}_x(t) = \hat{s}_x(0)\cos\omega_0 t + \hat{s}_y(0)\sin\omega_0 t$, $\hat{s}_y(t) = -\hat{s}_x(0)\sin\omega_0 t + \hat{s}_y(0)\cos\omega_0 t$. Since a localized spin interacts with its environment by exchange interaction and magnetic dipole interaction, the precession will dephase after a time τ_2, and the z-component of the spin relaxes to its equilibrium value s_{z0} within a relaxation time τ_1. This modifies the Bloch equations to the phenomenological equations,

$$\begin{aligned}
\partial_t \hat{s}_x &= \gamma_g(\hat{s}_y B_z - \hat{s}_z B_y) - \frac{1}{\tau_2}\hat{s}_x \\
\partial_t \hat{s}_y &= \gamma_g(\hat{s}_z B_x - \hat{s}_x B_z) - \frac{1}{\tau_2}\hat{s}_y \\
\partial_t \hat{s}_z &= \gamma_g(\hat{s}_x B_y - \hat{s}_y B_x) - \frac{1}{\tau_1}(\hat{s}_z - s_{z0}).
\end{aligned} \tag{2.5}$$

2.3 Spin Dynamics of Itinerant Electrons

2.3.1 Ballistic Spin Dynamics

Starting from Dirac equation we have seen that one obtains in addition to the Zeeman term a term which couples the spin $\mathbf{s}$ with the momentum $\mathbf{p}$ of the electrons, the spin-orbit coupling

$$H_{\text{SO}} = -\frac{\mu_B}{2m_{e0}c^2}\hat{\mathbf{s}}\ \mathbf{p} \times \mathbf{E} = -\hat{\mathbf{s}}\mathbf{B}_{\text{SO}}(\mathbf{p}), \tag{2.6}$$

where we set the gyromagnetic ratio $\gamma_g = 1$. $\mathbf{E} = -\nabla\varphi$, is an electrical field, and $\mathbf{B}_{\text{SO}}(\mathbf{p}) = \mu_B/(2m_{e0}c^2)\mathbf{p} \times \mathbf{E}$. Substitution into the Heisenberg equation yields the Bloch equation in the presence of spin-orbit interaction:

$$\partial_t \hat{\mathbf{s}} = \hat{\mathbf{s}} \times \mathbf{B}_{\text{SO}}(\mathbf{p}), \tag{2.7}$$

so that the spin performs a precession around the momentum dependent spin-orbit field $\mathbf{B}_{\text{SO}}(\mathbf{p})$. It is important to note, that the spin-orbit field does not break the invariance under time reversal ($\hat{\mathbf{s}} \to -\hat{\mathbf{s}}, \mathbf{p} \to -\mathbf{p}$), in contrast to an external magnetic field $\mathbf{B}$. Therefore, averaging over all directions of momentum, there is no spin polarization of the conduction electrons. However, injecting a spin-polarized electron with given momentum $\mathbf{p}$ into a translationally invariant wire, its spin precesses in the spin-orbit field as the electron moves through the wire. The spin will be oriented again in the initial direction after it moved a length L_{SO}, the spin precession length. The precise magnitude of L_{SO} does not only depend on the strength of the spin-orbit interaction but may also depend on the direction of its movement in the crystal, as we will discuss below.

2.3.2 Spin Diffusion Equation

Translational invariance is broken by the presence of disorder due to impurities and lattice imperfections in the conductor. As the electrons scatter from the disorder potential elastically, their momentum changes in a stochastic way, resulting in diffusive motion. That results in a change of the the local electron density $\rho(\mathbf{r}, t) = \sum_{\alpha=\pm} \mid \psi_\alpha(\mathbf{r}, t) \mid^2$, where $\alpha = \pm$ denotes the orientation of the electron spin, and $\psi_\alpha(\mathbf{r}, t)$ is the position and time dependent electron wave function amplitude. On length scales exceeding the elastic mean free path l_e, that density is governed by the diffusion equation

$$\frac{\partial \rho}{\partial t} = D_e \nabla^2 \rho, \tag{2.8}$$

where the diffusion constant D_e is related to the elastic scattering time τ by $D_e = v_{\text{F}}^2 \tau / d_D$, where v_{F} is the Fermi velocity, and d_D the diffusion dimension[1] of the electron system. That diffusion constant is related to the mobility of the electrons, $\mu_e = e\tau/m_e$ by the Einstein relation $\mu_e \rho = e 2\nu D_e$, where ν is the density of states (DOS) per spin at the Fermi energy E_{F} and m_e the effective electron mass.

---

[1] d_D can have a fractal value e.g. on quasi-periodic lattices

Injecting an electron at position $\mathbf{r_0}$ into a conductor with previously constant electron density ρ_0, the solution of the diffusion equation yields that the electron density spreads in space according to $\rho(\mathbf{r},t) = \rho_0 + \exp(-(\mathbf{r}-\mathbf{r_0})^2/4D_e t)/(4\pi D_e t)^{d_D/2}$. The dimension d_D is equal to the kinetic dimension d, $d_D = d$, if the elastic mean free path l_e is smaller than the size of the sample in all directions. If the elastic mean free path is larger than the sample size in one direction the diffusion dimension reduces by one, accordingly. Thus, on average the variance of the distance the electron moves after time t is $\langle(\mathbf{r}-\mathbf{r_0})^2\rangle = 2d_D D_e t$. This introduces a new length scale, the diffusion length $L_D(t) = \sqrt{D_e t}$. We can rewrite the density as $\rho = \langle\psi^\dagger(\mathbf{r},t)\psi(\mathbf{r},t)\rangle$, where $\psi^\dagger = (\psi_+^\dagger, \psi_-^\dagger)$ is the two-component vector of the up (+), and down (-) spin fermionic creation operators, and ψ the 2-component vector of annihilation operators, respectively, $\langle\ldots\rangle$ denotes the expectation value. Accordingly, the spin density $\mathbf{s}(\mathbf{r},t)$ is expected to satisfy a diffusion equation, as well. The spin density is defined by

$$\mathbf{s}(\mathbf{r},t) = \frac{1}{2}\langle\psi^\dagger(\mathbf{r},t)\boldsymbol{\sigma}\psi(\mathbf{r},t)\rangle, \tag{2.9}$$

where $\boldsymbol{\sigma}$ is the vector of Pauli matrices,

$$\sigma_x = \begin{pmatrix} 0 & 1 \\ 1 & 0 \end{pmatrix}, \sigma_y = \begin{pmatrix} 0 & -i \\ i & 0 \end{pmatrix}, \text{ and } \sigma_z = \begin{pmatrix} 1 & 0 \\ 0 & -1 \end{pmatrix}.$$

Thus the z-component of the spin density is half the difference between the density of spin up and down electrons, $s_z = (\rho_+ - \rho_-)/2$, which is the local spin polarization of the electron system. Thus, we can directly infer the diffusion equation for s_z, and, similarly, for the other components of the spin density, yielding, without magnetic field and spin-orbit interaction,[Tor56]

$$\frac{\partial \mathbf{s}}{\partial t} = D_e \nabla^2 \mathbf{s} - \frac{\mathbf{s}}{\hat{\tau}_s}. \tag{2.10}$$

Here, in the spin relaxation term we introduced the tensor $\hat{\tau}_s$, which can have non-diagonal matrix elements. In the case of a diagonal matrix, $\tau_{sxx} = \tau_{syy} = \tau_2$, is the spin dephasing time, and $\tau_{szz} = \tau_1$ the spin relaxation time. The spin diffusion equation can be written as a continuity equation for the spin density vector, by defining the spin diffusion current of the spin components s_i,

$$\mathbf{J}_{s_i} = -D_e \nabla s_i. \tag{2.11}$$

Thus, we get the continuity equation for the spin density components s_i,

$$\frac{\partial s_i}{\partial t} + \nabla \mathbf{J}_{s_i} = -\sum_j \frac{s_j}{(\hat{\tau}_s)_{ij}}. \tag{2.12}$$

2.3.3 Spin Orbit Interaction in Semiconductors

SOI in semiconductors is closely related to breaking of symmetries which lift spin degeneracy: In the case without magnetic field B we start with a twofold degeneracy: Time inversion symmetry, $E_\uparrow(\mathbf{k}) = E_\downarrow(-\mathbf{k})$ and space inversion symmetry, $E_\uparrow(\mathbf{k}) = E_\uparrow(-\mathbf{k})$. As a consequence we have $E_\uparrow(\mathbf{k}) = E_\downarrow(\mathbf{k})$. In the following, we show how the degeneracy is lifted in semiconductor devices in case of $B = 0$.

While silicon and germanium have in their diamond structure an inversion symmetry around every midpoint on each line connecting nearest neighbor atoms, this is not the case for III-V-semiconductors like GaAs, InAs, InSb, or ZnS. These have a zinc-blende structure which can be obtained from a diamond structure with neighbored sites occupied by the two different elements. Therefore, the inversion symmetry is broken, which results in spin-orbit coupling. This can be understood by noticing that pairs like Ga-As are local dipoles whose electric field is responsible for SOC if inversion symmetry is broken[2]. Similarly, that symmetry is broken in II-VI-semiconductors. This bulk inversion asymmetry (BIA) coupling, or often so-called Dresselhaus-coupling, is anisotropic, as given by [Dre55]

$$H_\mathrm{D} = \gamma_D \left[\sigma_x k_x (k_y^2 - k_z^2) + \sigma_y k_y (k_z^2 - k_x^2) + \sigma_z k_z (k_x^2 - k_y^2)\right], \tag{2.13}$$

where γ_D is the Dresselhaus-spin-orbit coefficient. Band structure calculations yield the following values: $\gamma_D = 27.6$ eVÅ(GaAs), $= 27.2$ eVÅ(InAs), $= 760.1$ eVÅ(InSb) [Win03]. Some values extracted in experiments are listed in Tab. A. Confinement in quantum wells with width a_z on the order of the Fermi wave length λ_F yields accordingly a spin-orbit interaction where the momentum in growth direction is of the order of $1/a_z$. Because of the anisotropy of the Dresselhaus term, the spin-orbit interaction depends strongly on the growth direction of the quantum well. Grown in [001] direction, one gets, taking the expectation value of Eq. (2.13) in the direction normal to the plane, noting that $\langle k_z \rangle = \langle k_z^3 \rangle = 0$, [Dre55]

$$H_{\mathrm{D}[001]} = \alpha_1(-\sigma_x k_x + \sigma_y k_y) + \gamma_D(\sigma_x k_x k_y^2 - \sigma_y k_y k_x^2). \tag{2.14}$$

where $\alpha_1 = \gamma_D \langle k_z^2 \rangle$ is the linear Dresselhaus parameter. Thus, inserting an electron with momentum along the x-direction, with its spin initially polarized in z-direction, it will

---

[2] Starting from an extended Kane model where p-like higher energy bands are included one gets a Hamiltonian with matrix elements which are only nonzero if the crystal has no center of inversion.[FMAE+07]

precess around the x-axis as it moves along. For narrow quantum wells, where $\langle k_z^2 \rangle \sim 1/a_z^2 \geq k_F^2$ the linear term exceeds the cubic Dresselhaus terms. For a typical value of $\langle k_z^2 \rangle = 0.036/\text{nm}^2$, one gets accordingly[Win04b], α_1 =0.99 meVnm (GaAs), 0.98 meVnm (InAs), 27.4 meVnm (InSb). A special situation arises for quantum wells grown in the [110]-direction, where it turns out that the spin-orbit field is pointing normal to the quantum well, as shown in Fig. 2.2, so that an electron whose spin is initially polarized along the normal of the plane, remains polarized as it moves in the quantum well.

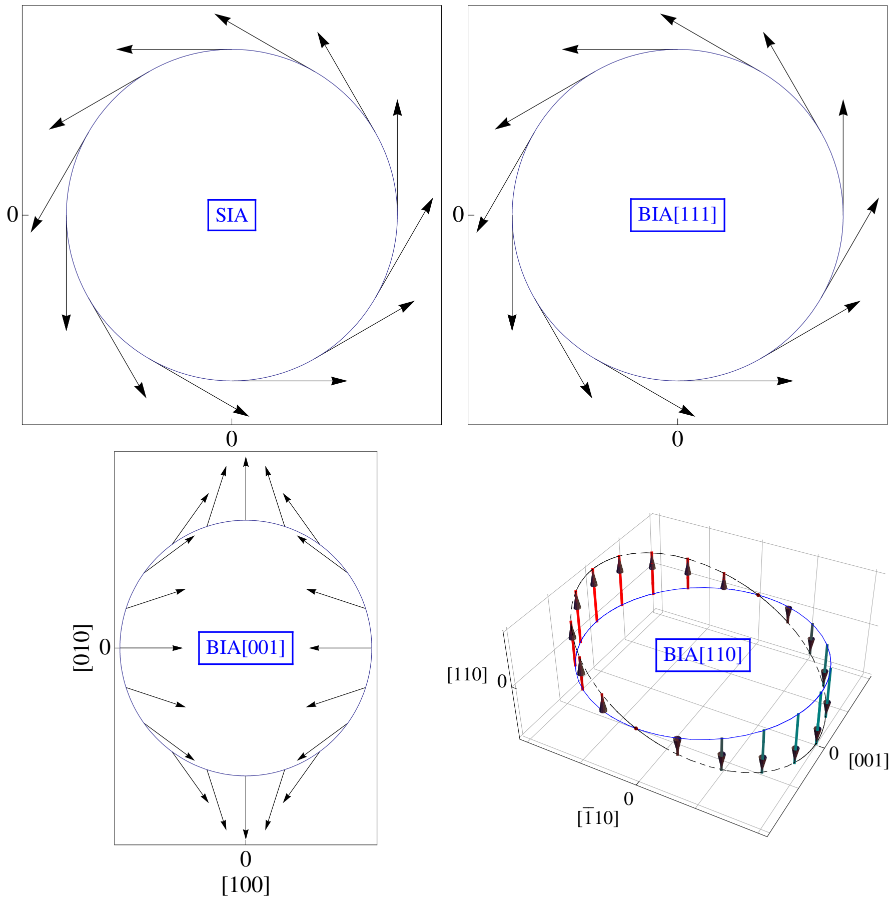

Figure 2.2: The spin-orbit vector fields for linear structure inversion asymmetry (Rashba) coupling, and for linear bulk inversion asymmetry (BIA) spin-orbit coupling for quantum wells grown in [111], [001] and [110] direction, respectively.

In quantum wells with asymmetric electrical confinement the inversion symmetry is broken as well. The resulting spin-orbit coupling, the structural inversion asymmetry coupling

(SIA), also-called Rashba-spin-orbit interaction[Ras60] is given by

$$H_{\mathrm{R}} = \alpha_2(\sigma_x k_y - \sigma_y k_x), \tag{2.15}$$

where α_2 depends on the asymmetry of the confinement potential $V(z)$ in the direction z, the growth direction of the quantum well, and can thus be deliberately changed by application of a gate potential. This dependence allows one, in principle, to control the electron spin with a gate potential, which can, therefore, be used as the basis of a spin transistor.[DD90] One should stress that the expectation value of the electrical field $\mathcal{E}_c = -\partial_z V(z)$ in the conduction band state vanishes if the effective mass m_e is not position dependent. However it can be shown that the parameter α_2 is modulated by the electric field in the valence band and the z-dependent Pauli splitting Δ_0.[FMAE$^+$07] Several measured values of α_2 are listed in Tab. A and ratios of α_2 and α_1 in Tab. A.

We can combine all spin-orbit couplings by introducing the spin-orbit field such that the Hamiltonian has the form of a Zeeman term:

$$H_{\mathrm{SO}} = -\mathbf{s}\mathbf{B}_{\mathrm{SO}}(\mathbf{k}), \tag{2.16}$$

where the spin vector is $\mathbf{s} = \boldsymbol{\sigma}/2$. But we stress again that since $\mathbf{B}_{\mathrm{SO}}(\mathbf{k}) \to \mathbf{B}_{\mathrm{SO}}(-\mathbf{k}) = -\mathbf{B}_{\mathrm{SO}}(\mathbf{k})$ under the time reversal operation, spin-orbit coupling does not break time reversal symmetry, since the time reversal operation also changes the sign of the spin, $\mathbf{s} \to -\mathbf{s}$. Only an external magnetic field $\mathbf{B}$ breaks the time reversal symmetry. Thus, the electron spin operator $\hat{\mathbf{s}}$ is for fixed electron momentum $\mathbf{k}$ governed by the Bloch equations with the spin-orbit field,

$$\frac{\partial \hat{\mathbf{s}}}{\partial t} = \hat{\mathbf{s}} \times (\mathbf{B} + \mathbf{B}_{\mathrm{SO}}(\mathbf{k})) - \frac{1}{\hat{\tau}_s}\hat{\mathbf{s}}. \tag{2.17}$$

The spin relaxation tensor is no longer necessarily diagonal in the presence of spin-orbit interaction as will be shown in Sec. 2.4.1.

In narrow quantum wells where the cubic Dresselhaus coupling is weak compared to the linear Dresselhaus and Rashba couplings, the spin-orbit field is given by

$$\mathbf{B}_{\mathrm{SO}}(\mathbf{k}) = -2 \begin{pmatrix} -\alpha_1 k_x + \alpha_2 k_y \\ \alpha_1 k_y - \alpha_2 k_x \\ 0 \end{pmatrix}, \tag{2.18}$$

which changes both its direction and its amplitude $\mid \mathbf{B}_{\mathrm{SO}}(\mathbf{k}) \mid = 2\sqrt{(\alpha_1^2 + \alpha_2^2)k^2 - 4\alpha_1\alpha_2 k_x k_y}$, as the direction of the momentum $\mathbf{k}$ is changed. Accordingly, the electron energy dispersion close to the Fermi energy is in general anisotropic as given by

$$E_{\pm}(\mathbf{k}) = \frac{1}{2m_e}k^2 \pm \alpha k \sqrt{1 - 4\frac{\alpha_1\alpha_2}{\alpha^2}\cos\theta\sin\theta}, \tag{2.19}$$

where $k = \mid \mathbf{k} \mid$, $\alpha = \sqrt{\alpha_1^2 + \alpha_2^2}$, and $k_x = k\cos\theta$. Thus, when an electron is injected with energy E, with momentum k along the [100]-direction, $k_x = k, k_y = 0$, its wave function is a superposition of plain waves with the positive momenta $k_{\pm} = \mp\alpha m_e + m_e(\alpha^2 + 2E/m_e)^{1/2}$. The momentum difference $k_- - k_+ = 2m_e\alpha$ causes a rotation of the electron eigenstate in the spin subspace. When at $x = 0$ the electron spin was polarized up spin, with the eigenvector

$$\psi(x=0) = \begin{pmatrix} 1 \\ 0 \end{pmatrix},$$

then, when its momentum points in x-direction, at a distance x, it will have rotated the spin as described by the eigenvector

$$\psi(x) = \frac{1}{2}\begin{pmatrix} 1 \\ \frac{\alpha_1 + i\alpha_2}{\alpha} \end{pmatrix} e^{ik_+x} + \frac{1}{2}\begin{pmatrix} 1 \\ -\frac{\alpha_1 + i\alpha_2}{\alpha} \end{pmatrix} e^{ik_-x}. \tag{2.20}$$

In Fig. 2.3 we plot the corresponding spin density as defined in Eq. (2.9) for pure Rashba coupling, $\alpha_1 = 0$. The spin will point again in the initial direction, when the phase difference between the two plain waves is 2π, which gives the condition for spin precession length as

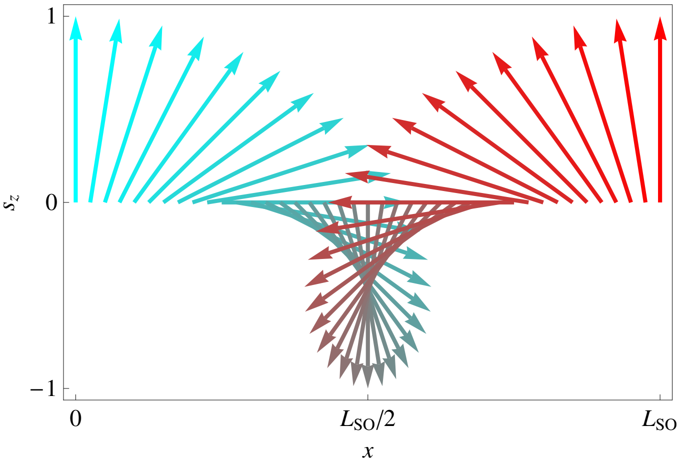

Figure 2.3: Precession of a spin injected at $x = 0$, polarized in z-direction, as it moves by one spin precession length $L_{\text{SO}} = \pi/m_e\alpha$ through the wire with linear Rashba spin-orbit coupling α_2.

$2\pi = (k_- - k_+)L_{\rm SO}$, yielding for linear Rashba and Dresselhaus coupling, and the electron moving in [100]- direction,

$$L_{\rm SO} = \pi/m_e\alpha. \tag{2.21}$$

We note that the period of spin precession changes with the direction of the electron momentum since the spin-orbit field, Eq. (2.18), is anisotropic.

2.3.4 Spin Diffusion in the Presence of Spin-Orbit Interaction

As the electrons are scattered by imperfections like impurities and dislocations, their momentum is changed randomly. Accordingly, the direction of the spin-orbit field $\mathbf{B}_{\rm SO}(\mathbf{k})$ changes randomly as the electron moves through the sample. This has two consequences: the electron spin direction becomes randomized, dephasing the spin precession and relaxing the spin polarization. In addition, the spin precession term is modified, as the momentum $\mathbf{k}$ changes randomly, and has no longer the form given in the ballistic Bloch-like equation, Eq. (2.17). One can derive the diffusion equation for the expectation value of the spin, the spin density Eq. (2.9) semiclassically, [MC00, SDGR06] or by diagrammatic expansion, as will be presented in Chapter 3. In order to get a better understanding on the meaning of this equation, we will give a simplified classical derivation, in the following. The spin density at time $t + \Delta t$ can be related to the one at the earlier time t. Note that for ballistic times $\Delta t \leq \tau$, the distance the electron has moved with a probability $p_{\Delta\mathbf{x}}$, $\Delta\mathbf{x}$, is related to that time by the ballistic equation, $\Delta\mathbf{x} = \mathbf{k}(t)\Delta t/m$ when the electron moves with the momentum $\mathbf{k}(t)$. On this time scale the spin evolution is still governed by the ballistic Bloch equation Eq. (2.17). Thus, we can relate the spin density at the position $\mathbf{x}$ at the time $t + \Delta t$, to the one at the earlier time t at position $\mathbf{x} - \Delta\mathbf{x}$:

$$\mathbf{s}(\mathbf{x}, t + \Delta t) = \sum_{\Delta\mathbf{x}} p_{\Delta\mathbf{x}} \left(\left(1 - \frac{1}{\hat{\tau}_s}\Delta t\right) \mathbf{s}(\mathbf{x} - \Delta\mathbf{x}, t) - \Delta t \left[\mathbf{B} + \mathbf{B}_{\rm SO}\left(\mathbf{k}(t)\right)\right] \times \mathbf{s}(\mathbf{x} - \Delta\mathbf{x}, t) \right). \tag{2.22}$$

Now, we can expand in Δt to first order and in $\Delta\mathbf{x}$ to second order. Next, we average over the disorder potential, assuming that the electrons are scattered isotropically, and substitute $\sum_{\Delta\mathbf{x}} p_{\Delta\mathbf{x}} \ldots = \int (\mathrm{d}\Omega/\Omega) \ldots$ where Ω is the total angle, and $\int d\Omega$ denotes the integral over all angles with $\int (\mathrm{d}\Omega/\Omega) = 1$. Also, we get $\left(\mathbf{s}(\mathbf{x}, t + \Delta t) - \mathbf{s}(\mathbf{x}, t)\right)/\Delta t \to \partial_t \mathbf{s}(\mathbf{x}, t)$ for $\Delta t \to 0$, and $\langle \Delta x_i^2 \rangle = 2D_e\Delta t$, where D_e is the diffusion constant. While the disorder average yields $\langle \Delta\mathbf{x} \rangle = 0$, and $\langle \mathbf{B}_{\rm SO}(\mathbf{k}(t)) \rangle = 0$, separately, for isotropic impurity scattering, averaging their product yields a finite value, since $\Delta\mathbf{x}$ depends on the momentum at time t, $\mathbf{k}(t)$, yielding $\langle \Delta\mathbf{x} B_{\mathrm{SOi}}(\mathbf{k}(t))\rangle = 2\Delta t \langle \mathbf{v}_{\mathrm{F}} B_{\mathrm{SOi}}(\mathbf{k}(t))\rangle$, where $\langle \dots \rangle$ denotes the average over the Fermi surface. This way, we can also evaluate the average of the spin-orbit term in Eq. (2.22), expanded to first order in $\Delta\mathbf{x}$, and get, substituting $\Delta t \to \tau$ the spin diffusion equation,

$$\frac{\partial \mathbf{s}}{\partial t} = -\mathbf{B} \times \mathbf{s} + D_e \nabla^2 \mathbf{s} + 2\tau \langle (\nabla \mathbf{v}_{\mathbf{F}}) \mathbf{B}_{\mathrm{SO}}(\mathbf{p}) \rangle \times \mathbf{s} - \frac{1}{\hat{\tau}_s} \mathbf{s}, \tag{2.23}$$

Spin polarized electrons injected into the sample spread diffusively, and their spin polarization, while spreading diffusively as well, decays in amplitude exponentially in time. Since, between scattering events the spins precess around the spin-orbit fields, one expects also an oscillation of the polarization amplitude in space. One can find the spatial distribution of the spin density which is the solution of Eq. (2.23) with the smallest decay rate Γ_s. As an example, the solution for linear Rashba coupling is, [SDGR06]

$$\mathbf{s}(\mathbf{x}, t) = \left(\hat{e}_q \cos(\mathbf{q}\mathbf{x}) + A \hat{e}_z \sin(\mathbf{q}\mathbf{x})\right) e^{-t/\tau_s}, \tag{2.24}$$

with $1/\tau_s = 7/16\tau_{s0}$ where $1/\tau_{s0} = 2\tau k_F^2 \alpha_2^2$ and where the amplitude of the momentum $\mathbf{q}$ is determined by $D_e q^2 = 15/16\tau_{s0}$, and $A = 3/\sqrt{15}$, and $\hat{e}_q = \mathbf{q}/q$. This solution is plotted in Fig. 2.4 for $\hat{e}_q = (1, 1, 0)/\sqrt{2}$. We will derive this solution in the context of local corrections to the static conductivity, Chapter 3. Thereby we show that by adding Dresselhaus SOC it will be even possible to create *persistent solutions*.

In Fig. 2.5 we plot the linearly independent solution obtained by interchanging cos and sin in Eq. (2.24), with the spin pointing in z-direction, initially. We choose $\hat{e}_q = \hat{e}_x$. Comparison with the ballistic precession of the spin, Fig 2.5 shows that the period of precession is enhanced by the factor $4/\sqrt{15}$ in the diffusive wire, and that the amplitude of the spin density is modulated, changing from 1 to $A = 3/\sqrt{15}$.

Injecting a spin-polarized electron at one point, say $\mathbf{x} = 0$, its density spreads the same way it does without spin-orbit interaction, $\rho(\mathbf{r}, t) = \exp(-r^2/4D_e t)/(4\pi D_e t)^{d_D/2}$, where r is the distance to the injection point. However, the decay of the spin density is periodically modulated as a function of $2\pi\sqrt{15/16} r/L_{\mathrm{SO}}$.[Fro01] The spin-orbit interaction together with the scattering from impurities is also a source of spin relaxation, as we discuss in the next Section together with other mechanisms of spin relaxation. We can find the classical spin diffusion current in the presence of spin-orbit interaction, in a similar way as one can derive the classical diffusion current: The current at the position $\mathbf{r}$ is a sum

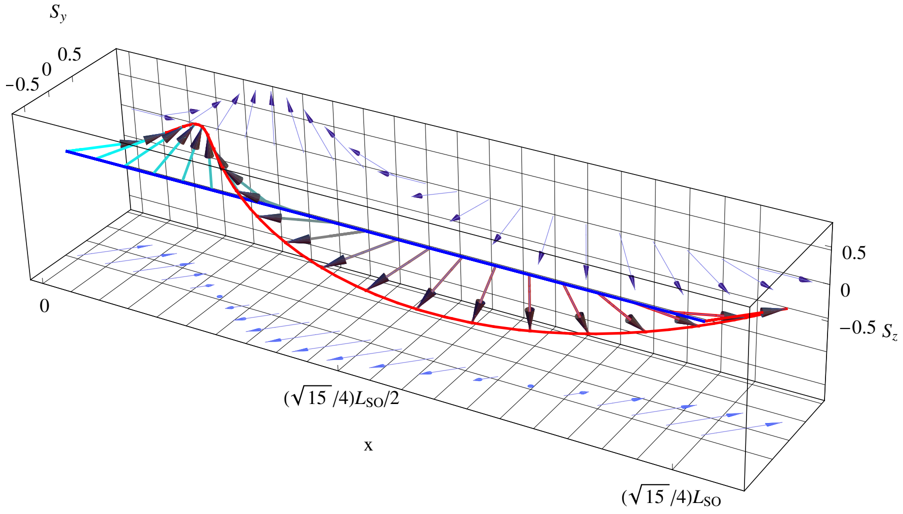

Figure 2.4: The spin density for linear Rashba coupling which is a solution of the spin diffusion equation with the relaxation rate $7/16\tau_s$. The spin points initially in the $x-y$-plane in the direction $(1, 1, 0)$.

over all currents in its vicinity which are directed towards that position. Thus, $\mathbf{j}(\mathbf{r}, t) = \langle \mathbf{v}\rho(\mathbf{r} - \Delta\mathbf{x})\rangle$ where an angular average over all possible directions of the velocity $\mathbf{v}$ is taken. Expanding in $\Delta\mathbf{x} = l_e\mathbf{v}/v$, and noting that $\langle \mathbf{v}\rho(\mathbf{r})\rangle = 0$, one gets $\mathbf{j}(\mathbf{r}, t) = \langle \mathbf{v}(-\Delta\mathbf{x})\nabla\rho(\mathbf{r})\rangle = -(v_F l_e/2)\nabla\rho(\mathbf{r}) = -D_e\nabla\rho(\mathbf{r})$. For the classical spin diffusion current of spin component S_i, as defined by $\mathbf{j}_{S_i}(\mathbf{r}, t) = \mathbf{v}S_i(\mathbf{r}, t)$, there is the complication that the spin keeps precessing as it moves from $\mathbf{r} - \Delta\mathbf{x}$ to $\mathbf{r}$, and that the spin-orbit field changes its direction with the direction of the electron velocity $\mathbf{v}$. Therefore, the 0-th order term in the expansion in $\Delta\mathbf{x}$ does not vanish, rather, we get

$$\mathbf{j}_{S_i}(\mathbf{r}, t) = \langle \mathbf{v}S_i^{\mathbf{k}}(\mathbf{r}, t)\rangle - D_e\nabla S_i(\mathbf{r}, t), \tag{2.25}$$

where $S_i^{\mathbf{k}}$ is the part of the spin density which evolved from the spin density at $\mathbf{r} - \Delta\mathbf{x}$ moving with velocity $\mathbf{v}$ and momentum $\mathbf{k}$. Noting that the spin precession on ballistic scales $t \leq \tau$ is governed by the Bloch equation, Eq. (2.17), we find by integration of Eq. (2.17), that $S_i^{\mathbf{k}} = -\tau\,[\mathbf{B}_{\text{SO}}(\mathbf{k}) \times \mathbf{S}]_i$ so that we can rewrite the first term yielding the total spin diffusion current as

$$\mathbf{j}_{S_i} = -\tau\langle \mathbf{v}_F\,[\mathbf{B}_{\text{SO}}(\mathbf{k}) \times \mathbf{S}]_i\rangle - D_e\nabla S_i. \tag{2.26}$$

Thus, we can rewrite the spin diffusion equation in terms of this spin diffusion current and

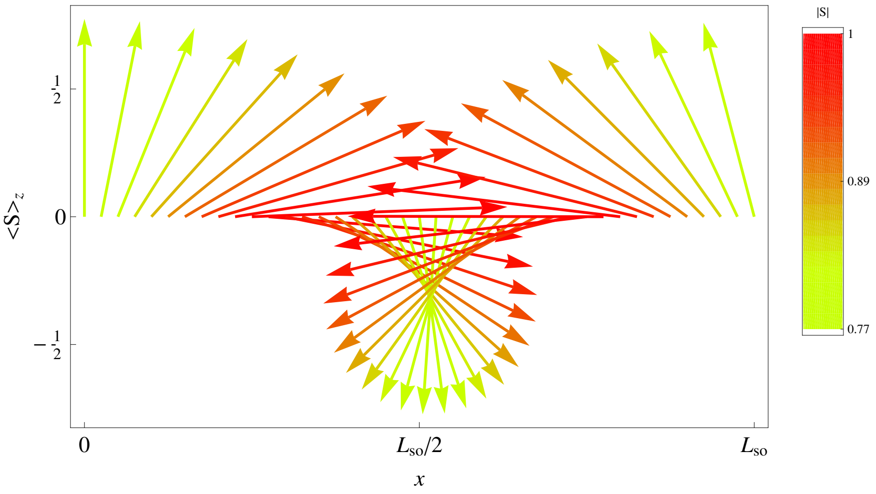

Figure 2.5: The spin density for linear Rashba coupling which is a solution of the spin diffusion equation with the relaxation rate $1/\tau_s = 7/16\tau_{s0}$. Note that, compared to the ballistic spin density, Fig. 2.3, the period is slightly enhanced by a factor $4/\sqrt{15}$. Also, the amplitude of the spin density changes with the position x, in contrast to the ballistic case. The color is changing in proportion to the spin density amplitude.

get the continuity equation

$$\frac{\partial \mathbf{s}_i}{\partial t} = -\nabla \mathbf{j}_{S_i} + \tau \langle \nabla \mathbf{v}_F \left(\mathbf{B}_{\,\mathrm{SO}}(\mathbf{k}) \times \mathbf{S} \right)_i \rangle - \frac{1}{(\hat{\tau}_s)_{ij}} \mathbf{s}_j. \tag{2.27}$$

It is important to note that in contrast to the continuity equation for the density, there are two additional terms, due to the spin-orbit interaction. The last one is the spin relaxation tensor which will be considered in detail in the next section. The other term arises due to the fact that Eq. (2.23) contains a factor 2 in front of the spin-orbit precession term, while the spin diffusion current Eq. (2.26) does not contain that factor. This has important physical consequences, resulting in the suppression of the spin relaxation rate in quantum wires and quantum dots as soon as their lateral extension is smaller than the spin precession length $L_{\,\mathrm{SO}}$, as we will see in Chapter 3.

2.4 Spin Relaxation Mechanisms

The intrinsic spin-orbit interaction itself causes the spin of the electrons to precess coherently, as the electrons move through a conductor, defining the spin precession length

$L_{\rm SO}$, Eq. (2.21). Since impurities and dislocations in the conductor randomize the electron momentum, the impurity scattering is transfered into a randomization of the electron spin by the spin-orbit interaction, which thereby results in spin dephasing and spin relaxation. This results in a new length scale, the spin relaxation length, L_s, which is related to the spin relaxation rate $1/\tau_s$ by

$$L_s = \sqrt{D_e \tau_s}. \tag{2.28}$$

2.4.1 D'yakonov-Perel' Spin Relaxation

D'yakonov-Perel' (DP) spin relaxation can be understood qualitatively in the following way: The spin-orbit field $\mathbf{B}_{\rm SO}(\mathbf{k})$ changes its direction randomly after each elastic scattering event from an impurity, that is, after a time of the order of the elastic scattering time τ, when the momentum is changed randomly as sketched in Fig. 2.6. Thus, the spin has the time τ to perform a precession around the present direction of the spin-orbit field, and can thus change its direction only by an angle of the order of $\mathbf{B}_{\rm SO}\tau$ by precession. After a time t with $N_t = t/\tau$ scattering events, the direction of the spin will, therefore, have changed by an angle of the order of $\mid B_{\rm SO} \mid \tau\sqrt{N_t} = \mid B_{\rm SO} \mid \sqrt{\tau t}$. Defining the spin relaxation time τ_s as the time by which the spin direction has changed by an angle of order one, we thus find that $1/\tau_s \sim \tau\langle \mathbf{B}_{\rm SO}(\mathbf{k})^2\rangle$, where the angular brackets denote integration over all angles. Remarkably, this spin relaxation rate becomes smaller, the more scattering events take place, because the smaller the elastic scattering time τ is, the less time the spin has to change its direction by precession. Such a behavior is also well known as *motional*, or *dynamic narrowing* of magnetic resonance lines[BPP48].

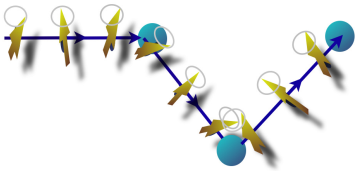

Figure 2.6: Elastic scattering from impurities changes the direction of the spin-orbit field around which the electron spin is precessing.

A more rigorous derivation for the kinetic equation of the spin density matrix yields additional interference terms, not taken into account in the above argument. It can be obtained by iterating the expansion of the spin density Eq. (2.22) once in the spin precession term, which yields the term

$$\left\langle \mathbf{s}(\mathbf{x},t) \times \int_0^{\Delta t} \mathrm{d}t' \, \mathbf{B}_{\,\mathrm{SO}}(\mathbf{k}(t')) \times \int_0^{\Delta t} \mathrm{d}t'' \, \mathbf{B}_{\,\mathrm{SO}}(\mathbf{k}(t'')) \right\rangle, \tag{2.29}$$

where $\langle \ldots \rangle$ denotes the average over all angles due to the scattering from impurities. Since the electrons move ballistically at times smaller than the elastic scattering time, the momenta are correlated only on time scales smaller than τ, yielding

$$\langle k_i(t') k_j(t'') \rangle = (1/2) k^2 \delta_{ij} \tau \delta(t' - t''). \tag{2.30}$$

Noting that $(\mathbf{A} \times \mathbf{B} \times \mathbf{C})_m = \epsilon_{ijk}\epsilon_{klm} A_i B_j C_l$ and $\sum \epsilon_{ijk}\epsilon_{klm} = \delta_{il}\delta_{jm} - \delta_{im}\delta_{jl}$ we find that Eq. (2.29) simplifies to $-\sum_i (1/\tau_{sij}) S_j$, where the matrix elements of the spin relaxation terms are given by [DP71c],

$$\frac{1}{(\hat{\tau}_s)_{ij}} = \tau \left(\langle \mathbf{B}_{\,\mathrm{SO}}(\mathbf{k})^2 \rangle \delta_{ij} - \langle B_{\,\mathrm{SO}}(\mathbf{k})_i B_{\,\mathrm{SO}}(\mathbf{k})_j \rangle \right), \tag{2.31}$$

where $\langle \ldots \rangle$ denotes the average over the direction of the momentum $\mathbf{k}$. In Chapter 3 we will focus on this kind of spin relaxation and show that these nondiagonal terms can diminish the spin relaxation and even result in vanishing spin relaxation. In the context of weak localization, which is presented in the next Chapter, we will show that the relaxation tensor Eq. (2.31) can be also derived from Cooperon equation (see Appendix C.3).

2.4.2 DP Spin Relaxation with Electron-Electron and Electron-Phonon Scattering

It has been noted, that the momentum scattering which limits the D'yakonov-Perel' mechanism of spin relaxation is not restricted to impurity scattering, but can also be due to electron-phonon or electron-electron interactions[GI02, GI04, PF06, DR04]. Thus the scattering time τ is the total scattering time as defined by, [GI02, GI04], $1/\tau = 1/\tau_0 + 1/\tau_{ee} + 1/\tau_{ep}$, where $1/\tau_0$ is the elastic scattering rate due to scattering from impurities with potential V, given by $1/\tau_0 = 2\pi\nu n_i \int (\mathrm{d}\theta/2\pi)\,(1 - \cos\theta) \mid V(\mathbf{k},\mathbf{k}') \mid^2$, where ν is the DOS per spin at the Fermi energy, n_i is the concentration of impurities with potential V, and $\mathbf{k}\mathbf{k}' = kk' \cos(\theta)$. Concerning the temperature dependence of the spin relaxation, for degenerate electrons in semiconductors ($E_{\mathbf{k}} = E_F$, with the Fermi energy E_F) it is given by the temperature dependence of $\tau(T)$. However, for a non-degenerate statistics one finds $1/\tau_s \sim T^3 \tau_m(T)$, where $\tau_m = \langle \tau(E_{\mathbf{k}}) E_{\mathbf{k}} \rangle \,/\, \langle E_{\mathbf{k}} \rangle$.

2.4.3 Elliott-Yafet Spin Relaxation

Because of the spin-orbit interaction the conduction electron wave functions are not eigenstates of the electron spin, but have an admixture of both spin up and spin down wave functions. Thus, a nonmagnetic impurity potential V can change the electron spin, by changing their momentum due to the spin-orbit coupling. This results in another source of spin relaxation which is stronger, the more often the electrons are scattered, and is thus proportional to the momentum scattering rate $1/\tau$[Ell54, Yaf63]. For degenerate III-V semiconductors one finds[Cha75, PT84]

$$\frac{1}{\tau_s} \sim \frac{\Delta_{\mathrm{SO}}^2}{(E_G + \Delta_{\mathrm{SO}})^2} \frac{E_{\mathbf{k}}^2}{E_G^2} \frac{1}{\tau(\mathbf{k})}, \tag{2.32}$$

where E_G is the gap between the valence and the conduction band of the semiconductor, $E_{\mathbf{k}}$ the energy of the conduction electron, and Δ_{SO} is the spin-orbit splitting of the valence band. Thus, the Elliott-Yafet spin relaxation (EYS) can be distinguished, being proportional to $1/\tau$, and thereby to the resistivity, in contrast to the DP spin scattering rate, Eq. (2.31), which is proportional to the conductivity. Since the EYS decays in proportion to the inverse of the band gap, it is negligible in large band gap semiconductors like Si and GaAs. The scattering rate $1/\tau$ is again the sum of the impurity scattering rate [Ell54], the electron-phonon scattering rate [Yaf63, GF97], and electron-electron interaction [Bog80], so that all these scattering processes result in EY spin relaxation. In degenerate semiconductors and in metals, the electron-electron scattering rate is given by the Fermi liquid inelastic electron scattering rate $1/\tau_{ee} \sim T^2/E_F$. The electron-phonon scattering time $1/\tau_{ep} \sim T^5$ decays faster with temperature. Thus, at low temperatures the Elliott-Yafet spin relaxation, Eq. (2.32), is dominated by elastic impurity scattering τ_0. In non-degenerate semiconductors, where the Fermi energy is below the conduction band edge, one finds $1/\tau_s \sim T^2/\tau(T)$.

2.4.4 Spin Relaxation due to Spin-Orbit Interaction with Impurities

The spin-orbit interaction, as defined in Eq. (2.6), arises whenever there is a gradient in an electrostatic potential. Thus, the impurity potential gives rise to the spin-orbit interaction

$$V_{\mathrm{SO}} = \frac{1}{2m^2c^2} \nabla V \times \mathbf{k}\ \mathbf{s}. \tag{2.33}$$

Perturbation theory yields then directly the corresponding spin relaxation rate

$$\frac{1}{\tau_s} = \pi \nu n_i \sum_{\alpha,\beta} \int \frac{\mathrm{d}\theta}{2\pi} (1 - \cos\theta) \mid V_{\mathrm{SO}}(\mathbf{k}, \mathbf{k}')_{\alpha\beta} \mid^2, \tag{2.34}$$

proportional to the concentration of impurities n_i. Here $\alpha, \beta = \pm$ denotes the spin indices. Since the spin-orbit interaction increases with the atomic number Z of the impurity element, this spin relaxation increases as Z^2, being stronger for heavier element impurities.

2.4.5 Bir-Aronov-Pikus Spin Relaxation

The exchange interaction J between electrons and holes in p-doped semiconductors results in spin relaxation, as well.[BAP76] Its strength is proportional to the density of holes p and depends on their itinerancy. If the holes are localized they act like magnetic impurities. If they are itinerant, the spin of the conduction electrons is transfered by the exchange interaction to the holes, where the spin-orbit splitting of the valence bands results in fast spin relaxation of the hole spin due to the Elliott-Yafet, or the D'yakonov-Perel' mechanism.

2.4.6 Magnetic Impurities

Magnetic impurities have a spin $\mathbf{S}$ which interacts with the spin of the conduction electrons by the exchange interaction J, resulting in a spatially and temporarily fluctuating local magnetic field

$$\mathbf{B}_{\mathrm{MI}}(\mathbf{r}) = -\sum_i J \delta(\mathbf{r} - \mathbf{R}_i) \mathbf{S}, \tag{2.35}$$

where the sum is over the position of the magnetic impurities $\mathbf{R}_i$. This gives rise to spin relaxation of the conduction electrons, with a rate given by

$$\frac{1}{\tau_{\mathrm{Ms}}} = 2\pi n_M \nu J^2 S(S+1), \tag{2.36}$$

where n_M is the density of magnetic impurities, and ν is the DOS at the Fermi energy. Here, S is the spin quantum number of the magnetic impurity, which can take the values $S = 1/2, 1, 3/2, 2 \ldots$. Antiferromagnetic exchange interaction between the magnetic impurity spin and the conduction electrons results in a competition between the conduction electrons to form a singlet with the impurity spin, which results in enhanced nonmagnetic and magnetic scattering. At low temperatures the magnetic impurity spin is screened by the conduction electrons resulting in a vanishing of the magnetic scattering rate. Thus, the spin scattering from magnetic impurities has a maximum at a temperature of the order of the Kondo temperature $T_K \sim E_F \exp(-1/\nu J)$[MACR06, MHEZ71, ZBvDA04]. In semiconductors T_K is exponentially small due to the small effective mass m_e (see Appendix A) and the resulting small DOS ν. Therefore, the magnetic moments remain free at the experimentally achievable temperatures. At large concentration of magnetic impurities, the RKKY-exchange interaction between the magnetic impurities quenches however the spin quantum dynamics, so that $S(S+1)$ is replaced by its classical value S^2. In Mn-p-doped GaAs, the exchange interaction between the Mn dopants and the holes can result in compensation of the hole spins and, therefore, a suppression of the Bir-Aronov-Pikus (BAP) spin relaxation[ADK$^+$08].

2.4.7 Nuclear Spins

Nuclear spins interact by the hyperfine interaction with conduction electrons. The hyperfine interaction between nuclear spins $\hat{\mathbf{I}}$ and the conduction electron spin, $\hat{s}$, results in a local Zeeman field given by [OW53]

$$\hat{\mathbf{B}}_N(\mathbf{r}) = -\frac{8\pi}{3}\frac{g_0\mu_B}{\gamma_g}\sum_n \gamma_n \hat{\mathbf{I}}\delta(\mathbf{r}-\mathbf{R}_n), \tag{2.37}$$

where γ_n is the gyromagnetic ratio of the nuclear spin. The spatial and temporal fluctuations of this hyperfine interaction field result in spin relaxation proportional to its variance, similar to the spin relaxation by magnetic impurities.

2.4.8 Magnetic Field Dependence of Spin Relaxation

The magnetic field changes the electron momentum due to the Lorentz force, resulting in a continuous change of the spin-orbit field, which similar to the momentum scattering results in motional narrowing and thereby a reduction of DP spin relaxation: [Ivc73, PT84, BB04],

$$\frac{1}{\tau_s} \sim \frac{\tau}{1+\omega_c^2\tau^2}. \tag{2.38}$$

Another source of a magnetic field dependence is the precession around the external magnetic field. In bulk semiconductors and for magnetic fields perpendicular to a quantum well, the orbital mechanism is dominating, however. This magnetic field dependence can be used to identify the spin relaxation mechanism, since the EYS does have only a weak magnetic field dependence due to the weak Pauli-paramagnetism.

In the next chapter, we will also analyze the effect of a Zeeman term on the crossover from weak localization to weak antilocalization. As we will see, this crossover can be controlled by spin relaxation rate.

Chapter 3

WL/WAL Crossover and Spin Relaxation in Confined Systems

3.1 Introduction

To build spin based devices which rely on coherent spin precession of conduction electrons[DD90, ZFD04], as presented in the introduction of this work, it has to be analyzed under which conditions, such as wire geometry, type and intensity of SOC, impurity density etc., spin relaxation rate can be minimized. We have shown in Sec. 2.4 that if electron momentum is randomized due to disorder, SO interaction is expected to result not only in a spin precession but in randomization of the electron spin with rate $1/\tau_s$.[DP72] In the following, we focus on the D'yakonov-Perel' spin relaxation mechanism.

3.1.1 One-Dimensional Wires

In one-dimensional wires, whose width W is of the order of the Fermi wave length λ_F, impurities can only reverse the momentum $p \rightarrow -p$. Therefore, the spin-orbit field can only change its sign, when a scattering from impurities occurs. $\mathbf{B}_{\text{SO}}(p) \rightarrow \mathbf{B}_{\text{SO}}(-p) = -\mathbf{B}_{\text{SO}}(p)$. Therefore, the precession axis and the amplitude of the spin-orbit field does not change, reversing only the spin precession, so that the D'yakonov-Perel'-spin relaxation is absent in one-dimensional wires[KK00, MFA02]. In an external magnetic field, the precession around the magnetic field axis, due to the Zeeman-interaction is competing with the spin-orbit field, however. Then, as the electrons are scattered from impurities, both the precession axis and the amplitude of the total precession field is changing, since

$$\mid \mathbf{B} + \mathbf{B}_{\text{SO}}(-\mathbf{p}) \mid = \mid \mathbf{B} - \mathbf{B}_{\text{SO}}(\mathbf{p}) \mid \neq \mid \mathbf{B} + \mathbf{B}_{\text{SO}}(\mathbf{p}) \mid,$$

resulting in spin dephasing and relaxation, as the sign of the momentum changes randomly.

3.1.2 Wires with $W > \lambda_F$

In this Chapter, we show, however, that the condition for a coherent spin precession is not only the 1d wire, $1/\tau_s$ is already strongly reduced in much wider wires: as soon as the wire width W is smaller than bulk spin precession length L_{SO}, which is the length on which the electron spin precesses a full cycle. This explains the reduction of the spin relaxation rate in quantum wires for widths exceeding both the elastic mean-free path l_e and λ_F, as observed with optical[HSM+06] as well as with WL measurements[DLS+05, LSK+07, SGP+06, WGZ+06, KKN09]. As an example we show two experiments in Fig. 3.1, where the significant dimensional reduction has been observed. Since L_{SO} can be several μm and is not changed significantly as the wire width W is reduced, such a reduction of spin relaxation can be very useful for applications: the spin of conduction electrons precesses coherently as it moves along the wire on length scale L_{SO}. It becomes randomized and relaxes on the longer length scale $L_s(W) = \sqrt{D_e \tau_s}$ only [$D_e = v_F l_e/2$ (v_F, Fermi velocity) is the 2D diffusion constant].

To understand the connection between the conductivity measurements and spin relaxation we recall that quantum interference of electrons in low-dimensional, disordered conductors is known to result in corrections to the electrical conductivity $\Delta\sigma$. This quantum correction, the WL effect, is a very sensitive tool to study dephasing and symmetry-breaking mechanisms in conductors.[AAKL82, Ber84, CS86] The entanglement of spin and charge by SO interaction reverses the effect of WL and thereby enhances the conductivity. This WAL effect was predicted by Hikami *et al.*[HLN80] for conductors with impurities of heavy elements. As conduction electrons scatter from such impurities, the SO interaction randomizes their spin. The resulting spin relaxation suppresses interference in spin triplet configurations. Since the time-reversal operation changes not only the sign of momentum but also the sign of the spin, the interference in singlet configuration remains unaffected. Since singlet interference reduces the electron's return probability, it enhances the conductivity, which is named the WAL effect. In weak magnetic fields, the singlet contributions are suppressed. Thereby, the conductivity is reduced and the magnetoconductivity becomes negative. The magnetoconductivity of wires is thus related to the magnitude of the spin relaxation rate. In Sec. 3.2, we first derive the quantum corrections to the conductivity for wires with general bulk SO interaction and relate it to the Cooperon propagator. In Sec. 3.3, we diagonalize the Cooperon for two-dimensional (2D) electron systems with Rashba SO interaction. We compare the spectrum of the triplet Cooperon with the one of the spin-diffusion equation. In Sec. 3.4, we present the solution of the Cooperon equation for a wire geometry. We review the solutions of the spin-diffusion equation in the wire geometry and compare the resulting spin relaxation rate with the one extracted from the Cooperon equation. Then we proceed to calculate the quantum corrections to the conductivity using the exact diagonalization of the Cooperon propagator. In the last part of this section, we consider two other kinds of boundary conditions. We calculate the spin relaxation rate in narrow wires with adiabatic boundaries, which arise in wires with smooth lateral confinement and regard also tubular wires. In Sec. 3.5, we study the influence of the Zeeman coupling to a magnetic field perpendicular to the quantum well in a system with sharp boundaries and analyze how the magnetoconductivity is modified. In Sec. 3.6, we draw the conclusions and compare with experimental results. In Appendix C.2, we give the derivation of the non-Abelian Neumann boundary conditions for the Cooperon propagator. In Appendix C.3, we show the connection between the effective vector potential $\mathbf{A_S}$ due to SO coupling and the spin relaxation tensor. In Appendix C.4, we give the exact quantum correction to the electrical conductivity in 2D. In Appendix C.5, we detail the diagonalization of the Cooperon propagator.

3.2 Quantum Transport Corrections

3.2.1 Diagrammatic Approach

As the temperature is lowered, we expect quantum mechanical coherence to be more important: The phase coherence length l_φ increases with decreasing temperature. If l_φ is much larger then the elastic scattering length but smaller then the sample size one would expect that all interference effects disappear due to self-averaging. However, it was found that one process seems to survive, as measurements show in logarithmically increasing resistance as temperature decreases, Fig. 3.2. In order to introduce the problem of dephasing and WL, we begin with a semiclassical picture of how an electron propagates from a point $\mathbf{r}$ to $\mathbf{r}'$: The corresponding probability amplitude P is given as the sum over

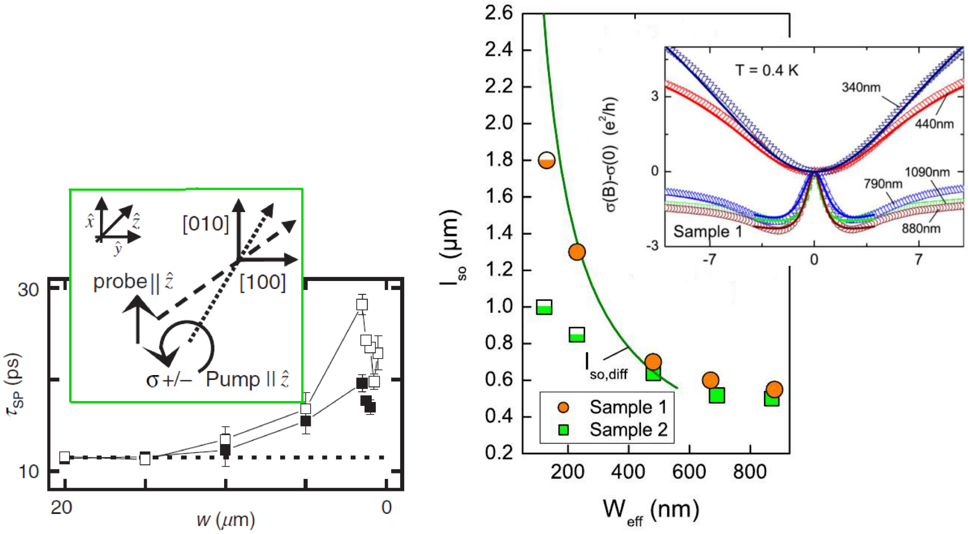

(a) (b)

Figure 3.1: Two different experimental approaches to extract the wire width dependence of spin relaxation rate. (a) Measurement by Kerr rotation (extracted from [HSM$^+$06]) and (b) using magnetoconductivity experiments (extracted from [LSK$^+$07]).

all classical paths α with their corresponding actions S_α

$$P(\mathbf{r},\mathbf{r}') \approx \sum_\alpha A_\alpha e^{iS_\alpha}. \tag{3.1}$$

It is intuitively clear that only this interference processes will survive self-averaging which are independent of the impurity position. Disadvantageous for conductivity is clearly, if an electron returns to the point he started from. This are paths where the relative phase is independent of the position of the impurities:

$$|P(\mathbf{r},\mathbf{r})|^2 \approx \sum_{\alpha,\beta} A_\alpha A_\beta e^{i(S_\alpha - S_\beta)}. \tag{3.2}$$

There are two possibilities, which cancel the phase factor: The first one is pure classic, namely representing a scattering that causes the electron to traverse the way α backwards. The reason for the second one is with the time-reversal-symmetry of the system, which allows to be β the time-reversed path of α, more specific

$$\begin{aligned} |P(\mathbf{r},\mathbf{r})|^2 &\approx \sum_\alpha \langle |A_\alpha^{\circlearrowright}|^2 + |A_\alpha^{\circlearrowleft}|^2\rangle + 2\Re \sum_\alpha \langle A_\alpha^{\circlearrowright} A_\alpha^{\circlearrowleft *}\rangle & (3.3)\\ &= |P_{\text{class}}(\mathbf{r},\mathbf{r})|^2 + |P_{\text{WL}}(\mathbf{r},\mathbf{r})|^2. & (3.4) \end{aligned}$$

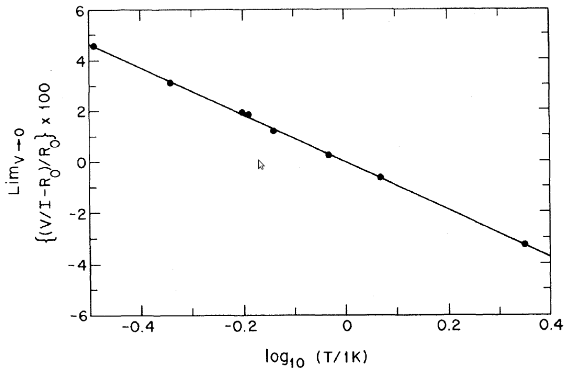

Figure 3.2: Measured WL corrections on a thin PdAu film, Ref. [DO79]. The resistivity increases logarithmically as the temperature decreases.

Summing over all possible paths will generally yield only the classical and the pure quantum-mechanical term. Other path have in general a large phase difference and will average out. Thus, the quantum-mechanical return-probability is twice the classical one. This effect is called WL. This effect can be destroyed if we think about the Aharonov-Bohm-Effect[AB59]: Switching on a magnetic field, Fig. (3.3), we can add an additional phase to the propagating electron which destroys the constructive interference, leading to an enhanced conductivity,

$$|P(r,r)|^2 \approx \sum_\alpha \langle (A_\alpha^{\circlearrowright} e^{i2\pi\varphi} + A_\alpha^{\circlearrowleft} e^{-i2\pi\varphi})(A_\alpha^{\circlearrowright *} e^{-i2\pi\varphi} + A_\alpha^{\circlearrowleft *} e^{i2\pi\varphi})\rangle \tag{3.5}$$

$$= \sum_\alpha \langle 2|A_\alpha^{\circlearrowright}|^2 (1+\cos(4\pi\varphi))\rangle \tag{3.6}$$

$$\text{with } \varphi = \phi/\phi_0, \phi_0 = \frac{h}{e}.$$

Because of $\langle (1+\cos(4\pi\varphi))\rangle = 1$ we have no quantum corrections on average in this case. The quantum correction to the conductivity appears therefore in the difference between the classical diffusion with the corresponding propagator (Diffuson) and the propagation which includes quantum interference between two possibilities for a particle to traverse a closed loop in opposite -time reversed- directions described by the Cooperon. To calculate this quantum correction at zero frequency ω, one applies Kubo formula (Appendix B.1) which yields

$$\sigma_{xx}(\omega=0) \equiv \sigma = \frac{e^2}{m_e^2}\frac{2\pi}{\mathrm{Vol}}\int_0^\infty \mathrm{d}E \left(-\frac{\partial f(E)}{\partial E}\right) \langle \mathrm{Tr}[\delta(E-H_0)p_x\delta(E-H_0)p_x]\rangle_{\mathrm{imp}}. \tag{3.7}$$

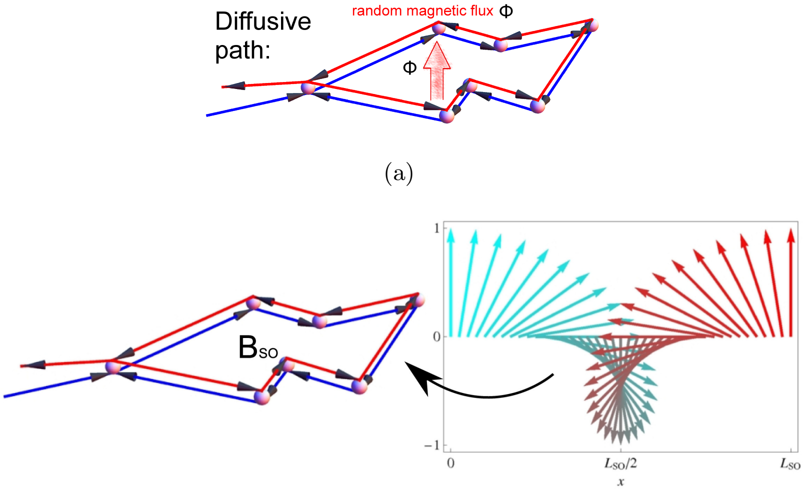

(a)

(b)

Figure 3.3: Exemplification of the second term in Eq. (3.4): Interference of electrons traveling in the opposite direction along the same path causes an enhanced backscattering, the WL effect. (a) Closed electron paths enclose a magnetic flux from an external magnetic field, indicated as the red arrow, breaking time reversal symmetry, breaking constructive interference. (b) The entanglement of spin and charge by SO interaction causes the spin to precess inbetween two scatterers around an axis which changes with the momentum vector of the itinerant electron. This effective field can cause WAL.

With the definition

$$G_E^{R/A}(\mathbf{p}',\mathbf{p}) = \left\langle \mathbf{p}' \left| \frac{1}{E-(H_0+V)\mp i\eta} \right| \mathbf{p} \right\rangle, \tag{3.8}$$

the conductivity can be rewritten to the following form

$$\sigma = \frac{e^2}{\pi m_e^2 \mathrm{Vol}} \sum_{\mathbf{p},\mathbf{p}'} p_x p_x' \times \langle G^R(\mathbf{p},\mathbf{p}') G^A(\mathbf{p}',\mathbf{p}) \rangle_{\text{imp}}, \tag{3.9}$$

with the propagator of density

$$\Gamma(\mathbf{p},\mathbf{p}') = \langle G^R(\mathbf{p},\mathbf{p}') G^A(\mathbf{p}',\mathbf{p}) \rangle_{\text{imp}}, \tag{3.10}$$

where impurity averaging products of Green's functions of the type $\langle G^R G^R \rangle$ and $\langle G^A G^A \rangle$ yield small corrections of order $1/E_F\tau$ and will be neglected (Appendix B.1).

The first approximation one can apply is to assume

$$\langle G^R(\mathbf{p},\mathbf{p}') G^A(\mathbf{p}',\mathbf{p}) \rangle_{\text{imp}} \approx \langle G^R(\mathbf{p}) \rangle_{\text{imp}} \langle G^A(\mathbf{p}) \rangle_{\text{imp}}, \tag{3.11}$$

where we used the definition $G^{R/A}(\mathbf{p}) \equiv G^{R/A}(\mathbf{p},\mathbf{p}')\delta_{\mathbf{p},\mathbf{p}'}$. The average over impurities can be depicted diagrammatically,

$$\langle G \rangle_{\text{imp}} =$$

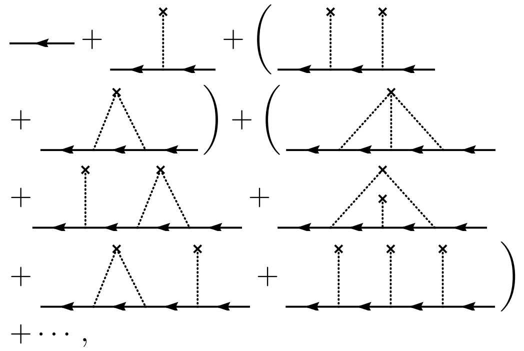

(3.12)

where the fermion line $\longleftarrow$ denotes the unperturbed Green's function. For uncorrelated disorder potential, $\langle V(\mathbf{x})V(\mathbf{x}')\rangle = \delta(\mathbf{x}-\mathbf{x}')/2\pi\nu\tau$, as we will use in the following, we perform the disorder average in first-order Born approximation and get

$$\mathcal{G}^R_E(\mathbf{p}) = \longrightarrow = \frac{1}{E - H_0(\mathbf{p}) + i\frac{1}{2\tau}}, \tag{3.13}$$

where $\mathcal{G}^A_E(\mathbf{p})$ is its complex conjugate, respectively. H_0 is the Hamiltonian without disorder potential V. The impurity vertex (the cross) is given by $1/2\pi\nu\tau$. Until now we have the same information in the scattering time τ as we would gain from the Drude formula. Assuming low temperature, we can simplify Eq. (3.9) to

$$\sigma = \frac{e^2}{\pi m_e^2 \mathrm{Vol}} \sum_{\mathbf{p}} p_x^2 \times \langle G^R(\mathbf{p})\rangle_{\text{imp}} \langle G^A(\mathbf{p})\rangle_{\text{imp}} \tag{3.14}$$

$$= \frac{e^2}{\pi m_e^2 \mathrm{Vol}} \sum_{\mathbf{p}} p_x^2 \times \mathcal{G}^R(\mathbf{p})\mathcal{G}^A(\mathbf{p}) \tag{3.15}$$

$$= \frac{e^2}{\pi m_e^2 \mathrm{Vol}} \sum_{\mathbf{p}} \frac{p_x^2}{(E_F - E_{\mathbf{p}})^2 + \left(\frac{1}{2\tau}\right)^2} \tag{3.16}$$

which can be simplified in the metallic regime, $E_F \gg 1/\tau$, where the dominant contribution is given by energies close to E_F, to

$$\approx \frac{e^2}{\pi m_e^2 \mathrm{Vol}} \int_0^\infty \mathrm{d}E \, (\mathrm{Vol}\,\rho(E)) \left(\frac{E2m_e}{d}\right) \frac{1}{(E_F - E)^2 + \left(\frac{1}{2\tau}\right)^2} \tag{3.17}$$

$$\approx 2\frac{e^2}{m_e}\rho(E_F)E_F\frac{1}{d}\int_\infty^\infty \mathrm{d}E \, \frac{1}{(E_F - E)^2 + \left(\frac{1}{2\tau}\right)^2} \tag{3.18}$$

$$= \frac{e^2 n\tau}{m_e}, \tag{3.19}$$

where d is the dimension. To get the quantum corrections to the Drude conductivity, we have to include the additional contribution by considering the connection of $\mathcal{G}^R$ and $\mathcal{G}^A$ due to the impurity potential V:

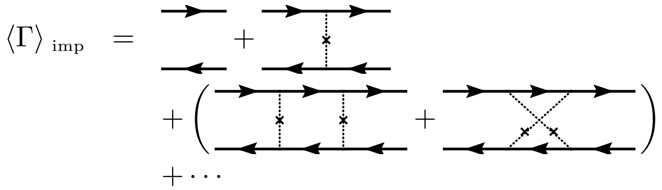

(3.20)

This sum can be separated into uncrossed and crossed diagrams. As known from standard literature both can be calculated in an analog way. Summing up only ladder diagrams will lead to the Diffuson $\hat{D}$

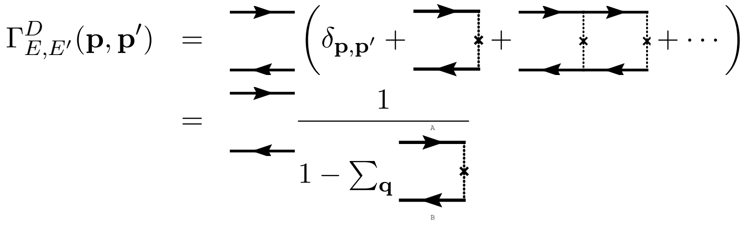

(3.21)

$$= \mathcal{G}^R_E(\mathbf{p})\mathcal{G}^A_{E'}(\mathbf{p}')\frac{1}{\tau}\hat{D}_{E,E'}(\mathbf{p},\mathbf{p}'), \tag{3.22}$$

It is important to notice that each ladder diagram is of the same order as the Drude diagram[1]. In contrast to this classical contribution, the diagrams where the impurity lines, which connect the advanced and retarded lines, cross are smaller by the factor $1/(p_F l)$ (see e.g. Ref. [Ram82]). Eq. (3.22) can be solved easily for $\hat{D}$ if we expand the Diffuson in $(E' - E)$ and $(\mathbf{p}' - \mathbf{p})$ (the pole stems from particle conservation):

$$\hat{D}_{E,E'}(\mathbf{p},\mathbf{p}') = \frac{1}{i(E-E') + D_e(\mathbf{p}'-\mathbf{p})^2}, \tag{3.23}$$

with the diffusion constant $D_e = v_F^2\tau/d$. If $\Re\sigma_{xx}$ is now calculated not only by using the bubble diagram, we end up with a correction of the momentum relaxation time τ in Eq. (3.19) being replaced by the transport time

$$\tau_0 \sim \int \mathrm{d}p_F \, |V(\mathbf{p_F} - \mathbf{p'_F})|^2 (1 - \mathbf{p_F}\cdot\mathbf{p'_F}). \tag{3.24}$$

However, we are interested in the calculation which goes beyond this class of diagrams. Time-reversal symmetry helps to sum up the group of crossed diagrams via unknotting

---

[1] bubble diagram

them:

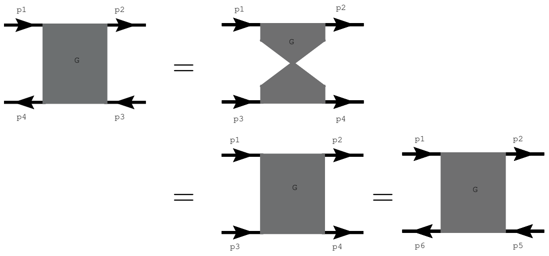

(3.25)

(3.26)

Exploiting Eq. (3.25) makes the calculation of the maximally crossed diagrams easier:

$$\Gamma^{C}_{E,E'}(\mathbf{p},\mathbf{p}') =$$

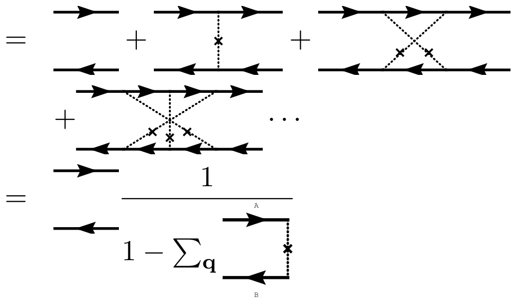

(3.27)

(3.28)

$$= \mathcal{G}^{R}_{E}(\mathbf{p})\mathcal{G}^{A}_{E'}(\mathbf{p}')\frac{1}{\tau}\hat{C}_{E,E'}(\mathbf{p},\mathbf{p}'), \tag{3.29}$$

with the Cooperon[2] propagator $\hat{C}$ for $E_F\tau \gg 1$ (E_F, Fermi energy) given by

$$\hat{C}_{\omega=E-E'}(\mathbf{Q}=\mathbf{p}+\mathbf{p}') = \tau\left(1-\sum_{\mathbf{q}}\qquad\right)^{-1}. \tag{3.30}$$

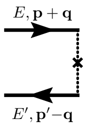

In contrast to the Diffuson, the infrared divergence is now at $\mathbf{p} = -\mathbf{p}'$, i.e. the correction to the conductivity for $\omega = 0$,

$$\Delta\sigma = 2\frac{e^2}{\pi}\frac{1}{m^2}\sum_{\mathbf{p},Q}(-p_x^2)\mathcal{G}^{R}(\mathbf{p})\mathcal{G}^{A}(\mathbf{p})\mathcal{G}^{R}(\mathbf{Q}-\mathbf{p})\mathcal{G}^{A}(\mathbf{Q}-\mathbf{p})\frac{1}{\tau}\hat{C}_{\omega=0}(\mathbf{Q}) \tag{3.31}$$

is due to the factor $(-p_x^2)$, in the case without magnetic field and SOC, negative. The divergent nature explains post hoc the choice of the maximally crossed diagrams.

Notice that one obtains the Cooperon using time-reversal symmetry from the Diffuson. We will use this later to map the Cooperon equation onto the spin diffusion equation.

---

[2] The name stems from the singularity at total momentum being zero, as in the case of a Cooper pair where the consequence is superconductivity.

3.2.2 Weak Localization in Quantum Wires

If the host lattice of the electrons provides SO interaction, quantum corrections to the conductivity have to be calculated in the basis of eigenstates of the Hamiltonian with SO interaction

$$H = \frac{1}{2m_e}(\mathbf{p} + e\mathbf{A})^2 + V(\mathbf{x}) - \frac{1}{2}\gamma_g \boldsymbol{\sigma}\left(\mathbf{B} + \mathbf{B}_{\text{SO}}(\mathbf{p})\right), \tag{3.32}$$

where m_e is the effective electron mass (see Appendix A for examples in semiconductors). $\mathbf{A}$ is the vector potential due to the external magnetic field $\mathbf{B}$. $\mathbf{B}_{\text{SO}}^T = (B_{\text{SO}x}, B_{\text{SO}y})$ is the momentum dependent SO field. $\boldsymbol{\sigma}$ is a vector, with components $\boldsymbol{\sigma}_i$, $i = x, y, z$, the Pauli matrices, γ_g is the gyromagnetic ratio with $\gamma_g = g\mu_{\text{B}}$ with the effective g factor of the material, and $\mu_{\text{B}} = e/2m_e$ is the Bohr magneton constant. In Sec. 2.3.3 we presented the dominant SO interactions in semiconductors: For example, the breaking of inversion symmetry in III-V semiconductors causes a SO coupling, which for quantum wells grown in the [001] direction is given by [Dre55]

$$-\frac{1}{2}\gamma_g \mathbf{B}_{\text{SO,D}} = \alpha_1(-\hat{e}_x p_x + \hat{e}_y p_y) + \gamma_D(\hat{e}_x p_x p_y^2 - \hat{e}_y p_y p_x^2). \tag{3.33}$$

Here, $\alpha_1 = \gamma_D \langle p_z^2 \rangle$ is the linear Dresselhaus parameter, which measures the strength of the term linear in momenta p_x, p_y in the plane of the 2DES. When $\langle p_z^2 \rangle \sim 1/a_z^2 \geq k_F^2$ (a_z is the thickness of the 2DES and k_F is the Fermi wavenumber), that term exceeds the cubic Dresselhaus terms which have coupling strength γ_D. Asymmetric confinement of the 2DES yields the Rashba term which does not depend on the growth direction

$$-\frac{1}{2}\gamma_g \mathbf{B}_{\text{SO,R}} = \alpha_2(\hat{e}_x p_y - \hat{e}_y p_x), \tag{3.34}$$

with α_2 the Rashba parameter.[BR84, Ras60] We consider the standard white-noise model for the impurity potential, $V(\mathbf{x})$, which vanishes on average $\langle V(\mathbf{x}) \rangle = 0$, is uncorrelated, $\langle V(\mathbf{x})V(\mathbf{x}') \rangle = \delta(\mathbf{x} - \mathbf{x}')/2\pi\nu\tau$, and weak, $E_F\tau \gg 1$. Going to momentum ($\mathbf{Q}$) and frequency (ω) representation, and proceeding as presented Sec. 3.2.1 but now taking into account the spin degree of freedom for a two electron interference, we yield the quantum correction to the static conductivity as [HLN80]

$$\Delta\sigma = -2\frac{e^2}{2\pi}\frac{D_e}{\text{Vol}} \sum_{\mathbf{Q}} \sum_{\alpha,\beta=\pm} C_{\alpha\beta\beta\alpha,\omega=0}(\mathbf{Q}), \tag{3.35}$$

where $\alpha, \beta = \pm$ are the spin indices, and the Cooperon propagator $\hat{C}$ is for $E_F\tau \gg 1$ (E_F, Fermi energy), given by Eq. (3.30). The summation over the spins is described in more detail in Appendix C.1. Thus, the problem reduces to the calculation in presence of SOC of the correlation function

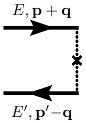

$$\sum_{\mathbf{q}} \quad = \frac{1}{2\pi\nu\tau} \sum_{\mathbf{q}} \mathcal{G}^{R}_{E,\sigma}(\mathbf{p}+\mathbf{q}) \mathcal{G}^{A}_{E',\sigma'}(\mathbf{p}'-\mathbf{q}), \tag{3.36}$$

which simplifies for weak disorder $\epsilon_F \tau \gg 1$ to

$$\approx \int \frac{\mathrm{d}\Omega}{2\pi} \frac{1}{1 - i\tau\hat{\Sigma}}, \tag{3.37}$$

where

$$\hat{\Sigma} = \epsilon_{\mathbf{p}'+\mathbf{q},\boldsymbol{\sigma}'} - \epsilon_{\mathbf{p}-\mathbf{q},\boldsymbol{\sigma}}. \tag{3.38}$$

For diffusive wires, for which the elastic mean-free path l_e is smaller than the wire width W, the integral is over all angles of velocity $\mathbf{v}$ on the Fermi surface. Using

$$\begin{aligned}
\epsilon_{\mathbf{p}} &= \frac{(\mathbf{p}+e\mathbf{A})^2}{2m_e} - \frac{1}{2}\gamma_g \boldsymbol{\sigma}(\mathbf{B} + \mathbf{B}_{\,\mathrm{SO}}(\mathbf{p})), \\
\mathbf{v} &= \frac{\mathbf{p} - \mathbf{q} + e\mathbf{A}}{m_e}, \\
\mathbf{S} &= \frac{1}{2}(\boldsymbol{\sigma} + \boldsymbol{\sigma}'), \\
\mathbf{Q} &= \mathbf{p} + \mathbf{p}',
\end{aligned}$$

we obtain to lowest order in $\mathbf{Q}$,

$$\hat{\Sigma} = -\mathbf{v}(\mathbf{Q} + 2e\mathbf{A} + 2m_e \hat{a}\mathbf{S}) + (\mathbf{Q} + 2e\mathbf{A})\hat{a}\boldsymbol{\sigma}' + \frac{1}{2}\gamma_g(\boldsymbol{\sigma}' - \boldsymbol{\sigma})\mathbf{B}. \tag{3.39}$$

Here, the SO couplings are combined in the matrix

$$\hat{a} = \begin{pmatrix} -\alpha_1 + \gamma_D k_y^2 & -\alpha_2 \\ \alpha_2 & \alpha_1 - \gamma_D k_x^2 \end{pmatrix}. \tag{3.40}$$

Thus, the Cooperon becomes

$$\hat{C}(\mathbf{Q})^{-1} = \frac{1}{\tau}\left(1 - \int \frac{\mathrm{d}\Omega}{2\pi} \frac{1}{1 + i\tau(\mathbf{v}(\mathbf{Q} + 2e\mathbf{A} + 2m_e\hat{a}\mathbf{S}) + H_{\sigma'} + H_Z)}\right), \tag{3.41}$$

where $H_{\sigma'} = -(\mathbf{Q} + 2e\mathbf{A})\hat{a}\boldsymbol{\sigma}'$ and the Zeeman coupling to the external magnetic field yields

$$H_Z = -\frac{1}{2}\gamma_g(\boldsymbol{\sigma}' - \boldsymbol{\sigma})\mathbf{B}. \tag{3.42}$$

It follows that for weak disorder and without Zeeman coupling, the Cooperon depends only on the total momentum $\mathbf{Q}$ and the total spin $\mathbf{S}$. Expanding the Cooperon to second order in $(\mathbf{Q}+2e\mathbf{A}+2m_e\hat{a}\mathbf{S})$ and performing the angular integral which is for 2D diffusion (elastic mean-free path l_e smaller than wire width W) continuous from 0 to 2π and yields

$$\hat{C}(\mathbf{Q}) = \frac{1}{D_e(\mathbf{Q}+2e\mathbf{A}+2e\mathbf{A_S})^2 + H_{\gamma_D}}. \tag{3.43}$$

The effective vector potential due to SO interaction, $\mathbf{A_S} = m_e\hat{\alpha}\mathbf{S}/e$ (where $\hat{\alpha} = \langle\hat{a}\rangle$ denotes the matrix Eq. (3.40), as averaged over angle), couples to total spin vector $\mathbf{S}$ whose components are four by four matrices. The cubic Dresselhaus coupling is found to reduce the effect of the linear one to

$$\tilde{\alpha}_1 := \alpha_1 - m_e\gamma_D E_F/2. \tag{3.44}$$

Furthermore, it gives rise to the spin relaxation term in Eq. (3.43),

$$H_{\gamma_D} = D_e(m_e^2 E_F \gamma_D)^2 (S_x^2 + S_y^2). \tag{3.45}$$

In the representation of the singlet, $|\rightleftarrows\rangle$ and triplet states $|\rightrightarrows\rangle, |\upuparrows\rangle, |\downdownarrows\rangle$ (Tab. 3.1), $\hat{C}$ de-

state	(index: electron-number)	m_s	S
$\|\rightleftarrows\rangle :=$	$\frac{1}{\sqrt{2}}(\|\uparrow\rangle_1\|\downarrow\rangle_2 - \|\uparrow\rangle_2\|\downarrow\rangle_1)$	0	0
$\|\upuparrows\rangle :=$	$\|\uparrow\rangle_1\|\uparrow\rangle_2$	1	1
$\|\rightrightarrows\rangle :=$	$\frac{1}{\sqrt{2}}(\|\uparrow\rangle_1\|\downarrow\rangle_2 + \|\uparrow\rangle_2\|\downarrow\rangle_1)$	0	1
$\|\downdownarrows\rangle :=$	$\|\downarrow\rangle_1\|\downarrow\rangle_2$	−1	1

Table 3.1: Singlet and triplet states

couples into a singlet and a triplet sector. Thus, the quantum conductivity is a sum of singlet and triplet terms

$$\Delta\sigma = -2\frac{e^2}{2\pi}\frac{D_e}{\mathrm{Vol}}\sum_{\mathbf{Q}}\left(\underbrace{-\frac{1}{D_e(\mathbf{Q}+2e\mathbf{A})^2}}_{\text{singlet contribution}} + \underbrace{\sum_{m=0,\pm1}\left\langle S=1,m\middle|\hat{C}(\mathbf{Q})\middle|S=1,m\right\rangle}_{\text{triplet contribution}}\right). \tag{3.46}$$

With the cutoffs due to dephasing $1/\tau_\varphi$ and elastic scattering $1/\tau$, we can integrate over all possible wave vectors $\mathbf{Q}$ in the 2D case analytically (Appendix C.4).

In 2D, one can treat the magnetic field nonperturbatively using the basis of Landau bands.-[HLN80, KSZ+96, MZM+03, AF01, LG98, Gol05] In wires with widths smaller than cyclotron length $k_F l_B^2$ (l_B, the magnetic length, defined by $Bl_B^2 = 1/e$), the Landau basis is not suitable. There is another way to treat magnetic fields: quantum corrections are due to the interference between closed time-reversed paths. In magnetic fields, the electrons acquire a magnetic phase, which breaks time-reversal invariance. Averaging over all closed paths, one obtains a rate with which the magnetic field breaks the time-reversal invariance, $1/\tau_B$. Like the dephasing rate $1/\tau_\varphi$, it cuts off the divergence arising from quantum corrections with small wave vectors $\mathbf{Q}^2 < 1/D_e\tau_B$. In 2D systems, τ_B is the time an electron diffuses along a closed path enclosing one magnetic flux quantum, $D_e\tau_B = l_B^2$. In wires of finite width W the area which the electron path encloses in a time τ_B is $W\sqrt{D_e\tau_B}$. Requiring that this encloses one flux quantum gives $1/\tau_B = D_e e^2 W^2 B^2/3$. For arbitrary magnetic field, the relation

$$\frac{1}{\tau_B} = D_e(2e)^2 B^2 \langle y^2 \rangle, \tag{3.47}$$

with the expectation value of the square of the transverse position $\langle y^2\rangle$, yields $1/\tau_B = \left(1 - 1/(1 + W^2/3l_B^2)\right) D_e/l_B^2$. Thus, it is sufficient to diagonalize the Cooperon propagator as given by Eq. (3.43) without magnetic field, as we will do in the next chapters, and to add the magnetic rate $1/\tau_B$ together with dephasing rate $1/\tau_\varphi$ to the denominator of $\hat{C}(\mathbf{Q})$ when calculating the conductivity correction, Eq. (3.46).

3.3 The Cooperon and Spin Diffusion in 2D

The Cooperon can be diagonalized analytically in 2D for pure Rashba coupling, $\alpha_1 = 0, \gamma_D = 0$. For this case, we define the Cooperon Hamilton operator as

$$H_c := \frac{\hat{C}^{-1}}{D_e} = \mathbf{Q}^2 + 2Q_{\text{SO}}(Q_y S_x - Q_x S_y) + Q_{\text{SO}}^2(S_y^2 + S_x^2), \tag{3.48}$$

with $Q_{\text{SO}} = 2m_e\alpha_2 = 2\pi/L_{\text{SO}}$, where L_{SO} is the spin precession length. In the representation of the singlet $|\rightleftarrows\rangle$ and triplet modes, $\{|\upuparrows\rangle, |\rightrightarrows\rangle, |\downdownarrows\rangle\}$ it becomes

$$H_c = \begin{pmatrix} \mathbf{Q}^2 & 0 & 0 & 0 \\ 0 & Q_{\text{SO}}^2 + \mathbf{Q}^2 & \sqrt{2}Q_{\text{SO}}Q_+ & 0 \\ 0 & \sqrt{2}Q_{\text{SO}}Q_- & 2Q_{\text{SO}}^2 + \mathbf{Q}^2 & \sqrt{2}Q_{\text{SO}}Q_+ \\ 0 & 0 & \sqrt{2}Q_{\text{SO}}Q_- & Q_{\text{SO}}^2 + \mathbf{Q}^2 \end{pmatrix}, \tag{3.49}$$

with $Q_\pm = Q_y \pm iQ_x$. Diagonalization yields the gapless singlet eigenvalues and the three triplet Cooperon eigenvalues with a gap due to the SO coupling (see Fig. 3.4),

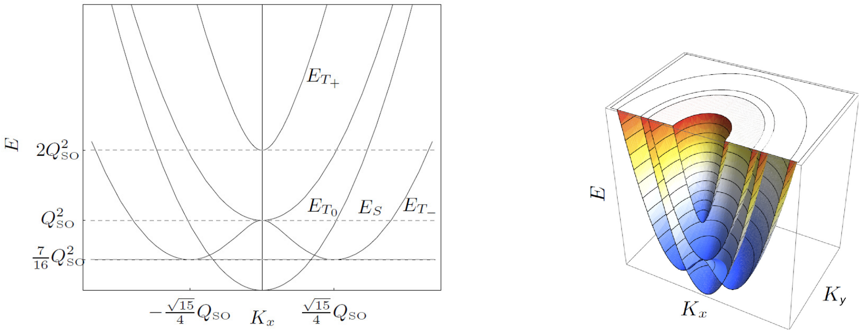

(a) (b)

Figure 3.4: 2D spectrum of H_c, $K_i = Q_i/Q_{\text{SO}}$. The physical meaning of the gaps in the triplet modes is more comprehensible if H_c is related to spin diffusion, where the gaps appear as spin relaxation rates.

$$E_S(Q)/D_e = \mathbf{Q}^2, \tag{3.50}$$

$$E_{T_0}(Q)/D_e = \mathbf{Q}^2 + Q^2_{\text{SO}}, \tag{3.51}$$

$$E_{T_\pm}(Q)/D_e = \mathbf{Q}^2 + \frac{3}{2}Q^2_{\text{SO}} \pm \frac{Q^2_{\text{SO}}}{2}\sqrt{1 + 16\frac{\mathbf{Q}^2}{Q^2_{\text{SO}}}}, \tag{3.52}$$

where E_S denotes the singlet eigenvalue and $E_{T_0}, E_{T_\pm}$ the three triplet eigenvalues. Notice that the two minima of the lowest triplet eigenmode are shifted to $Q = \pm(\sqrt{15}/4)Q_{\text{SO}}$ with a minimal eigenvalue of $E/D_e = (7/16)Q^2_{\text{SO}}$. As we show in the following, this gap in the triplet modes is directly related to the D'yakonov-Perel' spin relaxation rate $1/\tau_s$.

Spin Diffusion

We can get a better understanding of the spin relaxation induced by the SO coupling and impurity scattering by considering directly the spin-diffusion equation for the expectation value of the electron-spin vector [MC00]

$$\mathbf{s}(\mathbf{r},t) = \frac{1}{2}\langle \psi^\dagger(\mathbf{r},t)\boldsymbol{\sigma}\psi(\mathbf{r},t)\rangle, \tag{3.53}$$

where $\psi^\dagger = (\psi_+^\dagger, \psi_-^\dagger)$ is the two-component vector of the up (+), and down (-) spin fermionic creation operators and ψ the two-component vector of annihilation operators, respectively. In the presence of SO coupling, the spin-diffusion equation becomes for $v_F \mid \nabla_{\mathbf{r}}\mathbf{s} \mid \ll 1/\tau$,

$$0 = \partial_t \mathbf{s} + \frac{1}{\hat{\tau}_s}\mathbf{s} - D_e\nabla^2\mathbf{s} + \gamma_g(\mathbf{B} - 2\tau\langle(\nabla\mathbf{v}_F)\mathbf{B}_{\,\mathrm{SO}}(\mathbf{p})\rangle) \times \mathbf{s} \tag{3.54}$$

and we define accordingly the spin-diffusion Hamiltonian $H_{\,\mathrm{SD}}$

$$0 = \partial_t \mathbf{s} + D_e H_{\,\mathrm{SD}}\mathbf{s}, \tag{3.55}$$

where the matrix elements of the spin relaxation terms are given by [DP71b, DP71c] (Appendix C.3)

$$\frac{1}{(\hat{\tau}_s)_{ij}} = \tau\gamma_g^2\left(\langle \mathbf{B}_{\,\mathrm{SO}}(\mathbf{k})^2\rangle\delta_{ij} - \langle B_{\,\mathrm{SO}}(\mathbf{k})_i B_{\,\mathrm{SO}}(\mathbf{k})_j\rangle\right). \tag{3.56}$$

For pure Rashba SO interaction, the spin-diffusion operator $H_{\,\mathrm{SD}}$ is in momentum representation[SDGR06]

$$H_{\,\mathrm{SD}} = \begin{pmatrix} \frac{1}{D_e\tau_s} + \mathbf{k}^2 & 0 & -i2Q_{\,\mathrm{SO}}k_x \\ 0 & \frac{1}{D_e\tau_s} + \mathbf{k}^2 & -i2Q_{\,\mathrm{SO}}k_y \\ i2Q_{\,\mathrm{SO}}k_x & i2Q_{\,\mathrm{SO}}k_y & \frac{2}{D_e\tau_s} + \mathbf{k}^2 \end{pmatrix}, \tag{3.57}$$

with $1/D_e\tau_s = Q_{\,\mathrm{SO}}^2$. In the 2D case, diagonalization yields the eigenvalues

$$E_0(k) = \mathbf{k}^2 + \frac{1}{D_e\tau_s}, \tag{3.58}$$

$$E_\pm(k) = \mathbf{k}^2 + \frac{3}{2}\frac{1}{D_e\tau_s} \pm \frac{1}{2D_e\tau_s}\sqrt{1 + 16\frac{\mathbf{k}^2}{Q_{\,\mathrm{SO}}^2}}. \tag{3.59}$$

Thus, we find that the spectrum of the spin-diffusion operator and the one of the triplet Cooperon Hamiltonian are identical in 2D (Ref. [MCW97]) as long as time-reversal symmetry is not broken. This confirms that antilocalization in the presence of SO interaction, which has its cause in the suppression of the triplet modes in Eq. (3.46), is indeed a direct measure of the spin relaxation. Mathematically, there exists a unitary transformation

$$H_c = U_{\mathrm{CD}} H_{\mathrm{SD}} U^{\dagger}_{\mathrm{CD}}, \tag{3.60}$$

$$U_{\mathrm{CD}} = \begin{pmatrix} -\frac{1}{\sqrt{2}} & \frac{i}{\sqrt{2}} & 0 \\ 0 & 0 & 1 \\ \frac{1}{\sqrt{2}} & \frac{i}{\sqrt{2}} & 0 \end{pmatrix}, \tag{3.61}$$

with the according transformation between spin-density components s_i and the triplet components of the Cooperon density $\tilde{s}$,

$$\frac{1}{\sqrt{2}}(-s_x + i s_y) = \tilde{s}_{\uparrow\uparrow}, \tag{3.62}$$

$$s_z = \tilde{s}_{\rightrightarrows}, \tag{3.63}$$

$$\frac{1}{\sqrt{2}}(s_x + i s_y) = \tilde{s}_{\downarrow\downarrow}. \tag{3.64}$$

This is a consequence of the fact that the four-component vector of charge density $\rho = (\rho_+ + \rho_-)/2$ and spin-density vector $\mathbf{S}$ are related to the density vector $\hat{\rho}$ with the four components $\langle \psi^{\dagger}_{\alpha} \psi_{\beta} \rangle / \sqrt{2}$, where $\alpha, \beta = \pm$, by a unitary transformation.

Relation to the Diffuson

The classical evolution of the four-component density vector $\hat{\rho}$ is by definition governed by the diffusion operator, the Diffuson. The Diffuson is related to the Cooperon in momentum space by substituting $\mathbf{Q} \to \mathbf{p} - \mathbf{p}'$ and the sum of the spins of the retarded and advanced parts, $\boldsymbol{\sigma}$ and $\boldsymbol{\sigma}'$, by their difference. Using this substitution, Eq. (3.48) leads thus to the inverse of the Diffuson propagator

$$H_d := \frac{\hat{D}^{-1}}{D_e} = \mathbf{Q}^2 + 2Q_{\mathrm{SO}}(Q_y \widetilde{S}_x - Q_x \widetilde{S}_y) + Q^2_{\mathrm{SO}}(\widetilde{S}^2_y + \widetilde{S}^2_x), \tag{3.65}$$

with $\widetilde{\mathbf{S}} = (\boldsymbol{\sigma}' - \boldsymbol{\sigma})/2$, which has the same spectrum as the Cooperon, as long as the time-reversal symmetry is not broken. In the representation of singlet and triplet modes, the diffusion Hamiltonian becomes

$$H_d = \begin{pmatrix} 2Q^2_{\mathrm{SO}} + \mathbf{Q}^2 & \sqrt{2}Q_{\mathrm{SO}}Q_- & 0 & -\sqrt{2}Q_{\mathrm{SO}}Q_+ \\ \sqrt{2}Q_{\mathrm{SO}}Q_+ & Q^2_{\mathrm{SO}} + \mathbf{Q}^2 & 0 & 0 \\ 0 & 0 & \mathbf{Q}^2 & 0 \\ -\sqrt{2}Q_{\mathrm{SO}}Q_- & 0 & 0 & Q^2_{\mathrm{SO}} + \mathbf{Q}^2 \end{pmatrix}. \tag{3.66}$$

Comparing Eqs. (3.49) and Eq. (3.66), we see that diagonalization leads to Eqs. (3.50)-(3.52).

Influence of Dresselhaus SOC

It can be seen from Eqs. (3.58) and (3.59) that in the case of a homogeneous Rashba field, the spin-density has a finite decay rate as we pointed out in Sec. 2.3.4. However, if we go beyond the pure Rashba system and include a linear Dresselhaus coupling, the first term in Eq. (3.33), we can find spin states which do not relax and are thus persistent. The spin relaxation tensor, Eq. (3.56), acquires nondiagonal elements and changes to

$$\frac{1}{\hat{\tau}_s}(k_F) = 4\tau k_F^2 \begin{pmatrix} \frac{1}{2}\alpha^2 & -\alpha_1\alpha_2 & 0 \\ -\alpha_1\alpha_2 & \frac{1}{2}\alpha^2 & 0 \\ 0 & 0 & \alpha^2 \end{pmatrix}, \tag{3.67}$$

with $\alpha = \sqrt{\alpha_1^2 + \alpha_2^2}$. For $Q = 0$ and $\alpha_1 = \alpha_2 = \alpha_0$, we find indeed a vanishing eigenvalue with a spin-density vector parallel to the spin-orbit field, $\mathbf{s} = s_0(1,1,0)^T$. Moreover there are two additional modes which do not decay in time but are inhomogeneous in space: the persistent spin helices,[BOZ06, LCCC06, OTA+99, WOB+07, KWO+09]

$$\begin{aligned} \mathbf{S} = S_0 \begin{pmatrix} 1 \\ -1 \\ 0 \end{pmatrix} \sin\left(\frac{2\pi}{L_{\text{SO}}}(x-y)\right) \\ + S_0\sqrt{2} \begin{pmatrix} 0 \\ 0 \\ 1 \end{pmatrix} \cos\left(\frac{2\pi}{L_{\text{SO}}}(x-y)\right), \end{aligned} \tag{3.68}$$

(Fig. 3.5) and the linearly independent solution, obtained by interchanging cos and sin. Here, $L_{\text{SO}} = \pi/m_e\sqrt{2}\alpha_0$. One has to keep in mind that this solution is not an eigenstate anymore in a quantum wire. However, we will show that there exist also long persisting solutions in a quasi-1D case.

It is worth to mention that in the case where cubic Dresselhaus coupling in Eq. (3.33) cannot be neglected, the strength of linear Dresselhaus coupling α_1 is shifted[Ket07] to $\tilde{\alpha}_1 = \alpha_1 - m_e\gamma_D E_F/2$, as we noted before, Eq. (3.44), and, e.g., in the $Q = 0$ case, the spin relaxation rate becomes

$$\frac{1}{\tau_s} = 2p_F^2 \frac{\left(\alpha_2^2 - \tilde{\alpha}_1^2\right)^2}{\alpha_2^2 + \tilde{\alpha}_1^2}\tau + D_e(m_e^2 E_F \gamma_D)^2. \tag{3.69}$$

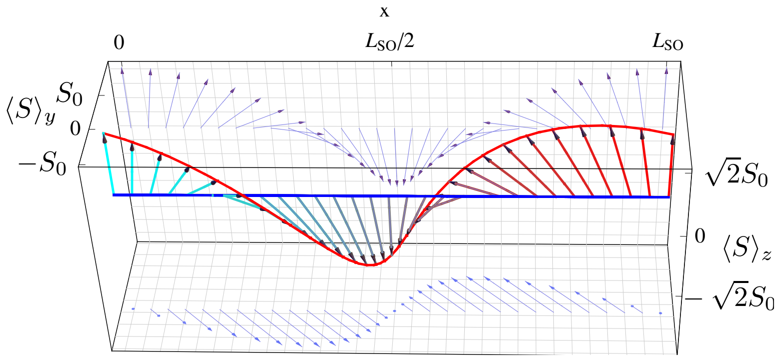

Figure 3.5: Persistent spin helix solution of the spin-diffusion equation for equal magnitude of linear Rashba and linear Dresselhaus coupling, Eq. (3.68).

The condition for persistence is thus rather $\tilde{\alpha}_1 = \alpha_2$. This has been confirmed in a recent measurement (Ref. [KWO$^+$09]). The existence of such long-living modes has an effect on the quantum corrections to the conductivity. In this case, $\tilde{\alpha}_1 = \alpha_2 = \alpha_0$, there is only WL in 2D.[PP95, SKK$^+$08] In the next sections, we will make use of the equivalence of the triplet sector of the Cooperon propagator and the spin-diffusion propagator in quantum wires with appropriate boundary conditions and show how long-living modes may change the quantum corrections to the conductivity.

3.4 Solution of the Cooperon Equation in Quantum Wires

3.4.1 Quantum Wires with Spin-Conserving Boundaries

The conductivity of quantum wires with width $W < L_\varphi = \sqrt{D_e \tau_\varphi}$ is without SO interaction dominated by the transverse zero-mode $Q_y = 0$. This yields the quasi-1D WL correction.[KCCC92] However, in the presence of SO interaction, setting simply $Q_y = 0$ is not correct. If we consider spin-conserving boundaries, rather one has to solve the Cooperon equation with the following modified boundary conditions as derived in Appendix C.2 (Refs. [AF01, MFA02]):

$$\left(-\frac{\tau}{D_e}\mathbf{n}\cdot\langle \mathbf{v}_F[\gamma_g \mathbf{B}_{\text{SO}}(\mathbf{k})\cdot\mathbf{S}]\rangle - i\partial_{\mathbf{n}}\right) C|_{\partial S} = 0, \tag{3.70}$$

where $\langle ... \rangle$ denotes the average over the direction of $\mathbf{v}_F$ and $\mathbf{k}$ which we rewrite using Eq. (C.28) for the given geometry as

$$(-i\partial_y + 2e(\mathbf{A_S})_y)C\left(x, y = \pm\frac{W}{2}\right) = 0, \;\; \forall x, \tag{3.71}$$

where $\mathbf{n}$ is the unit vector normal to the boundary ∂S and x is the coordinate along the wire. The transverse zero-mode $Q_y = 0$ does not satisfy this condition. Therefore, it is convenient to perform a non-Abelian gauge transformation,[AF01, MC00] so that the transformed problem has Neumann boundary conditions, and the transformed Cooperon Hamiltonian can, therefore, be diagonalized in zero-mode approximation for quantum wires. Since in quantum wires these boundary conditions apply only in the transverse direction, a transformation acting in the transverse direction is needed: $\hat{C} \to \tilde{\hat{C}} = U_A \hat{C} U_A^\dagger$, with $U_A = \exp(i2e(\mathbf{A_S})_y y)$. Then, the boundary condition simplifies to $-i\partial_y \tilde{C}(x, y = \pm W/2) = 0, \;\; \forall x$, and the Hamiltonian changes to

$$\begin{aligned}
\tilde{H}_c &= \mathbf{Q}^2 - 2Q_{\,\mathrm{SO}}Q_x[\cos(Q_{\,\mathrm{SO}}y)S_y - \sin(Q_{\,\mathrm{SO}}y)S_z] \\
&\quad + Q_{\mathrm{SO}}^2[\cos^2(Q_{\,\mathrm{SO}}y)S_y^2 + \sin^2(Q_{\,\mathrm{SO}}y)S_z^2 \\
&\quad - \sin(Q_{\,\mathrm{SO}}y)\cos(Q_{\,\mathrm{SO}}y)(S_yS_z + S_zS_y)] \qquad (3.72) \\
&= (\mathbf{Q} + 2e\tilde{\mathbf{A}}_s)^2. \qquad (3.73)
\end{aligned}$$

where the effective vector potential $\mathbf{A_S}$, as introduced in Eq. (3.43),

$$\mathbf{A_S} = \frac{m_e}{e}\hat{\alpha}\mathbf{S} = \frac{m_e}{e}\begin{pmatrix} 0 & -\alpha_2 & 0 \\ \alpha_2 & 0 & 0 \end{pmatrix}\begin{pmatrix} S_x \\ S_y \\ S_z \end{pmatrix}, \tag{3.74}$$

is transformed to the effective vector potential $\tilde{\mathbf{A}}_s$ after the transformation U_A has been applied to the Hamiltonian

$$\begin{aligned}
\tilde{\mathbf{A}}_s &\equiv \frac{m_e}{e}\tilde{\hat{\alpha}}(y)\mathbf{S} \\
&= \frac{m_e}{e}\begin{pmatrix} 0 & -\alpha_2\cos(Q_{\,\mathrm{SO}}y) & -\alpha_2\sin(Q_{\,\mathrm{SO}}y) \\ 0 & 0 & 0 \end{pmatrix}\begin{pmatrix} S_x \\ S_y \\ S_z \end{pmatrix}, \qquad (3.75)
\end{aligned}$$

which varies with the transverse coordinate y on the length scale of $L_{\,\mathrm{SO}}$. Now, we can see already that for narrow wires $W < L_{\,\mathrm{SO}}$, this vector potential varies linearly with y,

$\tilde{\mathbf{A}}_s \sim -m_e\alpha_2 Q_{\text{SO}} y/e$, like the vector potential of the external magnetic field $\mathbf{B}$. Thus, it follows, that for $W < L_{\text{SO}}$, the spin relaxation rate is $1/\tau_s \sim Q^2_{\text{SO}}\langle y^2\rangle \sim Q^2_{\text{SO}}W^2/12$, vanishing for small wire widths. As announced at the beginning, we thus see that the presence of boundaries diminishes the spin relaxation already at wire widths of the order of L_{SO}. If we include only pure Neumann boundaries to the Hamiltonian H_c, i.e., using the wrong covariant derivative, this would not affect the absolute spin relaxation minimum and it would be equal to the nonzero one in the 2D case. We give a more precise answer in the following.

3.4.2 Zero-Mode Approximation

For $W < L_\varphi$, we can use the fact that the nth transverse nonzero-modes contribute terms to the conductivity which are by a factor W/nL_φ smaller than the 0-mode term, with n a nonzero integer number. Therefore, it should be a good approximation to diagonalize the effective quasi-one-dimensional Cooperon propagator, which is the transverse 0-mode expectation value of the transformed inverse Cooperon propagator, Eq. (3.73), $\tilde{H}_{1D} = \langle 0 \mid \tilde{H}_c \mid 0\rangle$. It is crucial to note that $\tilde{H}_{1D}$ contains additional terms, created by the non-Abelian transformation, which shows that taking just the transverse zero-mode approximation of the untransformed Eq. (3.48) would yield a different, incorrect result. We can now diagonalize $\tilde{H}_{1D}$ and finally find the dispersion of quasi-1D triplet modes

$$\frac{E_{t0}}{D_e} = Q_x^2 + \frac{1}{2}Q^2_{\text{SO}}t_{\text{SO}}, \tag{3.76}$$

$$\frac{E_{t\pm}}{D_e} = Q_x^2 + \frac{1}{4}Q^2_{\text{SO}}\left(4 - t_{\text{SO}} \pm \sqrt{t^2_{\text{SO}} + 64\frac{Q_x^2}{Q^2_{\text{SO}}}(1 + c_{\text{SO}}(c_{\text{SO}} - 2))}\right), \tag{3.77}$$

where c_{SO} and t_{SO} are functions of the wire width W as given by

$$c_{\text{SO}} = 1 - \frac{2\sin(Q_{\text{SO}}W/2)}{Q_{\text{SO}}W}, \quad t_{\text{SO}} = 1 - \frac{\sin(Q_{\text{SO}}W)}{Q_{\text{SO}}W}. \tag{3.78}$$

One notices that in the limit of $Q_{\text{SO}}W \to \infty$ we do not recover the previous 2D solution. This boundary effect will be clarified later on.

Inserting Eq. (3.76) and Eq. (3.77) into the expression for the quantum correction to the conductivity Eq. (3.46), taking into account the magnetic field by inserting the magnetic rate $1/\tau_B(W)$ and the finite temperature by inserting the dephasing rate $1/\tau_\varphi(T)$, it remains to perform the integral over momentum Q_x, as has been done in Ref. [Ket07]. For $Q_{\text{SO}}W < 1$, the WL correction can then be written as

$$\Delta\sigma = \frac{\sqrt{H_W}}{\sqrt{H_\varphi + B^*(W)/4}} - \frac{\sqrt{H_W}}{\sqrt{H_\varphi + B^*(W)/4 + H_s(W)}} - 2\frac{\sqrt{H_W}}{\sqrt{H_\varphi + B^*(W)/4 + H_s(W)/2}} \tag{3.79}$$

in units of $e^2/2\pi$. We defined $H_W = 1/4eW^2$ and the effective external magnetic field

$$B^*(W) = \left(1 - \left(1 + \frac{W^2}{3l_B^2}\right)^{-1}\right) B. \tag{3.80}$$

The spin relaxation field $H_s(W)$ is for $Q_{\text{SO}}W < 1$,

$$H_s(W) = \frac{1}{12}(Q_{\text{SO}}W)^2 H_s, \tag{3.81}$$

suppressed in proportion to $(W/L_{\text{SO}})^2$ similar to $B^*(W)$, Eq. (3.80). Here, $H_s = 1/4eD_e\tau_s$, with $1/\tau_s = 2p_F^2\alpha_2^2\tau$. As mentioned above, the analogy to the suppression of the effective magnetic field, Eq. (3.80), is expected, since the SO coupling enters the transformed Cooperon, Eq. (3.73), like an effective magnetic vector potential.[Fal03]
Cubic Dresselhaus coupling, however, would give rise to an additional spin relaxation term, see Eqs. (3.45) and (C.35), which has no analogy to a magnetic field and is, therefore, not suppressed in diffusive wires. In Chapter 4 we will show that this additional term, though it cannot vanish for $Q_{\text{SO}}W \ll 1$, is width dependent, since the term Eq.(3.45) in the Cooperon Hamiltonian H_c is also transformed to obtain the modified Neumann boundaries by applying the transformation U_A, which is W dependent.
When W is larger than SO length L_{SO}, coupling to higher transverse modes may become relevant even if $W < L_\varphi$ is still satisfied, since the SO interaction may introduce coupling to higher transverse modes.[Ale06] We will study these corrections by numerical exact diagonalization in the next section. One can expect that in ballistic wires, $l_e > W$, the spin relaxation rate is suppressed in analogy to the flux cancellation effect, which yields the weaker rate, $1/\tau_s(W) = (W/Cl_e)(D_eW^2/12L_{\text{S}}^4)$, where $C = 10.8$.[BvH88a, DK84, KM02] Before we investigate the exact diagonalization in the pure Rashba case, we consider an anisotropic field with linear Rashba and Dresselhaus SO coupling to see which form the long persisting spin-diffusion modes have in narrow wires. Also, here, we can take advantage of the equivalence of Cooperon and spin-diffusion equation as far as time-reversal symmetry is not violated. We find three solutions whose spin relaxation rate decay proportional to W^2 for $\alpha_2 \neq \alpha_1$ and

which are persistent for $\alpha_2 = \alpha_1$. The first solution is $\mathbf{s} = s_0(\alpha_1, \alpha_2, 0)^T$ for $Q_x = 0$ which is aligned with the effective SO field $\mathbf{B}_{\,\text{SO}}(\mathbf{k}) = -2\gamma_g k_x(\alpha_1, \alpha_2, 0)^T$. In this case, we have according to Eq. (3.81) $H_{\,\text{s,RD1}}(W) = (1/12)(\tilde{Q}_{\,\text{SO}}W)^2 H_s$, with $\tilde{Q}^2_{\,\text{SO}} = (2m_e(\alpha_1^2 - \alpha_2^2))^2/\alpha^2$ and $1/\tau_s = 2p_F^2\alpha^2\tau$, $\alpha = \sqrt{\alpha_1^2 + \alpha_2^2}$. As mentioned above by transforming the vector potential $\mathbf{A_S}$, Eq. (3.75), this alignment occurs due to the constraint on the spin-dynamics imposed by the boundary condition as soon as the wire width W is smaller than the spin precession length $L_{\,\text{SO}}$. In addition, we find two spin helix solutions in narrow wires,

$$\mathbf{s} = s_0 \begin{pmatrix} -\frac{\alpha_2}{\alpha} \\ \frac{\alpha_1}{\alpha} \\ 0 \end{pmatrix} \sin\left(\frac{2\pi}{L_{\,\text{SO}}}x\right) + s_0 \begin{pmatrix} 0 \\ 0 \\ 1 \end{pmatrix} \cos\left(\frac{2\pi}{L_{\,\text{SO}}}x\right), \tag{3.82}$$

and the linearly independent solution, obtained by interchanging cos and sin in Eq. (3.82). The form of this long persisting spin helix depends therefore on the ratio of linear Rashba and linear Dresselhaus coupling strength, Fig. 3.6, and its spin relaxation rate is diminished as $H_{\,\text{s,RD2/3}} = (1/2)H_{\,\text{s,RD1}}$.

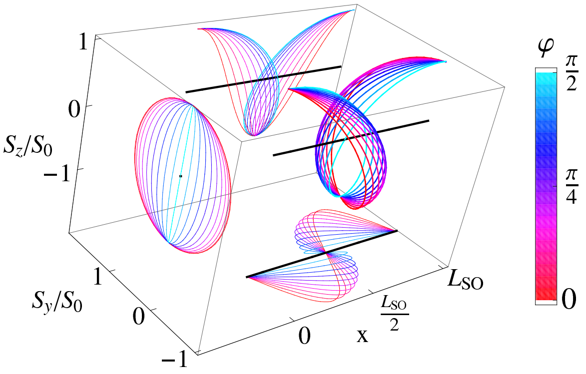

Figure 3.6: Long persisting spin helix solution of the spin-diffusion equation in a quantum wire whose width W is smaller than the spin precession length $L_{\,\text{SO}}$ for varying ratio of linear Rashba $\alpha_2 = \alpha \sin\varphi$ and linear Dresselhaus coupling, $\alpha_1 = \alpha\cos\varphi$, Eq. (3.82), for fixed α and $L_{\,\text{SO}} = \pi/m_e\alpha$.

3.4.3 Exact Diagonalization

The exact diagonalization of the inverse Cooperon propagator, as obtained after the non-Abelian transformation, Eq. (3.73), is performed in the basis of transverse standing waves, satisfying Neumann boundary conditions, $\left\{1/\sqrt{W}, \sqrt{2}/\sqrt{W}\cos\left((n\pi/W)(y - W/2)\right)\right\}$

with $n \in \mathbb{N}^*$, and the plane waves $\exp(iQ_x x)$ with momentum Q_x along the wire. The results of this calculation for different values of the dimensionless wire width $Q_{\text{SO}}W$ are shown in Fig. 3.7. The numerical data points are attributed to the different branches of the eigenenergy dispersion by comparing their eigenvectors. For small $Q_{\text{SO}}W$, the result is in accordance with the 0-mode approximation: For small wire widths W, the z-component of the total spin, S_z, is a good quantum number, as can be seen by expanding Eq. (3.75) in $Q_{\text{SO}}y$. Thus, one can identify the lowest modes with the transverse zero-modes of the triplet modes corresponding to the eigenvalues of S_z, $m = 0, \pm 1$, in the rotated spin axis frame, denoting them as $E_{\{t0,n=0\}}$ and $E_{\{t\pm,n=0\}}$. The minimum of the $E_{\{t0,n=0\}}$ mode is located at $Q_x = 0$. The minimum of $E_{\{t-,0\}}$ is located at finite $Q_x > 0$, in agreement with the 0-mode approximation. For larger $Q_{\text{SO}}W$, the modes mix with respect to the spin quantum number and the transverse quantization modes. As a consequence, energy level crossings which are present at small wire widths are lifted at larger widths, since the mixing of spin and transverse quantization modes results in level repulsion being seen in Fig. 3.7 as avoided level crossings. The branches, $E_{\{t0,0\}}$ and $E_{\{t-,0\}}$, evolve into two modes which become degenerate at large values of $Q_{\text{SO}}W$. These two modes are the only ones whose energy lies below the energy minimum which we obtained for the 2D modes, $E/D_e = (7/16)Q_{\text{SO}}^2$, for a finite K_x-interval around $K_x = 0$. Therefore, we can identify these modes with edge modes which are created by the Neumann boundary conditions. We can confirm that these are edge modes by considering their spatial distribution, shown in Fig. 3.8. Therefore, even in the limit of large widths W, we do get in addition to the spectrum obtained for the 2D system with open boundary conditions case the edge modes, whose energy is lowered as seen in Fig. 3.7. The presence of these edge states and the difference to the 2D system with open boundary conditions can be seen in Appendix C.5 in the nondiagonal elements which are proportional to the width times the functions Eqs. (C.65) and (C.66). Even in the limit of wide wires there are nondiagonal matrix elements which give a significant contribution which cannot be neglected. The modes above $E/D_e = (7/16)Q_{\text{SO}}^2$ are extended over the whole wire system and can thus be characterized as bulk-states, as seen in Figs. 3.8 (c) and (d).[Wen07] In Fig. 3.9, we compare the results which we obtained in the 0-mode approximation with the results of the exact diagonalization. We plot the absolute minima of the spectra as function of the dimensionless wire width parameter $Q_{\text{SO}}W/\pi = 2W/L_{\text{SO}}$. We confirm the parabolic suppression of the lowest eigenvalues for narrow wires $\sim W^2/L_{\text{SO}}^2$, obtained earlier.[MC00, Ket07] We note that the oscillatory behavior of the triplet eigen-

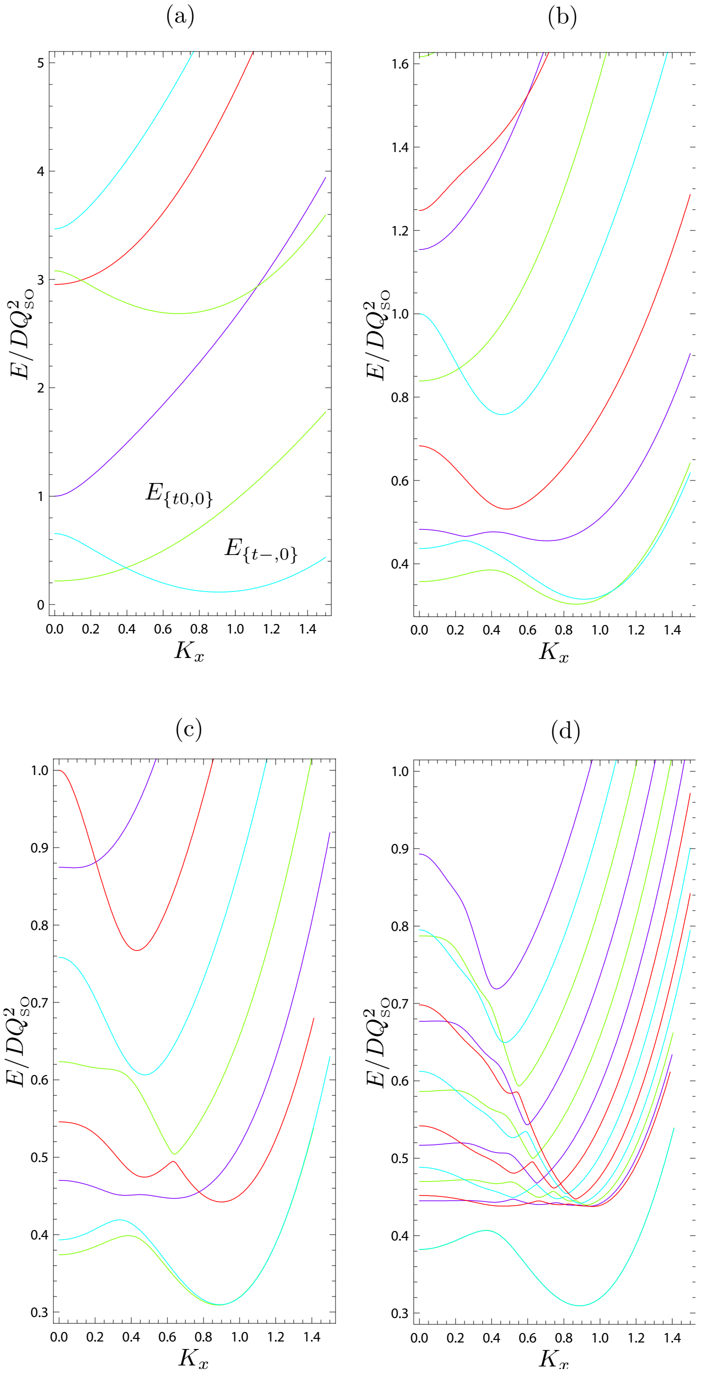

Figure 3.7: Dispersion of the triplet Cooperon modes for different dimensionless wire units $Q_{\mathrm{SO}}W$: (a) $Q_{\mathrm{SO}}W = 2$, (b) $Q_{\mathrm{SO}}W = 8$, (c) $Q_{\mathrm{SO}}W = 12$, (d) $Q_{\mathrm{SO}}W = 30$, plotted as function of $K_x = Q_x/Q_{\mathrm{SO}}$. For $Q_{\mathrm{SO}}W \gg 3$, $E_{\{t0,0\}}$ and $E_{\{t-,0\}}$ evolve into degenerate branches for large K_x. (For $Q_{\mathrm{SO}}W = 30$, not all high-energy branches are shown.)

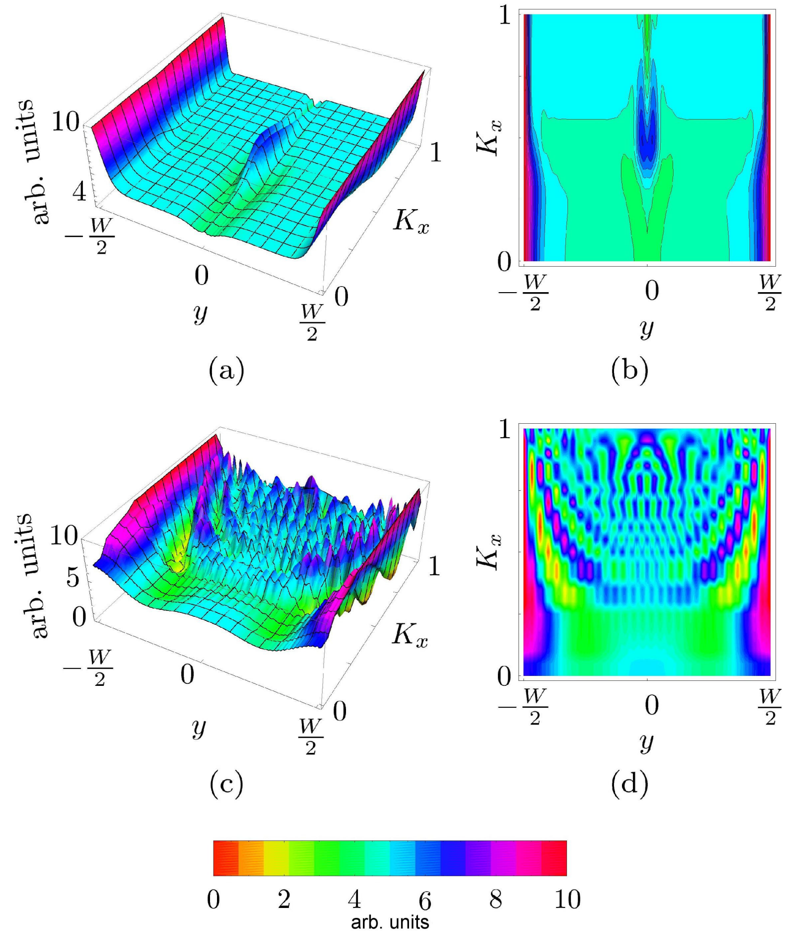

Figure 3.8: Probability density of the Cooperon eigenmodes in the wire for $Q_{\text{SO}}W/\pi = 30$. (a) 3D plot, (b) density plot for one of the two lowest branches, showing their edge mode character. (c) 3D plot and (d) density plot of the density of the third lowest mode, which shows bulk character.

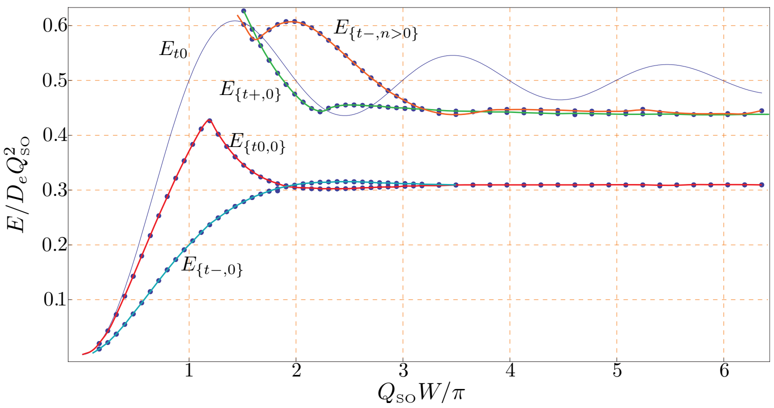

Figure 3.9: Absolute minima of the lowest eigenmodes $E_{\{t0,0\}}$, $E_{\{t-,0\}}$, and $E_{\{t+,0\}}$ plotted as function of $Q_{\text{SO}}W/\pi = 2W/L_{\text{SO}}$. We note that the minimum of $E_{\{t-,0\}}$ is located at $\pm K_x \neq 0$. For comparison, the solution of the zero-mode approximation E_{t0} is shown.

values as function of W, obtained in the 0-mode approximation,[Ket07] is diminished according to the exact diagonalization. However, there remains a sharp maximum of E_{t0} at $Q_{\text{SO}}W/\pi \approx 1.2$ and a shallow maximum of E_{t-} at $Q_{\text{SO}}W/\pi \approx 2.5$. As noted above, the values of the energy minima of E_{t0} and E_{t-} at larger widths W are furthermore diminished as a result of the edge mode character of these modes.

Comparison to Solution of Spin Diffusion Equation in Quantum Wires

As shown above, the spin-diffusion operator and the triplet Cooperon propagator have the same eigenvalue spectrum as soon as time-symmetry is not broken. Therefore, the minima of the spin-diffusion modes, which yield information on the spin relaxation rate, must be the same as the one of the triplet Cooperon propagator as plotted in Fig. 3.9. In Ref. [SDGR06], the value at $K_x = 0$, with $K_i = Q_i/Q_{\text{SO}}$, has been plotted, as shown in Fig. 3.10. We note, however, that this does not correspond to the global minimum plotted in Fig. 3.9. The two lowest states exhibit two minima as can be seen in Fig. 3.7: one local at $K_x = 0$ and one global, which is for large $Q_{\text{SO}}W$ at $K_x \approx 0.88$. The first one is equal to the results given by Ref. [SDGR06]. For the WL correction to the conductivity, however, it is important to retain the global minimum, which is dominant in the integral over the longitudinal momenta.

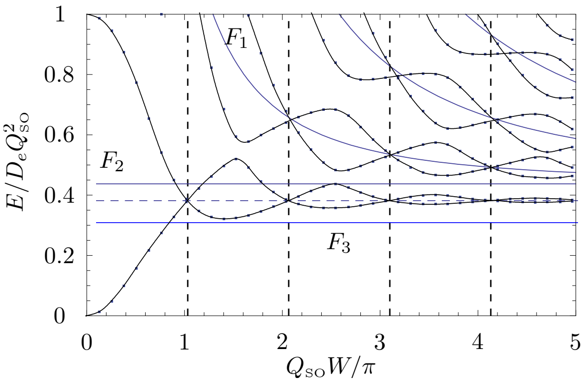

Figure 3.10: Lowest eigenvalues at $K_x = 0$ plotted against $Q_{\rm SO}W/\pi$. For comparison, the global minimum of the Cooperon spectrum for $Q_{\rm SO}W \gtrsim 9$ is plotted, F_3. Curves $F_1[n]$ are given by $7/16 + \left((n/(Q_{\rm SO}W/\pi))\sqrt{15}/4\right)^2$, $n \in \mathbb{N}$. F_2 shows the energy minimum of the 2D case, $F_2 \equiv F_1[n = 0]$. Vertical dotted lines indicate the widths at which the lowest two branches degenerate at $K_x = 0$. They are given by $n/(\sqrt{15}/4)$; consider that the wave vector for the minimum of the E_{T_-} mode is $(\sqrt{15}/4)Q_{\rm SO}$.

Magnetoconductivity

Now, we can proceed to calculate the quantum corrections to the conductivity using the exact diagonalization of the Cooperon propagator. In Fig. 3.11, we show the resulting conductivity as function of magnetic field and as function of the wire width W. Here, we have included for all wire widths the lowest seven singlet modes and the lowest 21 triplet modes. We choose this number of modes so that we included sufficient modes to describe correctly the widest wires considered with $Q_{\rm SO}W = 10$. Thus, for the considered low-energy cutoff, due to electron dephasing rate $1/\tau_\varphi$ of $1/D_eQ^2_{\rm SO}\tau_\varphi = 0.08$ and the high energy cutoff $1/D_eQ^2_{\rm SO}\tau = 4$ due to the elastic scattering rate, we estimate that seven singlet modes fall in this energy range. Since for every transverse mode there are one singlet and three triplet modes, we therefore have to include 21 triplet modes, accordingly. We note a change from positive to negative magnetoconductivity as the wire width becomes smaller than the spin precession length $L_{\rm SO}$, in agreement with the results obtained within the 0-mode approximation, as reported earlier,[Ket07] plotted for comparison in Fig. 3.11 (without shading). At the width, where the crossover occurs, there is a very weak magnetoconductance. This crossover width W_c does depend on the lower cutoff, provided by the temperature-dependent dephasing rate $1/\tau_\varphi$. To estimate the dependence of W_c on the dephasing rate, we have to analyze the contribution of each term in the denominator of

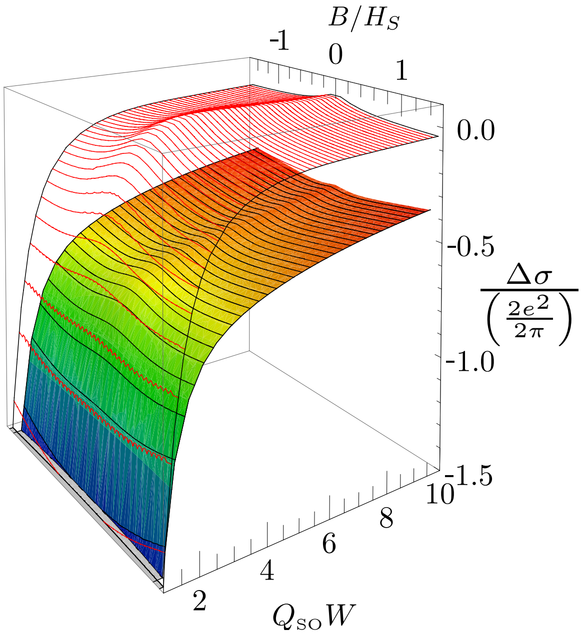

Figure 3.11: The quantum conductivity correction in units of $2e^2/2\pi$ as function of magnetic field B (scaled with bulk relaxation field H_s), and the wire width W scaled with $1/Q_{\mathrm{SO}}$ for pure Rashba coupling and cutoffs $1/D_e Q_{\mathrm{SO}}^2 \tau_\varphi = 0.08$, $1/D_e Q_{\mathrm{SO}}^2 \tau = 4$: Comparison of the zero-mode calculation (grid without shading) to the exact diagonalization where the lowest 21 triplet branches and seven singlet branches were taken into account.

singlet and triplet terms of the Cooperon. A significant change should arise if

$$\frac{1}{\tau_s}(W = W_c) = \frac{1}{\tau_\varphi}. \tag{3.83}$$

Assuming that this occurs for small wire widths, $Q_{\mathrm{SO}}W < 1$, as confirmed for the parameters we used, we apply Eq. (3.81) to Eq. (3.83) and conclude that

$$W_c \sim \frac{1}{\sqrt{\tau_\varphi}}. \tag{3.84}$$

If we calculate the crossover numerically in the 0-mode approximation we get the relation plotted in Fig. 3.13 which coincides with Eq. (3.84). We note that the change from WAL to WL may occur at a different width W_c than the change of sign in the correction to the electrical conductivity $\Delta\sigma(B = 0)$ occurs, W_{WL}. However, we find that the ratio W_c/W_{WL} is independent of the dephasing rate and the spin-orbit coupling strength Q_{SO}.

Furthermore, while there is quantitative agreement with the 0-mode approximation in the magnitude of the magnetoconductivity for all magnetic fields for small wire widths

$W < L_{\text{SO}}$, there is only qualitative agreement at larger wire widths. In particular, the total magnitude of the conductivity is reduced considerably in comparison with the 0-mode approximation. We can attribute this to the reduction of the energy of the lowest Cooperon triplet modes due to the emergence of edge modes, which is not taken into account when neglecting transversal spatial variations, as is done in the 0-mode approximation. Therefore, the 0-mode approximation overestimates the suppression of the triple modes, resulting in an overestimate of the conductivity. Similarly, the magnetic field at which the magnetoconductivity changes its sign from negative to positive is already at a smaller magnetic field, as seen by the shift in the minimum of the conductivity towards smaller magnetic fields (Fig. 3.12), in comparison to the 0-mode approximation (unshaded) in Fig. 3.11. This is in accordance with experimental observations, which showed clear deviations from the 0-mode approximation for larger wire widths, with a stronger magnetic field dependence than obtained in 0-mode approximation.[DLS+05, LSK+07, SGP+06, WGZ+06] Note that the nonmonotonous behavior of the triplet modes as function of the wire width, seen in Fig. 3.7, cannot be resolved in the width dependence of the conductivity.

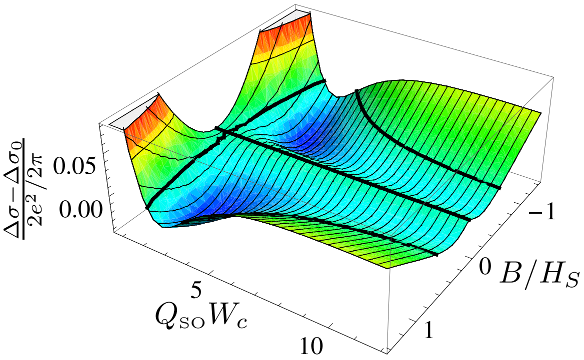

Figure 3.12: The relative magnetoconductivity $\Delta\sigma(B) - \Delta\sigma(B=0)$ in units of $2e^2/2\pi$, with the same parameters and number of modes as in Fig. 3.11.

3.4.4 Other Types of Boundary Conditions

Adiabatic Boundary Conditions

When the lateral confinement potential V is smooth compared to the SO splitting, that is, if $\lambda_F \partial_y V \ll \Delta_\alpha = 2k_F\alpha_2$, where λ_F is the Fermi wavelength, the boundaries do not preserve the spin, $s_{\text{in}} \neq s_{\text{out}}$, Eq. (3.70), since the spin may adiabatically evolve as the

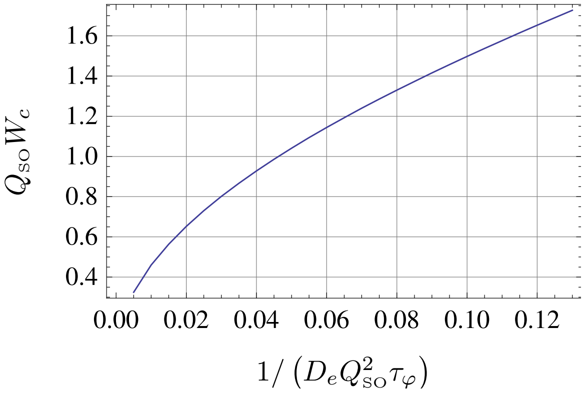

Figure 3.13: Width of wire $WQ_{\rm SO}$ at which there is a crossover from negative to positive magnetoconductivity as function of the lower cutoff $1/D_e Q_{\rm SO}^2 \tau_\varphi$.

electron is scattered from such a smooth boundary.[GKD04] If this applies, the potential is adiabatic and the spin of the scattered electron stays parallel to the field $\mathbf{B}_{\rm SO}$ as its momentum is changed. This leads to the boundary condition for the spin-density[SDGR06]

$$s_x|_{y=\pm W/2} = 0, \tag{3.85}$$

$$s_y|_{y=\pm W/2} = 0, \tag{3.86}$$

$$\partial_y s_z|_{y=\pm W/2} = 0. \tag{3.87}$$

We can transform this boundary condition to the one of the triplet Cooperon by using the unitary rotation between the spin density in the s_i representation and the triplet representation of the Cooperon, $\tilde{s}_i$, Eq. (3.62), which leads to the boundary condition

$$\frac{1}{\sqrt{2}}(-s_x + is_y)|_{y=\pm W/2} = \tilde{s}_{\Uparrow}|_{y=\pm W/2} = 0, \tag{3.88}$$

$$\partial_y s_z|_{y=\pm W/2} = \partial_y \tilde{s}_{\rightrightarrows}|_{y=\pm W/2} = 0, \tag{3.89}$$

$$\frac{1}{\sqrt{2}}(s_x + is_y)|_{y=\pm W/2} = \tilde{s}_{\Downarrow}|_{y=\pm W/2} = 0. \tag{3.90}$$

Now, if we require vanishing magnetization for the 1D case, then the diagonalization is done straightforwardly, plotted in Fig. 3.14 (see also Ref. [SDGR06]). We use a basis which satisfies the boundary conditions and therefore consists of $\sim\sin(qy)(1,0,0)^T$, $\sim\cos(qy)(0,1,0)^T$, and $\sim\sin(qy)(0,0,1)^T$, with $q = n\pi/W$, $n \in \mathbb{N}^*$. However, looking at the spin-diffusion operator [Eq. (3.57)], we see immediately that if we set $\mathbf{k}$ to zero and use the fact that $s_{x,y}$ must vanish at the boundary and s_z has to be constant for the chosen $\mathbf{k}$, we receive

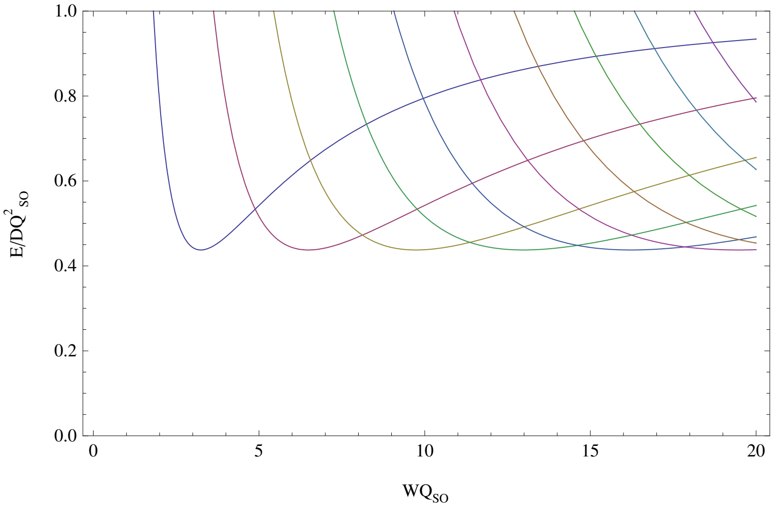

Figure 3.14: Spectrum in the case of adiabatic boundaries. Except for states which are polarized in z direction, the relaxation rates for all states diverge at small wire widths, $Q_{\text{SO}}W \ll 1$.

a polarized mode. Although this mode is a trivial solution, it differs from all other due to the fact that it has a finite spin relaxation time as $Q_{\text{SO}}W$ vanishes. For the choice of basis for diagonalization, this means: We set $q_i = n_i\pi/W$ for respective $\tilde{s}_i$ therewith one state is described by $\{n_1, n_2, n_3\} = \{n, n+p_2, n+p_3\}, \;\; n \in \mathbb{N}^*, \;\; p_2 \in \{-1, 0, 1, \cdots\}, \;\; p_3 \in \mathbb{N}$. In the case $\{n_1, n_2, n_3\} = \{n, n, n\}$ all branches diverge with reference to the eigenvalues in the limes of $Q_{\text{SO}}W \to 0$, so that the spin relaxation time goes to zero for small wires.[SDGR06] In contrast, there is an additional branch in the case of $p_2 = -1, p_3 = 0$ which has a finite eigenvalue and therefore finite spin relaxation time for small wire widths

$$\frac{E}{D_e Q_{\text{SO}}^2} = 2 + K_x^2 \left(1 - \frac{32(Q_{\text{SO}}W)^2}{\pi^4}\right) + \mathcal{O}[(Q_{\text{SO}}W)^4]. \tag{3.91}$$

The smallest spin relaxation rate for vanishing $Q_{\text{SO}}W$, $1/\tau_{s,1D}$, which is given for $k_x = 0$, is found to be an eigenstate polarized in z direction which relaxes with the rate $1/\tau_{s,1D} = 2/\tau_s$. It shows compared with the other modes a monotonous behavior as function of $Q_{\text{SO}}W$. If we allow magnetization for the 1D case, then the combination $p_1 = -1, p_2 = 0$ leads to a valid solution. For wide wires the smallest absolute minimum is the 2D minimum $E/D_e = (7/16)Q_{\text{SO}}^2$; there are no edge modes. But already at a width of $Q_{\text{SO}}W = \pi/\sqrt{5} \approx 1.4$ all modes except the z-polarized exceed the rate $1/\tau_{s,1D}$.

Tubular Wires

In tubular wires, such as carbon nanotubes, and InN nanowires in which only surface electrons conduct,[PHC+09] and radial core-shell InO nanowires,[JLS+08] the tubular topology of the electron system can be taken into account by periodic boundary conditions. In the following, we focus on wires where the dominant SO coupling is of Rashba type. If one requires furthermore that this SO-coupling strength is uniform and the wire curvature can be neglected,[PHC+09] the spectrum of the Cooperon propagator can be obtained by substituting in Eq. (3.52) the transverse momentum Q_y by the quantized values $Q_y = n2\pi/W$, n is an integer, when W is the circumference of the tubular wire. Thus, the spin relaxation rate remains unchanged, $1/\tau_s = (7/16)D_e Q_{\mathrm{SO}}^2$. If then a magnetic field perpendicular to the cylinder axis is applied as done in Ref. [PHC+09], there remains a negative magnetoconductivity due to the WAL, which is enhanced due to the dimensional crossover from the 2D correction to the conductivity Eq. (C.39) to the quasi-one-dimensional behavior of the quantum correction to the conductivity [Eq. (3.79)]. In tubular wires in which the circumference fulfills the quasi-one-dimensional condition $W < L_\varphi$, the WL correction can then be written as

$$\begin{aligned}\Delta\sigma = &\frac{\sqrt{H_W}}{\sqrt{H_\varphi + B^*(W)/4}} - \frac{\sqrt{H_W}}{\sqrt{H_\varphi + B^*(W)/4 + H_s(W)}} \\ &- 2\frac{\sqrt{H_W}}{\sqrt{H_\varphi + B^*(W)/4 + 7H_s(W)/16}}\end{aligned} \tag{3.92}$$

in units of $e^2/2\pi$. As in Eq. (3.79), we defined $H_W = 1/4eW^2$, but the effective external magnetic field differs due to the different geometry: Assuming that $W < l_B$, we have[Ket07]

$$\frac{1}{\tau_B} = D_e(2e)^2 B^2 \langle y^2 \rangle \tag{3.93}$$

$$= D_e(2e)^2 \frac{1}{2}\left(\frac{BW}{2\pi}\right)^2 \tag{3.94}$$

and the effective external magnetic field yields

$$B^*(W) = (2e)\left(\frac{BW}{2\pi}\right)^2 \tag{3.95}$$

$$= (2e)(Br_{\text{ tube}})^2, \tag{3.96}$$

with the tube radius $r_{\text{ tube}}$. The spin relaxation field H_s is $H_s = 1/4eD_e\tau_s$, with $1/\tau_s = 2p_F^2\alpha_2^2\tau$, or in terms of the effective Zeeman field $B_{\text{ SO}}$,

$$H_s = \frac{g\gamma_g}{16}\frac{B_{\text{ SO}}(\epsilon_{\text{F}})^2}{\epsilon_{\text{F}}}. \tag{3.97}$$

Thus the geometrical aspect, $\langle y^2\rangle_{\text{ tube}}/\langle y^2\rangle_{\text{ planar}} \approx 6.6$, might resolve the difference between measured and calculated SO coupling strength in Ref. [PHC$^+$09] where a planar geometry has been assumed to fit the data. This assumption leads in a tubular geometry to an underestimation of $H_s(W)$. The flux cancellation effect is as long as we are in the diffusive regime, $l_e \ll W$, negligible.

3.5 Magnetoconductivity with Zeeman splitting

In the following, we want to study if the Zeeman term, Eq. (3.42), is modifying the magnetoconductivity. Accordingly, we assume that the magnetic field is perpendicular to the 2DES. Taking into account the Zeeman term to first order in the external magnetic field $\mathbf{B} = (0, 0, B)^T$, the Cooperon is according to Eq. (3.43) given by

$$\hat{C}(\mathbf{Q}) = \frac{1}{D_e(\mathbf{Q} + 2e\mathbf{A} + 2e\mathbf{A}_{\mathbf{S}})^2 + i\frac{1}{2}\gamma_g(\boldsymbol{\sigma'} - \boldsymbol{\sigma})\mathbf{B}}. \tag{3.98}$$

This is valid for magnetic fields $\gamma_g B \ll 1/\tau$. Due to the term proportional to $(\boldsymbol{\sigma'} - \boldsymbol{\sigma})$, the singlet sector of the Cooperon mixes with the triplet one. We can find the eigenstates of C^{-1}, $|i\rangle$ with the eigenvalues $1/\lambda_i$. Thus, the sum over all spin up and down combinations $\alpha\beta, \beta\alpha$ in Eq. (3.35) for the conductance correction simplifies in the singlet-triplet representation to (Appendix C.1)

$$\begin{aligned}\sum_{\alpha\beta} C_{\alpha\beta\beta\alpha} = \sum_i \big(&- \langle\rightleftarrows|i\rangle\langle i|\rightleftarrows\rangle + \langle\upuparrows|i\rangle\langle i|\upuparrows\rangle \\ &+ \langle\rightrightarrows|i\rangle\langle i|\rightrightarrows\rangle + \langle\downdownarrows|i\rangle\langle i|\downdownarrows\rangle\big)\,\lambda_i.\end{aligned} \tag{3.99}$$

3.5.1 2DEG

The coupling of the singlet to the triplet sector lifts the energy level crossings at $K = \pm 1/\sqrt{2}$ of the singlet E_S and the triplet branch E_{T_-} as can be seen in Fig. 3.15 for a nonvanishing Zeeman coupling. The spectrum, which is not positive definite anymore for all wave vectors, $K = Q/Q_{\text{SO}}$, is given by

$$\begin{aligned}
E_{\text{B,2D,1}}/D_e Q_{\text{SO}}^2 &= 1 + K_x^2, &(3.100)\\
E_{\text{B,2D,2}}/D_e Q_{\text{SO}}^2 &= E_{\text{B,2D,1}} + \frac{f_1}{f_2^{1/3}} - \frac{1}{3} f_2^{1/3}, &(3.101)\\
E_{\text{B,2D,3/4}}/D_e Q_{\text{SO}}^2 &= E_{\text{B,2D,1}} - \frac{1}{2}\frac{\left(1 \pm i\sqrt{3}\right) f_1}{f_2^{1/3}} \\
&\quad + \frac{1}{6}\left(1 \mp i\sqrt{3}\right) f_2^{1/3}, &(3.102)
\end{aligned}$$

with

$$\begin{aligned}
f_1 &= \tilde{B}^2 - 4K_x^2 - 1, &(3.103)\\
f_2 &= 3\left(\sqrt{3}\sqrt{108K_x^4 + f_1^3} - 18K_x^2\right), &(3.104)\\
\tilde{B} &= g\mu_{\text{B}} B/D_e Q_{\text{SO}}^2, &(3.105)
\end{aligned}$$

Thus, there are spin states with the same real part of the Cooperon energy, so that they decay equally in time, but the imaginary part is different, so that they precess with different frequencies around the magnetic field axis. A significant change of the Cooperon spectrum appears when $g\mu_{\text{B}}B/D_e$ exceeds Q_{SO}^2, as can be seen in Fig. 3.16(b). All states with a low decay rate do precess now, due to a finite imaginary value of their eigenvalue. Associated with this change is also a change of the dispersion of the real part of $E_{\text{B,2D,3}}$ which changes for $K_y = 0$ from a nearly quadratic dispersion in K_x, $a_0 + a_1 K_x^2$ for $\tilde{B} < 1$ to one which changes more slowly as $a_0 + a_1 K_x^{2/3} + a_2 K_x^{4/3} + a_3 K_x^2$ for $\tilde{B} \geq 1$ [see Fig. 3.16 (a)].

Weak Field

In the case of a weak Zeeman field, $\tilde{B} \ll 1$, the singlet and triplet sectors are still approximately separated. A finite $\tilde{B} \ll 1$ lifts however the energy of the singlet mode to $E_{B,2D,2}(K = 0)/D_e Q_{\text{SO}}^2 = \tilde{B}^2/2 + \mathcal{O}(\tilde{B}^4)$, thus the singlet mode attains a finite gap, corresponding to a finite relaxation rate. The absolute minimum of two of the triplet modes is also lifted by $E_{B,2D,2}(K = \pm\sqrt{15}/4)/D_e Q_{\text{SO}}^2 = 7/16 + (3/4)\tilde{B}^2 + \mathcal{O}(\tilde{B}^4)$, while their value is independent of $\tilde{B}$ at $K = 0$. In contrast, the minimum of the triplet mode $E_{B,2D,3}$, which approaches E_{T_+} in the limit of no magnetic field (see Fig. 3.4) is diminished to $E_{B,2D,3}(K = 0)/D_e Q_{\text{SO}}^2 = 2 - \tilde{B}^2/2 + \mathcal{O}(\tilde{B}^4)$. So, in summary, a weak Zeeman field renders all four Cooperon modes gapfull and that gap can be interpreted as a finite relaxation rate

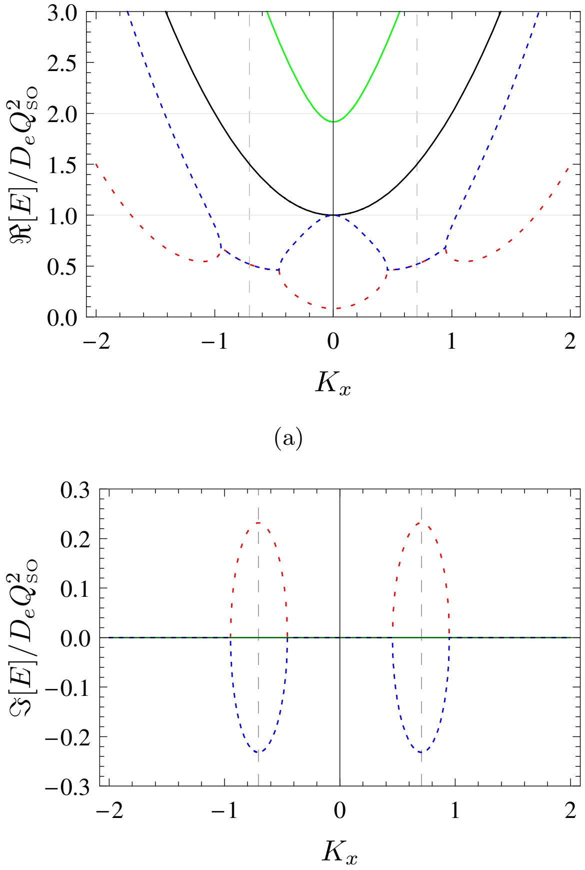

(a)

(b)

Figure 3.15: (a) Real and (b) imaginary parts of the spectrum of the 2D Cooperon with Zeeman term of strength $g\mu_{\rm B} B/D_e Q_{\rm SO}^2 = 0.4$. $E_{\rm B,2D,1}$ (black), $E_{\rm B,2D,2}$ (red dashed), $E_{\rm B,2D,3}$ (green), $E_{\rm B,2D,4}$ (blue dashed). Dashed vertical lines are located at $K_x = \pm 1/\sqrt{2}$, the wave vector where the triplet mode E_{T_-} and the singlet mode E_S are crossing each other (without loss of generality $K_y = 0$).

or dephasing rate as the Zeeman coupling mixes all the spin states, breaking time-reversal invariance.

Strong Field

If we expand the spectrum in $1/\tilde{B} \ll 1$, we find that all modes have the same gap proportional to the strength of the SO coupling, $D_e Q_{\mathrm{SO}}^2$, while two modes attain a finite imaginary part with opposite sign

$$\begin{aligned} E_{\mathrm{B,2D},1}/D_e Q_{\mathrm{SO}}^2 &= 1 + K_x^2, & (3.106)\\ E_{\mathrm{B,2D},2}/D_e Q_{\mathrm{SO}}^2 &= 1 + K_x^2 + \mathcal{O}(1/\tilde{B}), & (3.107)\\ E_{\mathrm{B,2D},3/4}/D_e Q_{\mathrm{SO}}^2 &= 1 + K_x^2 \mp i\tilde{B} + \mathcal{O}(1/\tilde{B}). & (3.108)\end{aligned}$$

Thus, a strong Zeeman field polarizes the spins and leads to their precession. The SO interaction, which is too weak to flip the spins, merely results in a relaxation of all modes, corresponding to a dephasing of the spin precession.

3.5.2 Quantum Wire with Spin-Conserving Boundary Conditions

In the following, we want to study if a Zeeman field modifies the magnetoconductivity and can shift the crossover from positive to negative Magnetoconductivity as function of wire width W. We have seen that for appropriate parameters the critical width W_c is small compared with L_{SO}. Therefore we stay in the 0-mode approximation to get a better overview of the physics. To do so, we first analyze the spectrum.

The modes with low decay rates are situated at $K_x = 0$ and $K_x \approx \pm 1$ for small widths and small enough Zeeman field, $\tilde{B} \lesssim 1$, as can be seen in Fig. 3.17. For $K_x = 0$, we have

$$E_{\min,0}/D_e Q_{\mathrm{SO}}^2 = \tilde{B}^2 + \tilde{B}^4 \left(1 + \frac{(Q_{\mathrm{SO}} W)^2}{12}\right) \tag{3.109}$$

and for $K_x = \pm 1$,

$$\begin{aligned} E_{\min,\pm 1}/D_e Q_{\mathrm{SO}}^2 = {} & \frac{(Q_{\mathrm{SO}} W)^2}{24} + \tilde{B}^2 \left(\frac{1}{2} - \frac{(Q_{\mathrm{SO}} W)^2}{96}\right) \\ & + \tilde{B}^4 \left(\frac{3}{16} - \frac{(Q_{\mathrm{SO}} W)^2}{384}\right). \end{aligned} \tag{3.110}$$

As in the 2D case, we have a mode which is independent of the Zeeman field and the spectrum is equal to E_{t0} with the eigenvector $(0,1,0,1)^T$. Using this spectrum, we estimate

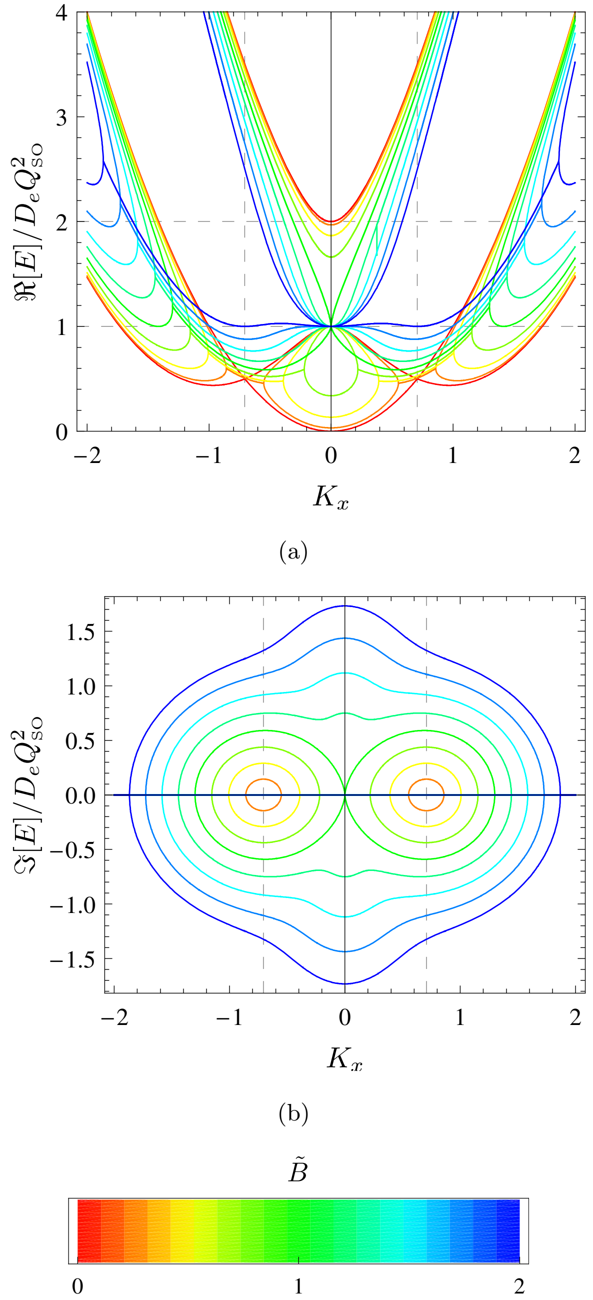

(a)

(b)

Figure 3.16: (a) Real and (b) imaginary parts of the spectrum of the 2D Cooperon with Zeeman term of the strength $g\mu_{\rm B}B/D_eQ^2_{\rm SO} = 0\ldots2$ in steps of 0.25 (w.l.o.g $K_y = 0$). The B independent mode E_{T_0} is not shown.

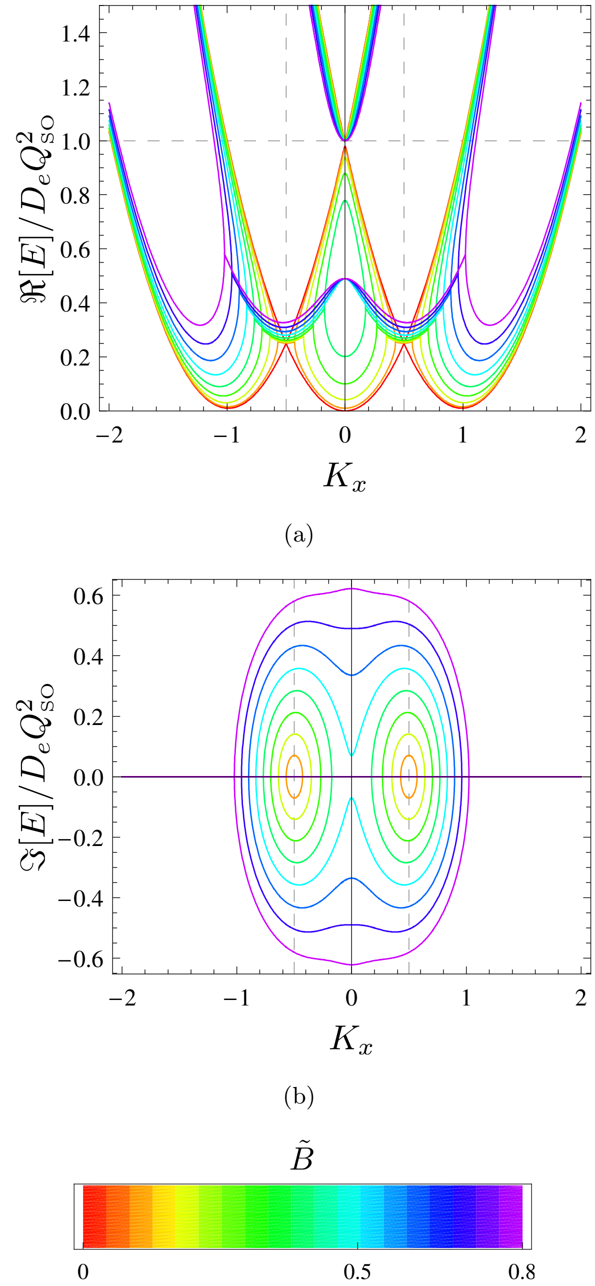

(a)

(b)

Figure 3.17: (a) Real and (b) imaginary parts of the spectrum of the Cooperon with Zeeman term of the strength $g\mu_{\mathrm{B}}B/D_e Q_{\mathrm{SO}}^2 = 0 \ldots 0.8$ in steps of 0.1 in a finite wire of the width $Q_{\mathrm{SO}}W = 0.5$. The B independent mode E_{t0} is not shown.

the correction to the static conductivity in the case of a magnetic field which we include by means of a Zeeman term together with an effective magnetic field appearing in the cutoff $1/\tau_B$ as described in Sec. 3.2. The $\tilde{g} = g/8m_eD_e$ factor is used as a material-dependent parameter. In Fig. 3.18, we see that for large enough $\tilde{g}$ factor, the system changes from positive magnetoconductivity—in the case without Zeeman field and a small-enough wire width—to negative magnetoconductivity at a finite Zeeman field for the same wire. Hence, the ratio W_c/W_{WL} changes and one has to be careful not to confuse the crossover defined by a change of the sign of the quantum correction, WL→WAL, and the crossover in the magnetoconductivity. To give an idea how the crossover W_c depends on $\tilde{g}$ and the strength of the Zeeman field we analyze two different systems as plotted in Fig. 3.19: The first one, plot (a), shows the drop of W_c in a system as just described where we have one magnetic field which we include with an orbital and a Zeeman part. For small $\tilde{g}$ we have $Q_{\text{SO}}W_c(\tilde{g}) = Q_{\text{SO}}W_c(\tilde{g} = 0) - \text{const}\,\tilde{g}^2$, where const is about 1 in the considered parameter space. In the second system [Fig. 3.19(b)], we assume that we can change the orbital and the Zeeman field separately. The critical width is plotted against the Zeeman field. To calculate W_c, we fix the Zeeman field to a certain value, horizontal axis in plot (b), while we vary the effective field and calculate if negative or positive magnetoconductivity is present. For different Zeeman fields B_Z/H_s we get different W_c. We see that W_c is shifted to larger widths as the Zeeman field is increased, $Q_{\text{SO}}W_c(B_Z/H_s) = Q_{\text{SO}}W_c(B_Z = 0) + \text{const}\,(B_Z/H_s)^2$, where const is about 1 in the considered parameter space, while $\Delta\sigma(1/\tau_{\text{B}} = 0)$ (not plotted) is lowered as long as we assume small Zeeman fields. If we notice that B_Z mixes singlet and triplet states it is understood that there is no gapless singlet mode anymore and therefore $\Delta\sigma(1/\tau_{\text{B}} = 0)$ must decrease for low Zeeman fields.

To estimate $\tilde{g}$, we take typical values for a GaAs/AlGaAs system and assume the electron density to be $n_s = 1.11\times10^{11}\,\text{cm}^{-2}$, the effective mass $m_e/m_{e_0} = 0.063$, the Landé factor $g = 0.75$ and an elastic mean-free path of $l_e = 10$ nm in a wire with $Q_{\text{SO}}W = 1$, corresponding to $W = 1.2\,\mu$m, if we assume a Rashba spin-orbit coupling strength of $\alpha_2 = 5$ meVÅ. We thus get $\tilde{g} \approx 0.1$ and find that the Zeeman coupling due to the perpendicular magnetic field can have a measurable, albeit small effect on the magnetoconductance in GaAs/AlGaAs systems.

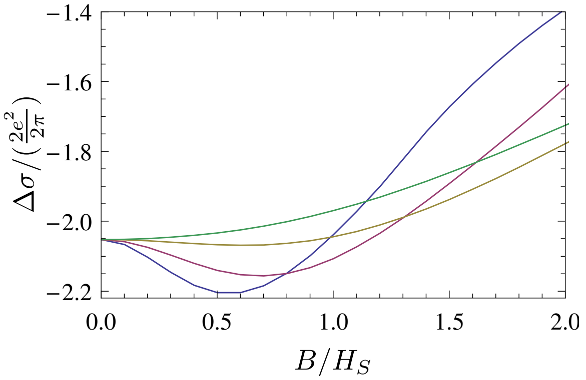

Figure 3.18: The magnetoconductance $\Delta\sigma(B)$ in a magnetic field perpendicular to the quantum well, where its coupling via the Zeeman term is considered by exact diagonalization while its effect on the orbital motion is considered effectively by the magnetic phase-shifting rate $1/\tau_B(W)$ for wire width $Q_{\mathrm{SO}}W = 1$, dephasing rate $1/\tau_\varphi = 0.06 D_e Q^2_{\mathrm{SO}}$, and elastic-scattering rate $1/\tau = 4 D_e Q^2_{\mathrm{SO}}$. The strength of the contribution of the Zeeman term is varied by the material-dependent factor $\tilde{g} = g\mu_{\mathrm{B}} H_s / D_e Q^2_{\mathrm{SO}}$ in the range $\tilde{g} = 0 \ldots 1.5$ in steps of 0.5: The system changes from positive magnetoconductivity ($\tilde{g} = 0$, green) to negative one ($\tilde{g} = 0.5 \ldots 1.5$, continuous decrease of the absolute minimum).

3.6 Conclusions

In conclusion, in wires with spin-conserving boundaries and a width W smaller than bulk spin precession length L_{SO}, the spin relaxation due to linear Rashba SO coupling is suppressed according to the spin relaxation rate $(1/\tau_s)(W) = (\pi^2/3)\,(W/L_{\mathrm{SO}})^2\,(1/\tau_s)$, where $1/\tau_s = 2p_F^2\alpha_2^2\tau$. The enhancement of spin relaxation length $L_s = \sqrt{D_e\tau_s(W)}$ can be understood as follows: The area an electron covers by diffusion in time τ_s is WL_s. This spin relaxation occurs if that area is equal L^2_{SO},[Fal03] which yields $1/L_s^2 \sim 1/D_e\tau_s \sim (W/L_{\mathrm{SO}})^2/L^2_{\mathrm{SO}}$, in agreement with Eq. (3.81). For larger wire widths, the exact diagonalization reveals a nonmonotonic behavior of the spin relaxation as function of the wire width of the long-living eigenstates. The spin relaxation rate is first enhanced before it is suppressed as the widths W is decreased. The longest living modes are found to exist at the boundary of wide wires. Since we identified a direct transformation from the spin-diffusion equation to the Cooperon equation, we could show that these edge modes affect the conductivity: the 0-mode approximation overestimates the conductivity for larger wire widths $Q_{\mathrm{SO}}W > 1$ since it does not take into account these edge modes. They add a larger contribution to the negative triplet term of the quantum

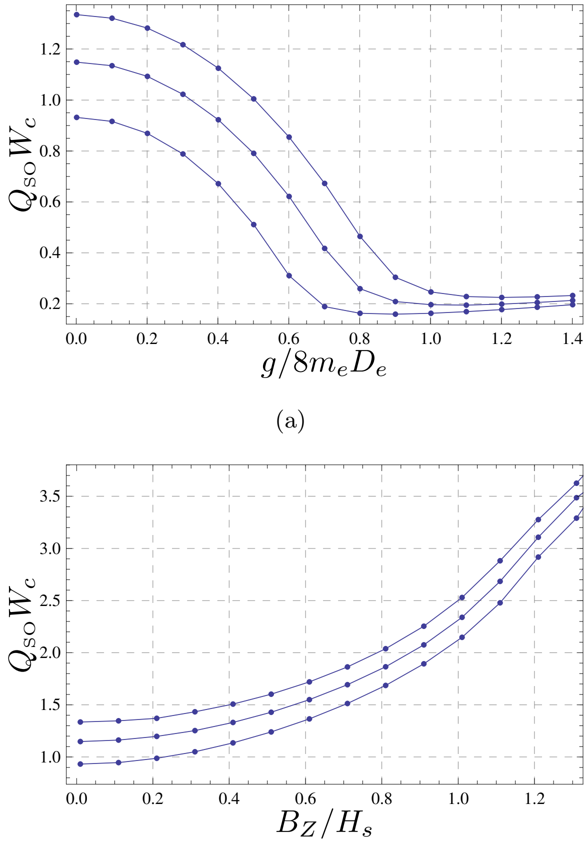

(a)

(b)

Figure 3.19: (a) Change of crossover width W_c with g factor: The magnetic field is included as an effective field $1/\tau_B$ and in the Zeeman term. The strength of the contribution of the Zeeman term is varied by the material dependent factor $\tilde{g} = g\mu_{\rm B} H_s / D_e Q_{\rm SO}^2$. (b) Change of crossover width W_c with Zeeman field: To calculate W_c, we fix the Zeeman field to a certain value, horizontal axis, while we vary the effective field independently and calculate if negative or positive magnetoconductivity is present. For different Zeeman fields B_Z/H_s, we find thereby a different width W_c. Here, we set $g/8m_eD_e = 1$. In (a) and (b), the cutoff due to dephasing is varied: $1/D_eQ_{\rm SO}^2\tau_\varphi = 0.04, 0.06, 0.08$ (lowest first).

correction than the bulk modes do, since they relax more slowly. This also results in a shift in the minimum of the conductivity towards smaller magnetic fields in comparison to the 0-mode approximation. The reduction of spin relaxation has recently been observed in optical measurements of n-doped InGaAs quantum wires[HSM+06] and in transport measurements.[DLS+05, LSK+07, SGP+06, WGZ+06, Mei05] Recently in Ref. [KKN09], the enhancement of spin lifetime due to dimensional confinement in gated InGaAs wires with gate-controlled SO coupling was reported. Reference [HSM+06] reports saturation of spin relaxation in narrow wires, $W \ll L_{\text{SO}}$, attributed to cubic Dresselhaus coupling.[Ket07] The contribution of the linear and cubic Dresselhaus SO interaction to the spin relaxation turns out to depend strongly on growth direction and will be studied in more detail in Chapter 4. Including both the linear Rashba and Dresselhaus SO coupling we have shown that there exist two long persisting spin helix solutions in narrow wires even for arbitrary strength of both SO coupling effects. This is in contrast to the 2D case, where the condition $\alpha_1 = \alpha_2$, respectively in the case where the cubic Dresselhaus term cannot be neglected, $\alpha_1 - m_e \gamma_g E_F/2 = \alpha_2$, is required to find persistent spin helices [BOZ06, LCCC06] as it was measured recently (Ref. [KWO+09]). Regarding the type of boundary, we found that the injection of polarized spins into a nonmagnetic material is favorable for wires with a smooth confinement, $\lambda_F \partial_y V < \Delta_\alpha = 2k_F \alpha_2$. With such adiabatic boundary conditions, states which are polarized in z direction relax with a finite rate for wires with widths $Q_{\text{SO}} W \ll 1$, while the spin relaxation rate of all other states diverges in that limit.

In tubular wires with periodic boundary conditions, the spin relaxation is found to remain constant as the wire circumference is reduced. Finally, by including the Zeeman coupling to the perpendicular magnetic field, we have shown that for spin-conserving boundary condition the critical wire width, W_c, where the crossover from negative to positive magnetoconductivity occurs, depends not only on the dephasing rate but also depends on the g factor of the material.

Chapter 4

Direction Dependence of Spin Relaxation and Diffusive-Ballistic Crossover

4.1 Introduction

In Chapter 3 it was shown how the spin relaxes in a quasi 1D electron system in a quantum well grown in the [001] direction, depending on the width of the wire, where the normal of the boundary was pointing in the [010] direction. In a system with only Rashba SOC or linear Dresselhaus SOC in a (111) quantum well it is clear from the vector fields plotted in Fig. 2.2 that a rotation in the plain should not effect the physics, i.e. the minimal spin relaxation rate will not reduce. The linear Rashba SOC does not depend on the growth direction at all. It is already known that on the other hand in a (001) 2D system with both BIA[Dre55] and SIA[BR84] we get an anisotropic spin-relaxation.[KRW03, CWd07, WJW10] This has also been studied numerically in quasi-1D GaAs wires[LLK$^+$10]. In this Chapter, Sec. 4.2, we present analytical results concerning this anisotropy for the 2D case as well as the case of quantum wire with spin and charge conserving boundaries. As in the previous chapter, also here we focus on materials where the dominant mechanism for spin relaxation is governed by the DP spin relaxation.

Furthermore, we extend our analysis to other growth directions, Sec. 4.3: Searching for long spin decoherence times at room temperature, the (110) quantum wire attracted attention.

[AOMO01, DHR$^+$04] The properties of spin relaxation in systems with this growth direction have also been related to WL measurements, Ref. [HPB$^+$97]. We present analytical explanations for dimensional spin relaxation reduction and discuss the crossover from WL to WAL, Sec. 4.4.

It was shown in the previous chapter that the cubic Dresselhaus SOC leads to a term, Eq. (3.45), which hinders the spin relaxation to vanish for small wire widths $Q_{\text{SO}}W \ll 1$ but $W \gg l_e$, with the wire width W and the elastic mean free path l_e. As we will show in the following sections, this term is width dependent but the finite spin relaxation rate is not reduced if the wire is rotated in the (001) plane. However some of the experiments are done on ballistic wires, i.e. in the regime where $W \gg l_e$ does not hold, and we need to modify the theory used in Ref. [Ket07] and presented in the previous chapter to enable us to study the crossover from diffusive to ballistic wires. In Sec. 4.5 we show how the spin relaxation which is due to cubic Dresselhaus SOC reduces with the number of channels in the quantum wire.

We consider again the Hamiltonian with SOC, Eq. (3.32)

$$H = \frac{1}{2m_e}(\mathbf{p} + e\mathbf{A})^2 + V(\mathbf{x}) - \frac{1}{2}\gamma_g \boldsymbol{\sigma}\left(\mathbf{B} + \mathbf{B}_{\text{SO}}(\mathbf{p})\right), \tag{4.1}$$

where m_e is the effective electron mass. $\mathbf{A}$ is the vector potential due to the external magnetic field $\mathbf{B}$. $\mathbf{B}^T_{\text{SO}} = (B_{\text{SO}x}, B_{\text{SO}y})$ is the momentum dependent SO field. $\boldsymbol{\sigma}$ is a vector, with components $\boldsymbol{\sigma}_i$, $i = x, y, z$, the Pauli matrices, γ_g is the gyromagnetic ratio with $\gamma_g = g\mu_{\text{B}}$ with the effective g factor of the material, and $\mu_{\text{B}} = e/2m_e$ is the Bohr magneton constant. To analyze the spin relaxation for different wire directions we use for the SO interaction which is caused by BIA to lowest order in the wave vector $\mathbf{k}$ the general form, Eq. (2.13),

$$-\frac{1}{2}\gamma_g \mathbf{B}_{\text{SO,D}} = \gamma_D \sum_i \hat{e}_i p_i (p_{i+1}^2 - p_{i+2}^2) \tag{4.2}$$

where the principal crystal axes are given by $i \in \{x, y, z\}, i \to ((i-1) \mod 3) + 1$ and the spin-orbit coefficient for the bulk semiconductor γ_D. We consider the standard white-noise model for the impurity potential as in the previous chapter, $V(\mathbf{x})$, which vanishes on average $\langle V(\mathbf{x})\rangle = 0$, is uncorrelated, $\langle V(\mathbf{x})V(\mathbf{x}')\rangle = \delta(\mathbf{x} - \mathbf{x}')/2\pi\nu\tau$, and weak, $E_F\tau \gg 1$. To address both, the WL corrections as well as the spin relaxation rates in the system, our starting point is also here the Cooperon[HLN80]

$$\hat{C}(\mathbf{Q})^{-1} = \frac{1}{\tau}\left(1 - \int \frac{d\varphi}{2\pi} \frac{1}{1 + i\tau(\mathbf{v}(\mathbf{Q} + 2e\mathbf{A} + 2m_e\hat{a}\mathbf{S}) + H_{\sigma'} + H_Z)}\right), \tag{4.3}$$

as presented in Eq. (3.41). Expanding the Cooperon to second order in $(\mathbf{Q} + 2e\mathbf{A} + 2m_e\hat{a}\mathbf{S})$ and performing the angular integral which is for 2D diffusion (elastic mean free path l_e smaller than wire width W) continuous from 0 to 2π, yields:

$$\hat{C}(\mathbf{Q}) = \frac{1}{D_e(\mathbf{Q} + 2e\mathbf{A} + 2e\mathbf{A}_\mathbf{S})^2 + H_{\gamma_D}}. \tag{4.4}$$

The effective vector potential due to SO interaction is $\mathbf{A}_\mathbf{S} = m_e\hat{\alpha}\mathbf{S}/e$, where $\hat{\alpha} = \langle\hat{a}\rangle$ is averaged over angle. The SO term H_{γ_D}, which cannot be rewritten as a vector potential, is in our case due to the appearance of cubic Dresselhaus SOC.

4.1.1 Example

To get an idea of the procedure we recall the situation presented in Ref. [Ket07] and Chapter 3 and take up the remark about the additional term due to cubic Dresselhaus SOC, Eq.(3.45) concerning the width dependence: Starting with the Cooperon Hamiltonian, in the case of Rashba and lin. and cubic Dresselhaus SOC,

$$H_c := \frac{\hat{C}^{-1}}{D_e} = (\mathbf{Q} + 2e\mathbf{A}_\mathbf{S})^2 + (m_e^2 E_F\gamma_D)^2(S_x^2 + S_y^2), \tag{4.5}$$

with the effective vector potential

$$\mathbf{A}_\mathbf{S} = \frac{m_e}{e}\hat{\alpha}\mathbf{S} = \frac{m_e}{e}\begin{pmatrix} -\tilde{\alpha}_1 & -\alpha_2 & 0 \\ \alpha_2 & \tilde{\alpha}_1 & 0 \end{pmatrix}\begin{pmatrix} S_x \\ S_y \\ S_z \end{pmatrix}, \tag{4.6}$$

with $\tilde{\alpha}_1 = \alpha_1 - m_e\gamma_D E_F/2$,
it can be easily shown that the Hamiltonian Eq. (4.5) has only non vanishing eigenvalues due to the last term in Eq. (4.5), which is due to cubic Dresselhaus SOC, if we assume no boundaries except the lateral confinement. This term is neither reduced by reason of the boundary in the diffusive case, as has been shown in the previous chapter for quantum wires in [100] direction and will be extended now to other directions, too. However two triplet eigenvalues of this term depend on the wire width,

$$E_{QD1} = \frac{q_{s3}^2}{2}, \tag{4.7}$$

$$E_{QD2,3} = \frac{q_{s3}^2}{2}\left(\frac{3}{2} \pm \frac{\sin(Q_{\,\mathrm{SO}}W)}{2Q_{\,\mathrm{SO}}W}\right), \tag{4.8}$$

with $q_{s3}^2/2 = (m_e^2 E_F\gamma_D)^2$. In the following we are going to diagonalize the whole Hamiltonian and change the direction of the wire in the (001) plane.

4.2 Spin Relaxation anisotropy in the (001) system

4.2.1 2D system

We rotate the system in-plane through the angle θ (the angle $\theta = \pi/4$ is equivalent to [110]). This does not effect the Rashba term but changes the Dresselhaus one to[CWd07, WJW10]

$$\begin{aligned}\frac{1}{\gamma_D} H_{D[001]} &= \sigma_y k_y \cos(2\theta)(\langle k_z^2\rangle - k_x^2) - \sigma_x k_x \cos(2\theta)(\langle k_z^2\rangle - k_y^2)\\ &- \sigma_y k_x \frac{1}{2}\sin(2\theta)(k_x^2 - k_y^2 - 2\langle k_z^2\rangle)\\ &+ \sigma_x k_y \frac{1}{2}\sin(2\theta)(k_x^2 - k_y^2 + 2\langle k_z^2\rangle),\end{aligned} \tag{4.9}$$

with the wave vectors k_i. The resulting Cooperon Hamiltonian, including Rashba and Dresselhaus SOC, reads then

$$H_c = (Q_x + \alpha_{x1} S_x + (\alpha_{x2} - q_2) S_y)^2 + (Q_y + (\alpha_{x2} + q_2) S_x - \alpha_{x1} S_y)^2 + \frac{q_{s3}^2}{2}(S_x^2 + S_y^2), \tag{4.10}$$

where we set

$$\begin{aligned}\frac{q_{s3}^2}{2} &= \left(m_e^2 E_F \gamma_D\right)^2, &(4.11)\\ \alpha_{x1} &= \frac{1}{2} m_e \gamma_D \cos(2\theta)((m_e v)^2 - 4\langle k_z^2\rangle), &(4.12)\\ \alpha_{x2} &= -\frac{1}{2} m_e \gamma_D \sin(2\theta)((m_e v)^2 - 4\langle k_z^2\rangle) &(4.13)\\ &= \left(q_1 - \sqrt{\frac{q_{s3}^2}{2}}\right)\sin(2\theta) &(4.14)\\ &= 2 m_e \tilde{\alpha}_1 \sin(2\theta), &(4.15)\end{aligned}$$

with $q_1 = 2m_e\alpha_1$, $q_2 = 2m_e\alpha_2$. We see that the part of the Hamiltonian which cannot be written as a vector field and is due to cubic Dresselhaus SOC does not depend on the wire direction in the (001) plane.

Special case: Only lin. Dresselhaus SOC equal to Rashba SOC

As a special example for the 2D case we set $q_{s3} = 0$ and $q_1 = q_2$. To simplify the search for vanishing spin relaxation we go to polar coordinates. Applying free wave functions (with k_x, k_y) to H_c, Eq. (4.10), we end up with (singlet part left out)

$$\frac{H_c}{q_2^2} = \begin{pmatrix} 2+Q^2 & f_{\theta\phi} & -2i\exp(2i\theta) \\ & 4+Q^2 & f_{\theta\phi} \\ \text{c.c.} & & 2+Q^2 \end{pmatrix} \tag{4.16}$$

with $k_x/q_2 = Q\cos(\phi)$, $k_y/q_2 = Q\sin(\phi)$ and

$$f_{\theta\phi} = (i-1)\sqrt{2}\exp(i\theta)(\cos(\phi+\theta) - \sin(\phi+\theta))Q. \tag{4.17}$$

Vanishing spin relaxation is found at $Q = 0$ for arbitrary values of θ (the spin with vanishing spin relaxation is pointing along the [110] direction[SEL03]). Another solution is found at $Q = 2$ with the condition $\theta + \phi = 3\pi/4$, which is equivalent to the $[\bar{1}10]$ crystallographic direction.[CWd07]

4.2.2 Quasi-1D wire

In the following we consider spin and charge conserving boundaries. Due to the SOC we have, as in the previous chapter, Eq. (3.70), modified Neumann condition with the slight change which is the angle dependency of the vector potential:

$$\left(-\frac{\tau}{D_e}\mathbf{n}\cdot\langle\mathbf{v}_F[\gamma_g\mathbf{B}_{\text{SO}}(\mathbf{k})\cdot\mathbf{S}]\rangle - i\partial_{\mathbf{n}}\right)C|_{\partial S} = 0, \tag{4.18}$$

where $\langle\ldots\rangle$ denotes the average over the direction of $\mathbf{v}_F$ and $\mathbf{k}$ which we rewrite for the rotated x-y system

$$(-i\partial_y + 2e(\mathbf{A_S})_y)C\left(x, y = \pm\frac{W}{2}\right) = 0,\ \ \forall x, \tag{4.19}$$

where $\mathbf{n}$ is the unit vector normal to the boundary ∂S and x is the coordinate along the wire. In order to do a diagonalization taking only the zero-mode into account, we have to simplify the boundary condition. A transformation acting in the transverse direction is needed according to Eq. (4.10): $\hat{C} \to \tilde{\hat{C}} = U_A\hat{C}U_A^\dagger$, by using the transformation

$$U = \mathbb{1}_4 - i\sin(q_s y)\frac{1}{q_s}A_y + (\cos(q_s y) - 1)\frac{1}{q_s^2}A_y^2 \tag{4.20}$$

with $A_y = (\alpha_{x2} + q_2)S_x - \alpha_{x1}S_y$ and $q_s = \sqrt{(\alpha_{x2}+q_2)^2 + \alpha_{x1}^2}$.

Spin relaxation

We diagonalize the Hamiltonian, Eq. (4.10), after applying the transformation U, taking only the lowest mode into account similar to the calculation presented in Sec. 3.4.2. The spectrum of the Hamiltonian for small wire width, $Wq_s < 1$, is given by

$$\begin{aligned} E_{1/2}(k_x > 0) = k_x^2 \pm k_x &\left(2q_{sm} - \frac{\left(\alpha_{x1}^2 + \alpha_{x2}^2 - q_2^2\right)^2}{12 q_{sm}} W^2 \right) \\ &+ \frac{3}{2}\frac{q_{s3}^2}{2} + q_{sm}^2 \mp \frac{q_{s3}^2}{2k_x} \frac{\left(\alpha_{x1}^2 + \alpha_{x2}^2 - q_2^2\right)^2 W^2}{96 q_{sm}} \\ &- \frac{\left(\frac{q_{s3}^2}{2} + q_{sm}^2\right)\left(\alpha_{x1}^2 + \alpha_{x2}^2 - q_2^2\right)^2}{24 q_{sm}^2} W^2 \,, \end{aligned} \tag{4.21}$$

$$E_1(k_x = 0) = q_{s3}^2 + q_{sm}^2 - \frac{(\alpha_{x1}^2 + \alpha_{x2}^2 - q_2^2)^2 + \frac{q_{s3}^2}{2} q_s^2}{12} W^2, \tag{4.22}$$

$$E_2(k_x = 0) = \frac{q_{s3}^2}{2} + q_{sm}^2 + \frac{q_{s3}^2}{2}\frac{q_2^2 \alpha_{x1}^2}{3 q_{sm}^2} W^2, \tag{4.23}$$

$$E_3 = k_x^2 + \frac{q_{s3}^2}{2} + \frac{\left(\frac{q_{s3}^2}{2} + q_{sm}^2\right)\left(\alpha_{x1}^2 + \alpha_{x2}^2 - q_2^2\right)^2}{12 q_{sm}^2} W^2, \tag{4.24}$$

with $q_{sm} = \sqrt{(\alpha_{x2} - q_2)^2 + \alpha_{x1}^2}$. First we notice that the only θ dependence is in the term q_{sm}, which disappears if the Dresselhaus SOC strength $\tilde{\alpha}_1$, which is shifted due to the cubic term, equals the Rashba SOC strength α_2 and the angle of the boundary is $\theta = (1/4 + n)\pi,\ n \in \mathbb{Z}$. Assuming the term proportional to W^2/k_x to be small, the absolute minimum can be found at

$$E_{1/2,min} = \frac{3}{2}\frac{q_{s3}^2}{2} + \frac{\left(q_{sm}^2 - \frac{q_{s3}^2}{2}\right)\left(\alpha_{x1}^2 + \alpha_{x2}^2 - q_2^2\right)^2}{24 q_{sm}^2} W^2 \tag{4.25}$$

which is independent of the width W if $\alpha_{x1}(\theta = 0) = -q_2$ and/or the direction of the wire is pointing in

$$\theta = \frac{1}{2} \arcsin\left(\frac{2\langle k_z^2\rangle (m_e\gamma_D)^2((m_e v)^2 - 2\langle k_z^2\rangle) - q_2^2}{(m_e^3 v^2 \gamma_D - 4\langle k_z^2\rangle m_e \gamma_D)\, q_2} \right). \tag{4.26}$$

The second possible absolute minimum, which dominates for sufficient small width W and $q_{sm} \neq 0$ (compare with $E_2(k_x = 0)$), is found at

$$E_{3,min} = \frac{q_{s3}^2}{2} + \frac{\left(\frac{q_{s3}^2}{2} + q_{sm}^2\right)\left(\alpha_{x1}^2 + \alpha_{x2}^2 - q_2^2\right)^2}{12 q_{sm}^2} W^2. \tag{4.27}$$

The minimal spin-relaxation rate is found by analyzing the prefactor of W^2 in Eq. (4.27), Fig. (4.1). We see immediately that in the case of vanishing cubic Dresselhaus or in the case where $\alpha_{x1}(\theta = 0) = -q_2$ we have no direction dependence of the minimal spin relaxation. Notice the shift of the absolute minimum away from $q_1 = q_2$ due to $q_{s3} \neq 0$. In the case of $q_1 < (q_{s3}/\sqrt{2})$ we find the minimum at $\theta = (1/4+n)\pi,\ \ n \in \mathbb{Z}$, else at $\theta = (3/4+n)\pi,\ \ n \in \mathbb{Z}$, which is indicated by the dashed line in Fig. (4.1).

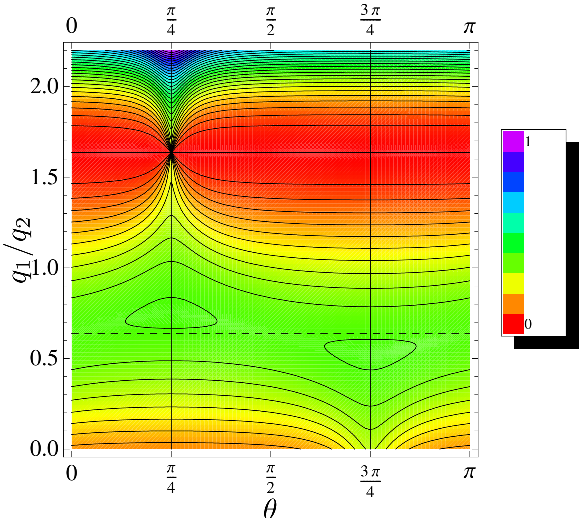

Figure 4.1: Dependence of the W^2 coefficient in Eq. (4.27) on the lateral rotation (θ). The absolute minimum is found for $\alpha_{x1}(\theta = 0) = -q_2$ (here: $q_1/q_2 = 1.63$) and for different SO strength we find the minimum at $\theta = (1/4+n)\pi,\ \ n \in \mathbb{Z}$ if $q_1 < (q_{s3}/\sqrt{2})$ (dashed line: $q_1 = (q_{s3}/\sqrt{2})$) and at $\theta = (3/4+n)\pi,\ \ n \in \mathbb{Z}$ else. Here we set $q_{s3} = 0.9$. The scaling is arbitrary.

Spin dephasing

Concerning spintronic devices it is interesting to know how an ensemble of spins initially oriented along the [001] direction dephases in the wire of different orientation θ. To do this analysis we only have to know that the eigenvector for the eigenvalue E_1 at $k_x = 0$, Eq. (4.22), is the triplet state $|S = 1; m = 0\rangle = (|\uparrow\downarrow\rangle + |\downarrow\uparrow\rangle)/\sqrt{2} \equiv |\rightrightarrows\rangle \hat{=} (0,1,0)^T$, Eqs. (3.62). This is equal to the z-component of the spin density whose evolution is described by the spin diffusion equation, Eq. (3.54). As an example we assume the case where cubic Dresselhaus term can be neglected and where the Rashba and lin. Dresselhaus SOC are equal. We notice that the dephasing is then width independent.

At definite angles the dephasing time diverges - as for the in-plane polarized states with eigenvalue $E_2(k_x = 0)$ - ,

$$\frac{1}{\tau_s(W)} = 2D_e q_2^2(1 - \sin(2\theta)) \tag{4.28}$$

which is plotted in Fig. (4.2). We have longest spin dephasing time at $\theta = (1/4+n)\pi, \;\; n \in \mathbb{Z}$. For $\theta = (3/4+n)\pi, \;\; n \in \mathbb{Z}$ we get the 2D result $T_2 = 1/(4q_2^2 D_e)$. We notice that this is the eigenvalue to the triplet state $|S = 1; m = 0\rangle$ of the spin relaxation tensor [DP71b, DP71c],

$$\frac{1}{(\hat{\tau}_s)_{ij}} = \tau\gamma_g^2 \left(\langle \mathbf{B}_{\text{SO}}(\mathbf{k})^2\rangle\delta_{ij} - \langle B_{\text{SO}}(\mathbf{k})_i B_{\text{SO}}(\mathbf{k})_j\rangle\right) \tag{4.29}$$

which we derived in Sec. 3.3.

This gives an analytical description of numerical calculation done by J.Liu *et al.*, Ref.-[LLK$^+$10].

Switching on cubic Dresselhaus SOC leads to finite spin dephasing time for all angles θ. In addition, T_2 is then width dependent. In the case of strong cubic Dresselhaus SOC where $q_{s3}^2/2 = q_1^2 = q_2^2$, the dephasing time T_2 is angle independent and for $q_{s3}^2/2 > q_1^2 = q_2^2$ the minima in $T_2(\theta)$ change to maxima and vice versa.

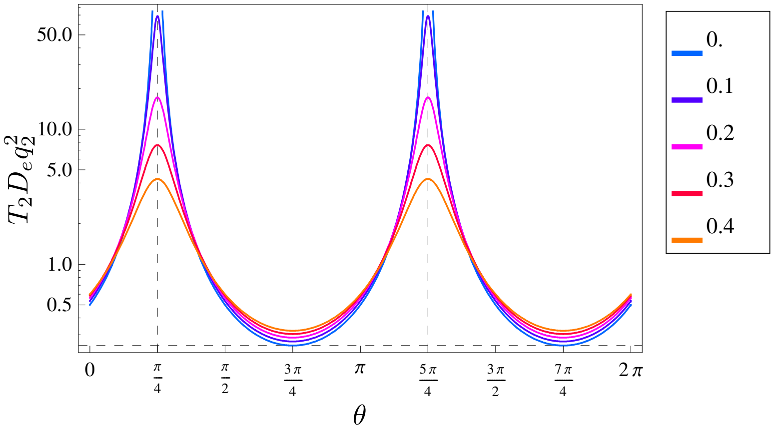

Figure 4.2: The spin dephasing time T_2 of a spin initially oriented along the [001] direction in units of $(D_e q_2^2)$ for the special case of equal Rashba and lin. Dresselhaus SOC. The different curves show different strength of cubic Dresselhaus in units of q_{s3}/q_2. In the case of finite cubic Dresselhaus SOC we set $W = 0.4/q_2$. If $q_{s3} = 0$: T_2 diverges at $\theta = (1/4+n)\pi, \;\; n \in \mathbb{Z}$ (dashed vertical lines). The horizontal dashed line indicated the 2D spin dephasing time, $T_2 = 1/(4q_2^2 D_e)$.

Special case: $\theta = 0$

In this case the longitudinal direction of the wire is [100].
If we neglect the term proportional to W^2/k_x in Eq. (4.21) the lowest spin relaxation is found to be

$$\frac{1}{D_e \tau_s} = \frac{q_{s3}^2}{2} + \frac{\left(\alpha_{x1}^2 - q_2^2\right)^2 \left(q_s^2 + \frac{q_{s3}^2}{2}\right) W^2}{12 q_s^2} \tag{4.30}$$

or

$$\frac{1}{D_e \tau_s} = \frac{3q_{s3}^2}{4} + \frac{\left(\alpha_{x1}^2 - q_2^2\right)^2 \left(q_s^2 - \frac{q_{s3}^2}{2}\right) W^2}{24 q_s^2}, \tag{4.31}$$

depending whether

$$-\frac{q_{s3}^2}{4} + \frac{\left(\alpha_{x1}^2 - q_2^2\right)^2 \left(q_s^2 + 3\frac{q_{s3}^2}{2}\right) W^2}{24 q_s^2} \tag{4.32}$$

is negative or positive. This shows that the cubic Dresselhaus term adds not only to the relaxation rate by a constant term but is also width dependent. However, this width dependence does not reduce the spin relaxation rate below $q_{s3}^2/2$.

4.3 Spin relaxation in quasi-1D wire with [110] growth direction

To get the spin-relaxation in a [110] quantum wire with Rashba and Dresselhaus SOC again we have to rotate the spacial coordinate system of the Dresselhaus Hamiltonian Eq.(4.2) but now with the rotation matrix

$$R = \begin{pmatrix} \frac{1}{\sqrt{2}} & 0 & \frac{1}{\sqrt{2}} \\ -\frac{1}{\sqrt{2}} & 0 & \frac{1}{\sqrt{2}} \\ 0 & 1 & 0 \end{pmatrix}. \tag{4.33}$$

We get

$$\begin{aligned} \frac{H_{D[110]}}{\gamma_D} &= \sigma_x(-k_x^2 k_z - 2k_y^2 k_z + k_z^3) \\ &+ \sigma_y(4k_x k_y k_z) \\ &+ \sigma_z(k_x^3 - 2k_x k_y^2 - k_x k_z^2). \end{aligned} \tag{4.34}$$

The confinement in z-direction ($z \equiv$[110]) leads to $\langle k_z \rangle = \langle k_z^3 \rangle = 0$, and $\langle k_z^2 \rangle = \int \mathrm{d}z\, |\nabla\phi|^2$. The Hamiltonian for the quantum wire in [110] direction has then the following form

[HPB+97]

$$H_{[110]} = -\gamma_D \sigma_z k_x \left(\frac{1}{2} \langle k_z^2 \rangle - \frac{1}{2} (k_x^2 - 2k_y^2) \right). \tag{4.35}$$

Including the Rashba SOC (q_2), noting that its Hamiltonian does not depend on the orientation of the wire,[HPB+97] we end up with the following Cooperon Hamiltonian

$$\frac{C^{-1}}{D_e} = (Q_x - \tilde{q}_1 S_z - q_2 S_y)^2 + (Q_y + q_2 S_x)^2 + \frac{\tilde{q}_3^2}{2} S_z^2, \tag{4.36}$$

$$\text{with} \qquad \tilde{q}_1 = 2m_e \frac{\gamma_D}{2} \langle k_z^2 \rangle - \frac{\gamma_D}{2} \frac{m_e E_F}{2}, \tag{4.37}$$

$$q_2 = 2m_e \alpha_2, \tag{4.38}$$

$$\text{and} \qquad \tilde{q}_3 = (3m_e E_F^2 (\gamma_D/2)). \tag{4.39}$$

We see immediately that in the 2D case states polarized in the z-direction have vanishing spin relaxation as long as we have no Rashba SOC. Compared with the (001) system the constant term due to cubic Dresselhaus does not mix spin directions. Here we set the appropriate Neumann boundary condition as follows:

$$(-i\partial_y + 2m_e \alpha_2 S_x) C \left(x, y = \pm \frac{W}{2} \right) = 0, \ \ \forall x. \tag{4.40}$$

The presence of Rashba SOC adds a vector potential proportional to S_x. Applying a non-abelian gauge transformation as before to simplify the boundary condition, we diagonalize the transformed Hamiltonian (App. (D.1)) up to second order in $q_2 W$ in the 0-mode approximation.

4.3.1 Special case: without cubic Dresselhaus SOC

The spectrum is found to be

$$E_1 = k_x^2 + \frac{1}{12} \Delta^2 (q_2 W)^2, \tag{4.41}$$

$$\begin{aligned} E_{2,3} = {} & k_x^2 + \frac{1}{24} \Delta^2 \left(24 - (q_2 W)^2 \right) \\ & \pm \frac{\Delta}{24} \sqrt{\Delta^2 (q_2 W)^4 + 4k_x^2 (24 - (q_2 W)^2)^2}, \end{aligned} \tag{4.42}$$

with the lowest spin relaxation rate found at finite wave vectors $k_{x\ \min} = \pm \frac{\Delta}{24} (24 - (q_2 W)^2)$,

$$\frac{1}{D_e \tau_s} = \frac{\Delta^2}{24} (q_2 W)^2. \tag{4.43}$$

We set $\Delta = \sqrt{\tilde{q}_1^2 + q_2^2}$.

4.3.2 With cubic Dresselhaus SOC

If cubic Dresselhaus SOC cannot be neglected, the absolute minimum of spin relaxation can also shift to $k_{x\ \mathrm{min}} = 0$. This depends on the ratio of Rashba and lin. Dresselhaus SOC:

If $q_2/q_1 \ll 1$, we find the absolute minimum at $k_{x\ \mathrm{min}} = 0$,

$$E_{min1} = \frac{\tilde{q}_3 + \tilde{q}_1^2 + q_2^2}{2} - \Delta_c + \frac{1}{12}\Delta_c (q_2 W)^2, \tag{4.44}$$

with

$$\Delta_c = \frac{1}{2}\sqrt{(\tilde{q}_3 + \tilde{q}_1^2)^2 + 2(\tilde{q}_1^2 - \tilde{q}_3) q_2^2 + q_2^4}. \tag{4.45}$$

If $q_2/q_1 \gg 1$, we find the absolute minimum at $k_{x\ \mathrm{min}} \approx \pm\frac{\Delta}{24}(24 - (q_2 W)^2)$,

$$\begin{aligned} E_{min2} = {} & k_{x\ \mathrm{min}}^2 - k_{x\ \mathrm{min}} q_2 \left(\frac{\tilde{q}_1^2}{q_2^2} + 2\right) - \frac{\tilde{q}_3^2}{16 k_{x\ \mathrm{min}} q_2} \\ & + \Delta^2 + \frac{\tilde{q}_3}{2}\left(\frac{\tilde{q}_1^2}{q_2^2} + 1\right) \\ & - \Bigg(\frac{\tilde{q}_3 \tilde{q}_1^2}{12} - \frac{\tilde{q}_3^2 q_2}{3072 k_{x\ \mathrm{min}}^3} - \frac{q_2^2}{24}(\tilde{q}_3 - \tilde{q}_1^2) \\ & + \frac{q_2^4}{24} - \left(\frac{\tilde{q}_1^2}{24} + \frac{q_2^2}{12}\right) q_2 k_{x\ \mathrm{min}} \\ & - \frac{q_2}{k_{x\ \mathrm{min}}}\left(\left(\frac{\tilde{q}_3^2}{128} + \frac{\tilde{q}_3 \tilde{q}_1^2}{192}\right) - \frac{\tilde{q}_3 q_2^2}{96}\right)\Bigg) W^2. \end{aligned} \tag{4.46}$$

We can conclude that reducing wire width W will not cancel the contribution due to cubic Dresselhaus SOC to the spin relaxation rate.

4.4 Weak Localization

In Ref. [Ket07] and the previous chapter the crossover from WL to WAL due to change of wire width and SOC strength was explained in the case of a (001) system. Whether WL or WAL is present depends on the suppression of the triplet modes of the Cooperon. The suppression, in turn, is dominated by the absolute minimum of the spectrum of the Cooperon Hamiltonian H_c. The findings presented in Sec. 4.2.2 therefore point out that e.g. the crossover width, at which the system changes from WL to WAL, can shift with the wire direction θ. Recently experimental results on WL/WAL by J. Nitta *et al.*, Ref. [Nit06], seem to show a strong dependence on growth direction. Our presented results can also support the method proposed in Ref. [SKK+08] -to determine the relative strength of Rashba and Dresselhaus SOC from WL/WAL measurements without fitting parameters-with the inclusion of cubic Dresselhaus term for wire directions different from [100] and [010] in an analytical manner.

In the (110) system the situation is different: In the 2D case it was shown by Pikus *et al.*, Ref. [HPB+97], that in the absence of the Rashba terms the negative magnetoconductivity cannot be observed. In the case of a wire geometry, we can conclude from Eqs. (4.41-4.46) that we have no width dependence if Rashba SOC vanishes. A change of the quantum correction to the static conductivity therefore cannot be achieved in this wire geometry by changing the wire width. The reason is the vector potential in the boundary condition, Eq. (4.40), which only depends on the Rashba SOC.

4.5 Diffusive-Ballistic Crossover

In the following we assume a (001) 2D system with both, Rashba and linear and cubic Dresselhaus SO coupling.

Experiments measuring WL in diffusive quantum wires with SOC[LSK+07, SGB+09] are in great agreement with theoretical calculations by S. Kettemann, Ref. [Ket07]. But considering e.g. the works Ref. [KKN09, KHG+10], one realizes that the scope of application of the theory has to be extended to describe also the crossover to the ballistic regime, $l_e > W$. In Fig. 4.3 we show an example of an experiment done by Kunihashi *et al.*[KKN09]. The lines show a fit using Eq. (10) in the paper by S. Kettemann[Ket07] which is equal to the results presented in Sec. 4.2.2 if the width dependence of the term due to cubic Dresselhaus SOC is neglected. To get the solid lines the term due to cubic Dresselhaus SOC was neglected, the dashed include it. When checking Fig. 4.3 (a) the condition $l_e < W$ is not fulfilled at all wire width. It follows that this additional term is suppressed if the condition of a diffusive system does not hold anymore.

We have shown in Sec. 4.2.2 that the presence of cubic Dresselhaus SOC in the sample leads to a finite spin relaxation even for wire widths $Q_{\mathrm{SO}} W \ll 1$, regardless of the boundary direction in a (001) system. To account for the ballistic case we have to modify the derivation of the Cooperon Hamiltonian, Eq. (4.5). In the case of a wire where the mean

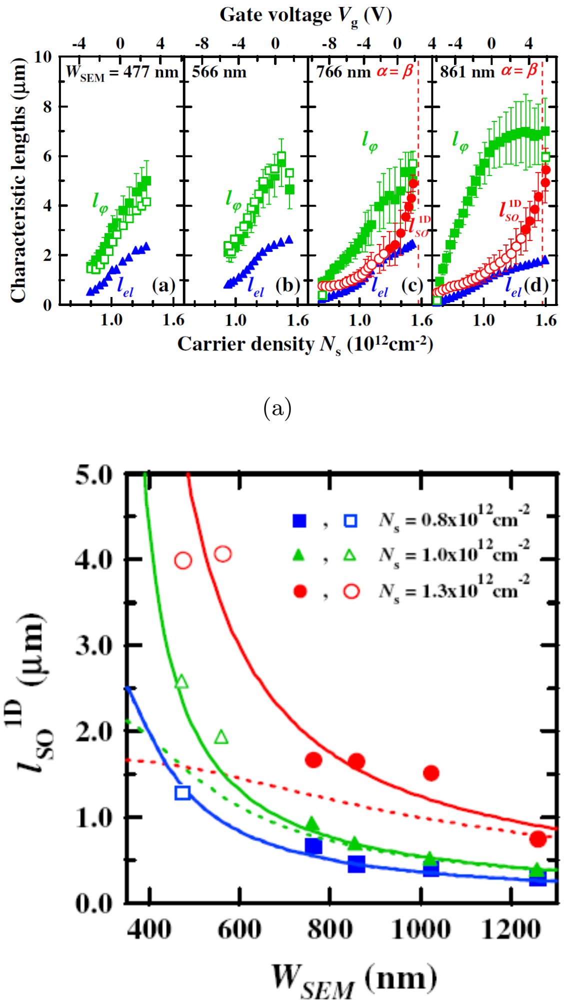

(a)

(b)

Figure 4.3: Example of an experiment done by Kunihashi *et al.*[KKN09]. The width dependence of the spin relaxation length l_{SO}^{1D} of different carrier density. Solid lines and dashed lines in (b) show the l_{SO}^{1D} calculated from the theory presented in this work, with neglecting cubic Dresselhaus term and taking into account full SOIs, respectively.

free path l_e is comparable to the wire width W, we cannot perform the step from

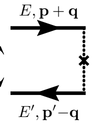

$$\sum_{\mathbf{q}} \quad = \frac{1}{2\pi\nu\tau}\sum_{\mathbf{q}} \mathcal{G}^{R}_{E,\sigma}(\mathbf{p}+\mathbf{q})\,\mathcal{G}^{A}_{E',\sigma'}(\mathbf{p'}-\mathbf{q}) \tag{4.47}$$

to

$$\int_0^{2\pi} \frac{\mathrm{d}\varphi}{2\pi}\,\left(1 + i\tau v\mathbf{e}_{\varphi}\left(\mathbf{Q} + 2m_e\mathbf{a}(\varphi).\mathbf{S}\right)\right)^{-1} \tag{4.48}$$

and integrate in Eq. (4.3) over the Fermi surface in a continuous way. Instead, we assume k_F/W to be finite and sum over the number of discrete channels $N = [k_F W/\pi]$, where $[\ldots]$ is the integer part. Because $H_{\gamma D} \sim E_F^2$ this constant term due to cubic Dresselhaus should reduce if we reduce the number of channels. If we expand the Cooperon to second order in $(\mathbf{Q} + 2e\mathbf{A} + 2m_e\hat{a}\mathbf{S})$ before averaging over the Fermi surface, $\langle\ldots\rangle$, and use the Matsubara trick, we get

$$\begin{aligned}\frac{C^{-1}}{D_e} &= 2f_1\left(Q_y + 2\alpha_2 S_x + 2\left(\alpha_1 - \gamma_D v^2\frac{f_3}{f_1}\right)S_y\right)^2 \\ &\quad + 2f_2\left(Q_x - 2\alpha_2 S_y - 2\left(\alpha_1 - \gamma_D v^2\frac{f_3}{f_2}\right)S_x\right)^2 \\ &\quad + 8\gamma_D^2 v^4\left[\left(f_4 - \frac{f_3^2}{f_2}\right)S_x^2 + \left(f_5 - \frac{f_3^2}{f_1}\right)S_y^2\right],\end{aligned} \tag{4.49}$$

with $m_e = 1$ and functions $f_i(\varphi)$ (App. E) which depend on the number of transverse modes N. In the diffusive case we can perform the continuous sum over the angle φ in Eq. (E.3)-(E.7), and we receive the old result with $f_1 = f_2 = 1/2$, $f_3 = 1/8$ and $f_4 = f_5 = 1/16$:

$$\begin{aligned}H_c = {}&(Q_y + 2\alpha_2 S_x + 2\left(\alpha_1 - \frac{1}{2}\gamma_D E_F\right)S_y)^2 + (Q_x - 2\alpha_2 S_y - 2\left(\alpha_1 - \frac{1}{2}\gamma_D E_F\right)S_x)^2 \\ &+ (\gamma_D E_F)^2(S_x^2 + S_y^2).\end{aligned} \tag{4.50}$$

4.5.1 Spin Relaxation at $Q_{\mathrm{SO}}W \ll 1$

In the first section we analyzed the lowest spin relaxation in wires of different direction in a (001) system. We have shown, that for every direction there is still a finite spin relaxation at wire width which fulfill the condition $Q_{\mathrm{SO}}W \ll 1$ due to cubic Dresselhaus SOC. It is clear that this finite spin relaxation vanishes when the width is equal to the Fermi wave length λ_F. In the following we show how this finite spin relaxation depends on the number of transverse channels N. We show in Ref. [WK] that the findings are consistent with calculations going beyond the perturbative ansatz. This is possible in a similar manner as has been done previously in Ref. [KM02] for wires without SOC, which showed the crossover of the magnetic phase shifting rate, which had been known before in the diffusive and ballistic limit, only.

To find the spectrum of the Cooperon Hamiltonian with boundary conditions as in Sec. 4.2.2, we stay in the 0-mode approximation in the Q space and proceed as before: According to Eq. (4.49), the non-Abelian gauge transformation for the transversal direction y is given by

$$U = \exp\left(-i\left[2\alpha_2 S_x + 2\left(\alpha_1 - \gamma_D v^2 \frac{f_3}{f_1}\right) S_y\right] y\right). \tag{4.51}$$

To concentrate on the constant width independent part of the spectrum we extract the absolute minimum at $Q = 0$, Fig. (4.4) and Fig. (4.5). A clear reduction of the absolute minimum is visible. Due to the factor f_3/f_1 in the transformation U, the decrease of the minimal spin relaxation depends also on the ratio of Rashba and linear Dresselhaus SOC.

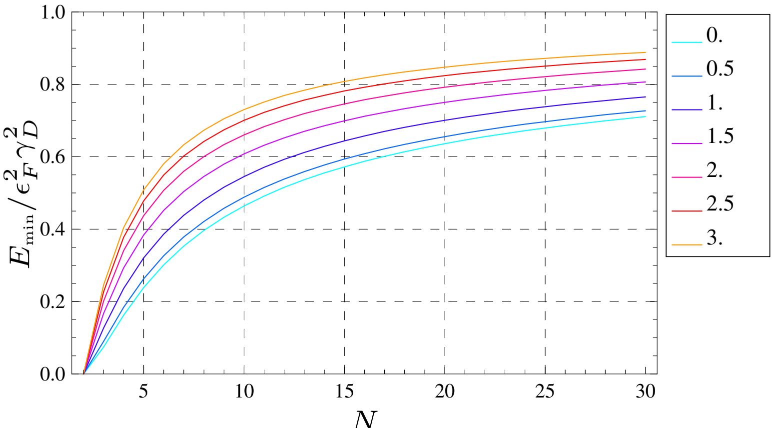

Figure 4.4: The lowest eigenvalues of the confined Cooperon Hamiltonian Eq. (4.49), equivalent to the lowest spin relaxation rate, are shown for $Q = 0$ for different number of modes $N = k_F W/\pi$. Different curves correspond to different values of α_2/q_s.

From Eq. (4.49) it is clear, that not only the H_{γ_D} is affected by the reduction of the number of channels N but also the shift of the lin. Dresselhaus SOC, α_1, in the orbital part. A model to extract the ratio of Rashba and lin. Dresselhaus SOC developed in Ref. [SANR09] by Scheid *et al.* did not show much difference between the strict 1D case and the non-diffusive case with wire of finite width. The results presented here should allow for extending the model to finite cubic Dresselhaus SOC. Deducing from our theory, the direction of the SO field should change with the number of channels due to the mentioned N dependent shift.

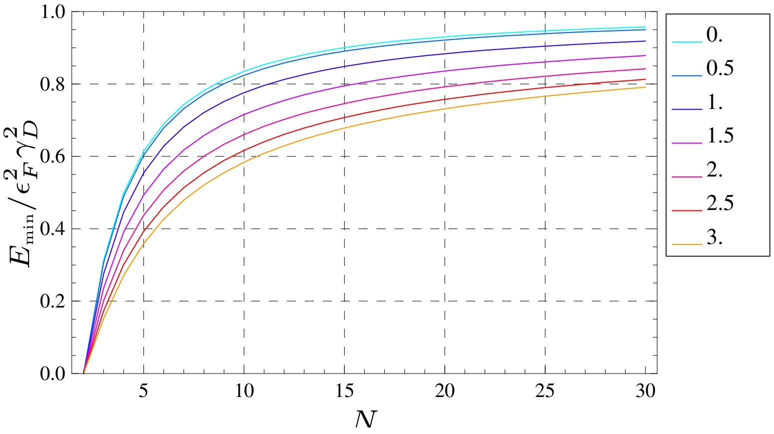

Figure 4.5: The lowest eigenvalues of the confined Cooperon Hamiltonian Eq. (4.49), equivalent to the lowest spin relaxation rate, are shown for $Q = 0$ for different number of modes $N = k_F W/\pi$. Different curves correspond to different values of α_1/q_s.

4.6 Conclusions

Summarizing the results of this chapter, we have characterized the anisotropy and width dependence of spin relaxation in a (001) quantum wire. There are special angles θ which are optimal for spin transport in quantum wires of finite width: The [110] and the [$\bar{1}$10] direction. At [110] we find the longest spin dephasing time T_2. If the absolute minimum of spin relaxation is found at [110] or [$\bar{1}$10] direction depends on the strength of cubic Dresselhaus and wire width. The findings for the spin dephasing time are in agreement with numerical results. The analytical expression for T_2 allows seeing directly the interplay between the cubic Dresselhaus SOC and the dimensional reduction, having effect on T_2. In addition, we analyzed the special case of a (110) system and found the minimal spin relaxation rates depending on Rashba and lin. and cubic Dresselhaus SOC in the presence of boundaries. This results can be used to understand width and direction dependent WL measurements in quantum wires. Finally, we have shown how the reduction of channels in the wire reduces the finite spin relaxation rate which is due to cubic Dresselhaus SOC and does not reduce if the wire is small, $Wq_s \ll 1$, and diffusive, $W \gg l_e$. The change in channel number also changes the shift of lin. Dresselhaus SOC strength, $\tilde{\alpha}_1$. This has to be considered if extracting SOC strength from wires with only few transverse channels.

Chapter 5

Spin Hall Effect

5.1 Introduction

In order to realize spintronic devices like the spin field effect transistor, one needs to induce spin polarized electrons in low dimensional electron systems (LDES)[icvacFDS04, DD90]. Spin polarized electrons can be generated by injecting a current with ferromagnetic metallic leads into the LDES. However, it has been found that in practice the efficiency of such spin injection is poor because of the conductivity mismatch. Therefore, recently there has been a strong effort to find new ways for generating polarized spin currents. One possibility is to use a T-shaped conductor with SOC as proposed by Yamamoto[YDKO06], whose efficiency is restricted however strongly by impurity scattering and is therefore only applicable to narrow wires with few channels. Another approach is to dope the semiconductor with magnetic impurities: When doped with several percents one speaks of dilute magnetic semiconductors. With transition metal atoms, like Mn, these materials become ferromagnetic, such as $\mathrm{In}_{1-x}\mathrm{Mn}_x\mathrm{As}$ which has been discovered by Ohno to have a ferromagnetic phase with a relatively high critical temperature[OMP$^+$92]. Due to the still relatively small concentration of impurities this system can still be manipulated in a wide range of carrier density, impurity concentration, and acceptor level energy: As these impurities not only provide spin, but also dope the system with holes, the density of charge carriers, and the Fermi energy can be changed, by changing their concentration. By choosing different elements, also the acceptor level energy can be changed. This together with the disorder provided by these magnetic impurities does change the magnetic properties substantially, since the effective magnetic coupling between the magnetic ions does depend itself on the

DOS, their average distance and the disorder strength [SBK+10].

Another way for efficiently injecting spin currents into semiconductors is to make use of the spin Hall effect (SHE). This effect was first proposed by D'yakonov and Perel [DP71a] and describes in today's terminology the extrinsic SHE which requires spin dependent impurity scattering. It was experimentally confirmed by the angle-resolved optical detection of spin polarization at the edges of a two-dimensional layer [WKSJ05, KMGA04]. The theory of the SHE has been developed in the last 10 years, as reviewed in Refs. [Sch06, ERH07].

The spin transport not only occurs due to the spin precession in the bulk but is affected by the scattering from nonmagnetic impurities, which can depend on the direction of the spin itself due to the so-called skew scattering and the side jump mechanism[Sch06]. In the first part of the following chapter, we will outline the formalism to calculate analytically the SHE which arises even in the absence of impurities, the so-called intrinsic SHE, which is due to the bulk SOC. For the clean case, we will include both, Rashba and Dresselhaus SOC. In the second part we focus on numerical methods: The first attempt is application of exact diagonalization which has of course strong limitations concerning the system size. To overcome this limitations, we apply the Kernel Polynomial Method (KPM) in the last part of this thesis. It is first applied to treat the metal-insulator transition (MIT) in a symplectic system, finally we calculate the SHE using the KPM.

5.1.1 About the Definition of Spin Current

We have learned in Sec. 2.3.4 that in presence of the spin-orbit interaction, the spin current components are not conserved[CSS+04, SZXN06] even if we assume no spin relaxation: In the continuity equation

$$\frac{\partial s_z}{\partial t} + D_e \nabla \mathbf{J}_{\text{spin}} = T_s - \frac{1}{(\hat{\tau}_s)_{ij}} \mathbf{s}_j \tag{5.1}$$

$$= \tau \langle \nabla \mathbf{v}_F \left(\mathbf{B}_{\text{SO}}(\mathbf{k}) \times \mathbf{S} \right)_i \rangle - \frac{1}{(\hat{\tau}_s)_{ij}} \mathbf{s}_j . \tag{5.2}$$

an additional torque term T_s appears in contrast to Eq. 2.12 besides the term which describes the spin relaxation rate $1/\tau_s$. It follows that Noether's theorem is not applicable to define the spin current. This is a reason why the comparison between results done with Kubo formalism and calculations using Landauer-Büttiker approach is not trivial, where the spin current in the latter is defined by[MM05]

$$I^s_{p,\mu} = \frac{1}{4\pi} \sum_{p \neq q,\, \nu} \mathrm{Tr}[\Gamma^\mu_p G^R \Gamma^\nu_q G^A](V_p - V_q), \tag{5.3}$$

where

$$\Gamma^\mu_p = i(\Sigma^\mu_p - (\Sigma^\mu_p)^\dagger), \tag{5.4}$$

with the retarded self energy Σ^μ_p due to coupling of lead p, which has voltage V_p, and sample for spin channel μ and advanced and retarded Green's function $G^{A/R}$. However, in an experiment the SHE can be measured. This measurement has to be connected to the theoretical description using linear response to a transverse electrical field with the frequency ω which yields, Appendix B, Eq. (B.16),

$$\sigma_{\mu\nu}(\omega) = \frac{i}{V} \sum_{m,n} \frac{(f(E_m) - f(E_n))}{E_n - E_m} \frac{\langle m\,|j_\nu|\,n\rangle\,\langle n\,|j_\mu|\,m\rangle}{E_n - E_m + \omega + i\eta}. \tag{5.5}$$

To calculate the spin Hall conductivity (SHC) the correlation function consists, in contrast to charge conductivity, of the charge current and a current which contains a spin operator. In the simplified model we use the spin current which is given by the anticommutator of the spin and the group velocity $\mathbf{v} = i[\mathbf{H}, \mathbf{r}]$,

$$\mathbf{J}^z = \frac{\hbar}{4}\{\sigma_z, \mathbf{v}\}. \tag{5.6}$$

This spin current does not differ from the one defined in Sec. 2.3.[ESL05, BNnM04] Note that this quantity is dissipationless, because the spin current is even under the time-reversal operation.

5.2 SHE without Impurities: Exact Calculation

We consider the Hamiltonian for a lattice which provides linear Rashba, Eq. (2.15), and linear and cubic Dresselhaus SOC, Eq. (2.14), as introduced in Sec. 2.3.3. The confinement to generate the 2D electron gas is in [001] direction. In order to do calculations numerically, one needs to define a tight binding model on a discrete lattice of finite lattice spacing a. It has the following characterization:

- square lattice,

- localized site orbitals are of s symmetry.

Applying this assumptions the tight-binding version of the Hamiltonian is given by

$$\begin{aligned}
H &= H_0 + H_R + H_{D,lin} + H_{D,cubic}, \qquad (5.7)\\
&= \sum_{i,\sigma} \epsilon_i c^\dagger_{i,\sigma} c_{i,\sigma} - t \sum_{\langle i,j\rangle,\sigma} c^\dagger_{i,\sigma} c_{j,\sigma}\\
&\quad + \frac{\alpha_2}{2a} \sum_{\substack{\sigma,\sigma'\\ l,m}} \{ c^\dagger_{l,m,\sigma'} (i\sigma_y)_{\sigma\sigma'} c_{l+1,m,\sigma} - c^\dagger_{l,m,\sigma'} (i\sigma_x)_{\sigma\sigma'} c_{l,m+1,\sigma} \}\\
&\quad + \frac{\alpha_1}{2a} \sum_{\substack{\sigma,\sigma'\\ l,m}} \{ c^\dagger_{l,m,\sigma'} (i\sigma_x)_{\sigma\sigma'} c_{l+1,m,\sigma} - c^\dagger_{l,m,\sigma'} (i\sigma_y)_{\sigma\sigma'} c_{l,m+1,\sigma} \}\\
&\quad + \frac{\gamma_D}{a^3} \Bigg\{ \sum_{\substack{\sigma,\sigma'\\ l,m}} \{ c^\dagger_{l,m,\sigma'} (-i\sigma_x)_{\sigma\sigma'} c_{l+1,m,\sigma} + c^\dagger_{l,m,\sigma'} (i\sigma_y)_{\sigma\sigma'} c_{l,m+1,\sigma} \}\\
&\quad + \frac{1}{2} \sum_{\substack{\sigma,\sigma'\\ l,m}} \{ c^\dagger_{l,m,\sigma'} (i(\sigma_x - \sigma_y))_{\sigma\sigma'} c_{l+1,m+1,\sigma} + c^\dagger_{l,m,\sigma'} (i(\sigma_x + \sigma_y))_{\sigma\sigma'} c_{l+1,m-1,\sigma} \} \Bigg\}\\
&\quad + h.c.. \qquad (5.8)
\end{aligned}$$

where $c^\dagger_{i,\sigma}$ is the creation operator at site index i with spin $\sigma = \uparrow, \downarrow$ and $c^\dagger_{l,m,\sigma}$ the creation operator at site $(\mathrm{index}_x, \mathrm{index}_y) = (l, m)$. The hopping coupling t is given by $t = 1/(2m_e a^2)$ with the lattice constant a. In the following we take the cubic Dresselhaus term only as a shift of, $\tilde{\alpha}_1 = \alpha_1 - 2\gamma_D/a^2$, according to Eq. (3.44), and assume a clean system, i.e the on-site energy is set to $\epsilon_i = 0$. Applying a Fourier transformation to Eq. (5.7) and going to momentum space we get (we set $a \equiv 1$)

$$\begin{aligned}
H = \sum_{\substack{kx,ky\\ \sigma,\sigma'}} \Bigg\{ & \underbrace{-2t(\cos(k_x) + \cos(k_y))}_{E_0} \delta_{\sigma\sigma'} c^\dagger_{k,\sigma'} c_{k,\sigma}\\
& + (\alpha_2 \sin(k_y) - \tilde{\alpha}_1 \sin(k_x)) c^\dagger_{k,\sigma'} (\sigma_x)_{\sigma\sigma'} c_{k,\sigma}\\
& + (\tilde{\alpha}_1 \sin(k_y) - \alpha_2 \sin(k_x)) c^\dagger_{k,\sigma'} (\sigma_y)_{\sigma\sigma'} c_{k,\sigma} \Bigg\}. \qquad (5.9)
\end{aligned}$$

The corresponding eigenvalues are

$$E_\pm(\mathbf{k}) = E_0(\mathbf{k}) \pm \Delta(\mathbf{k}) \qquad (5.10)$$

with $\Delta(\mathbf{k}) = \sqrt{(\alpha_2^2 + \tilde{\alpha}_1^2)(\sin(k_x)^2 + \sin(k_y)^2) - 4\alpha_2\tilde{\alpha}_1 \sin(k_x)\sin(k_y)}$ ($E_-(\mathbf{k})$ is plotted in Fig. 5.1). The eigenvectors are given by

$$|+/-\rangle = \frac{1}{\sqrt{2}} \begin{pmatrix} \frac{\mp(\{\tilde{\alpha}_1 \sin(k_x) - \alpha_2 \sin(k_y)\} + i\{\tilde{\alpha}_1 \sin(k_y) - \alpha_2 \sin(k_x)\})}{\Delta} \\ 1 \end{pmatrix} \tag{5.11}$$

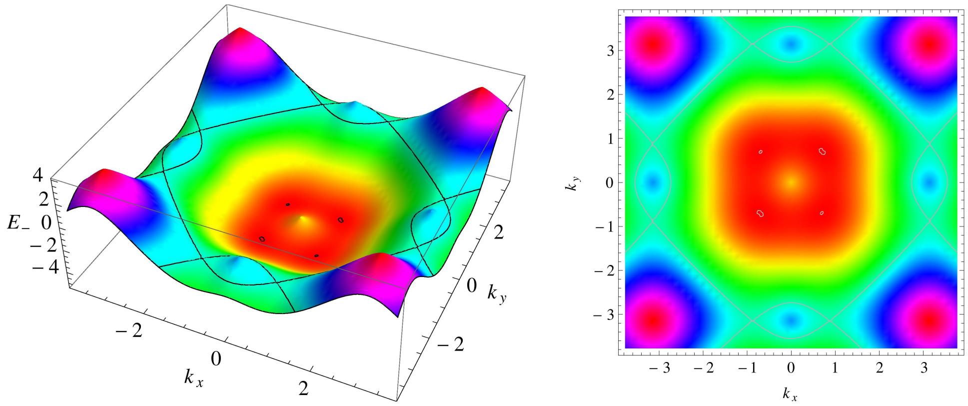

(a)

(b)

Figure 5.1: Energy band $E_-(\mathbf{k})$, Eq. (5.10) is plotted for pure Rashba SOC as function of wave vector $\mathbf{k}$. The contour lines indicate the energy at which one finds a Van Hove singularity in the DOS (below half-filling).

To calculate the SHE using Kubo formula, Eq. (5.5), we have to calculate the matrix elements of spin current operator and velocity operator. In the site basis of our lattice they have the following form:

$$\langle n| \mathbf{v} |m\rangle = \langle 0| \sum_{\substack{ij \\ \alpha\beta}} \psi_n^*(i,\alpha) c_{i\alpha} \mathbf{v} \psi_m(j,\beta) c_{j\beta}^\dagger |0\rangle \,, \tag{5.12}$$

$$= \langle 0| \sum_{\substack{ij \\ \alpha\beta}} \psi_n^*(i,\alpha) c_{i\alpha} \frac{1}{i} [\mathbf{r}, \mathbf{H}] \psi_m(j,\beta) c_{j\beta}^\dagger |0\rangle \,, \tag{5.13}$$

with $\mathbf{r} = \sum_{k\sigma} r_k c_{k\sigma}^\dagger c_{k\sigma}$

$$= \frac{1}{i} \langle 0| \sum_{k\gamma} \sum_{\substack{ij \\ \alpha\beta}} \psi_n^*(i,\alpha) c_{i\alpha} [r_k c_{k\gamma}^\dagger c_{k\gamma}] \mathbf{H} c_{j\beta}^\dagger \psi_m(j,\beta)$$

$$- \psi_n^*(i,\alpha) c_{i\alpha} \frac{1}{i} \mathbf{H} [c_{k\gamma}^\dagger c_{k\gamma} r_k] c_{j\beta}^\dagger \psi_m(j,\beta) |0\rangle \,, \tag{5.14}$$

with $c_{i\alpha}c^{\dagger}_{i\alpha}c_{i\alpha}\left|0\right\rangle = c_{i\alpha}\left|0\right\rangle$ and $c_{i\alpha}c^{\dagger}_{j\beta}c_{j\beta} = c^{\dagger}_{j\beta}c_{j\beta}c_{i\alpha}$

$$= \frac{1}{i}\sum_{\substack{ij\\ \alpha\beta}}\psi^{*}_{n}(i,\alpha)[(r_i - r_j)H^{\alpha\beta}_{ij}]\psi_m(j,\beta), \tag{5.15}$$

$$\mathbf{v} = \frac{1}{i}\sum_{\substack{ij\\ \alpha\beta}}(r_i - r_j)H^{\alpha\beta}_{ij}, \tag{5.16}$$

where we used i, j and k as site indices and the other for spin. Using the definition of the spin current, Eq. (5.6), we get accordingly

$$\left\langle n\right|\mathbf{J}^{z}\left|m\right\rangle = \frac{e}{4i}\sum_{\substack{ij\\ \alpha\beta}}(r_i - r_j)\psi_n(i,\alpha)\{\sigma_z, H\}^{\alpha\beta}_{ij}\psi_n(j,\beta). \tag{5.17}$$

Going into momentum space we are left with

$$\mathbf{v}_y = \sum_{k_y} 2t\sin(k_y)\mathbb{1} + (\alpha_2\sigma_x + \tilde{\alpha}_1\sigma_y)\cos(k_y), \tag{5.18}$$

and for the spin current

$$\mathbf{J}^{z}_{x} = \sum_{k_x} t\sin(k_x)\sigma_z. \tag{5.19}$$

The last Eq. follows from $\{\sigma_z, H_D\} = \{\sigma_z, H_R\} = 0$. To evaluate the rhs of Eq. (5.5) we need the matrix elements of both operators in the eigenvalue basis, which yields the pure imaginary result

$$\left\langle\mp\right|J^{z}_{x}\left|\pm\right\rangle\left\langle\pm\right|v_y\left|\mp\right\rangle = \pm it(\alpha_2^2 - \tilde{\alpha}_1^2)\frac{\sin(k_x)^2\cos(k_y)}{\Delta(\mathbf{k})}. \tag{5.20}$$

Assuming zero temperature to calculate σ^{z}_{xy} , Eq. (5.5) finally simplifies to[NSSM05, MMF08]

$$\sigma^{z}_{xy} \equiv \sigma_{\text{SH}} = -\frac{ie}{V}\sum_{m,n}\frac{f(E_m) - f(E_n)}{E_m - E_n}\frac{\left\langle m\right|J^{z}_{x}\left|n\right\rangle\left\langle n\right|v_y\left|m\right\rangle}{(E_m - E_n) + i\eta}, \tag{5.21}$$

$$= 2\frac{e}{V}\sum_{E_m<E_F<E_n}\frac{\Im(\left\langle m\right|J^{z}_{x}\left|n\right\rangle\left\langle n\right|v_y\left|m\right\rangle)}{(E_n - E_m)^2 + \eta^2}. \tag{5.22}$$

Applying this to the lattice case with L^2 sites, we get

$$\sigma_{\text{SH}} = \frac{e}{L^2}\sum_{kx,ky}\left\{(f_{E^-(k)} - f_{E^+(k)})\frac{\Im(\left\langle -\right|J^{z}_{x}\left|+\right\rangle\left\langle +\right|v_y\left|-\right\rangle)}{(E^+(k) - E^-(k))^2 + \eta^2}\right.$$
$$\left. + (f_{E^+(k)} - f_{E^-(k)})\frac{\Im(\left\langle +\right|J^{z}_{x}\left|-\right\rangle\left\langle -\right|v_y\left|+\right\rangle)}{(E^-(k) - E^+(k))^2 + \eta^2}\right\}, \tag{5.23}$$

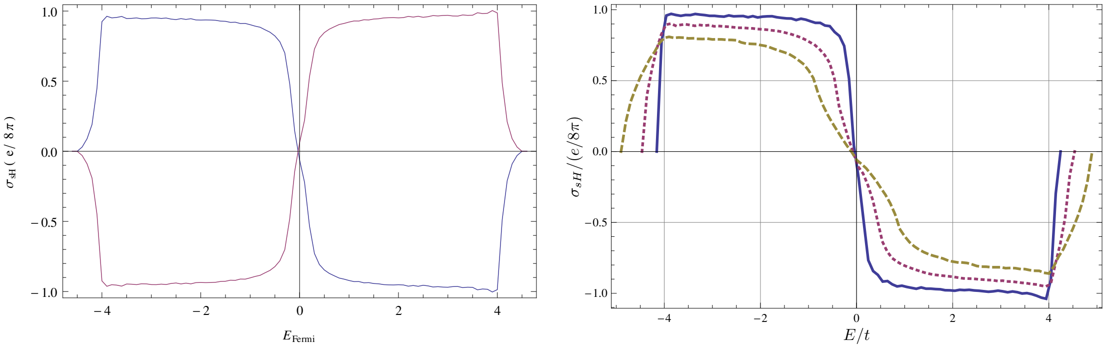

(a) (b)

Figure 5.2: (a) SHC $\sigma_{\rm SH}$ as a function of Fermi energy E_F, in a clean system of size $L^2 = 170 \times 170$ with both Rashba and linear Dresselhaus SOC with $\alpha_2 > \alpha_1$ (blue curve) and $\alpha_2 < \alpha_1$ (red curve). (b) SHC $\sigma_{\rm SH}$ as a function of Fermi energy E_F, in a clean system of size $V = 150 \times 150$ with only Rashba SOC of strength $\alpha_2 = 0.8t$ (blue/solid), $\alpha_2 = 1.4t$ (red/dotted) and $\alpha_2 = 2t$ (yellow/dashed).

where we used Eq. (5.20). The level broadening η is introduced for regularization in finite-size systems [NSSM05, MMF08]. It is chosen to be of the order of the level spacing δE, vanishing in the thermodynamic limit. Integration over the Brillouin zone we finally arrive at the clean solution for the SHC which is plotted in Fig. (5.2).

Results and Discussion

The SHC shows electron-hole symmetry: The SHC vanishes at half-filling, $E_F = 0$, and is an odd function of E_F. From Eq. (5.18) one can see that the sign-change is due to the term which is proportional to the SOC strength. It is worth noticing that an evaluation of the commutator $[\mathbf{r}, \mathbf{H}]$ in Eq. (5.13) will lead to

$$\mathbf{v} = -\frac{i}{m_e}\partial_{\mathbf{R}}\mathbb{1}_{2\times 2} + \alpha_2(\sigma_x\mathbf{e}_y - \sigma_y\mathbf{e}_x) + \alpha_1(\sigma_y\mathbf{e}_y - \sigma_x\mathbf{e}_x) \tag{5.24}$$

(compare for pure Rashba case e.g. with [SCN$^+$04]). A straight forward tight binding formulation of the velocity operator in this form would yield, in contrast to Eq. (5.16), on-site matrix elements proportional to the spin-orbit interaction which could yield unphysical results: The contribution of the velocity operator to the SHC would give $\langle +|\, v_y\, |-\rangle = i\alpha_2 \sin(k_x)/\Delta(\mathbf{k})$. Obviously the missing $\cos(k_y)$ factor leads to an even and therefore wrong SHC function of E_F. Because the linear in momentum SO interactions can be interpreted

as an effective magnetic field, which however does not break time reversal symmetry, this is very similar to the case where a Peierls substitution is applied,[Pei33] i.e. where a Peierls phase is added to the electron whenever it hops in the direction of finite vector field.
The sign changes according to the sign of $\alpha_2^2 - \tilde{\alpha}_1^2$ and exhibits the value $e/(8\pi)$ for small filling with the condition that both bands, $E_\pm$, are filled, independent of the strength of SOC. This can bee seen by expanding the spectrum around the Γ point which yields[She04]

$$\begin{aligned} \sigma_{\text{SH}} &= \frac{e}{16 m_e \pi^2} \int_0^{2\pi} \mathrm{d}\varphi \, \frac{(\alpha_2^2 - \tilde{\alpha}_1^2)\cos^2(\varphi)(k_+ - k_-)}{(\alpha_2^2 + \tilde{\alpha}_1^2 - 2\alpha_2\tilde{\alpha}_1 \sin(2\varphi))^{\frac{3}{2}}}, && (5.25) \\ &= \frac{e}{8\pi} \frac{\alpha_2^2 - \tilde{\alpha}_1^2}{|\alpha_2^2 - \tilde{\alpha}_1^2|}, && (5.26) \end{aligned}$$

with $k_x = k\cos(\varphi)$ and $k_x = k\sin(\varphi)$.
Looking at the results from the calculation on a clean lattice, Fig. (5.2) (b), it can be seen that the value $e/(8\pi)$ decreases with increasing SOC strength in the case of pure Rashba SOC. This can be understood by noticing that the value of the SHC[SCN$^+$04]

$$\sigma_{\text{SH}} = \frac{e}{16 m_e \pi \alpha_2}(k_{F+} - k_{F-}) \tag{5.27}$$

is diminished when we add corrections to the parabolic assumption: On the lattice we have

$$\begin{aligned} (k_{F+} - k_{F-}) &= \arccos\left(\frac{2}{1 + \left(\frac{\alpha_2}{2t}\right)^2} - 1\right) && (5.28) \\ &= 2m_e\alpha_2 - \frac{2}{3}(m_e\alpha_2)^3 + \mathcal{O}(m_e\alpha_2)^4 && (5.29) \end{aligned}$$

and therefore the diminishment is given by

$$\sigma_{\text{SH}} = \frac{e}{8\pi} - \frac{e}{24\pi}(m_e\alpha_2)^2. \tag{5.30}$$

5.3 Numerical Analysis of SHE

5.3.1 Exact Diagonalization

For linear Rashba coupling, the value $\sigma_{\text{SH}} = e^2/(8\pi)$, as presented in the previous section, has been obtained both by analytical calculations in the continuum model, and by numerical calculations of the tight binding model[Sch06]. However, in the presence of nonmagnetic impurities, the DC spin Hall conductance is diminished to exactly zero, as soon as the system size L exceeds the elastic mean free path l_e. In the case of δ-function potential and pure linear Rashba SOC, in the thermodynamic limit this result is even independent of the impurity strength, as discovered by Schwab and Raimondi[RS05] by using self-consistent Born approximation: The vertex correction in the ladder approximation cancel exactly the term coming from the one-loop part. Following Rashba, Ref. [Ras04], this can be understood as follows: Corresponding to Eq. (5.10) and Eq. (5.22) we have, at low filling, positive contribution to σ_{SH} due to interbranch transitions between the occupied (E_+) and unoccupied (E_-) states. Adding a perturbation by applying an infinitesimal small magnetic field, intrabranch transitions at the Fermi energy give rise to a negative contribution. Surprisingly, this additional contribution cancels the first and we are left with zero SHC. This counterintuitive finding led to several controversies because the first numerical calculations in this field showed finite SHC when extrapolated to infinite large samples[NSJ$^+$05]. However, new numerical results, e.g. Ref. [NSJ$^+$06] as an erratum to Ref. [NSJ$^+$05], showed agreement with the analytical predictions. In contrast, taking into account also spin-orbit terms which are cubic in momentum, as they are present in any system with broken inversion symmetry (cubic Dresselhaus terms), or in quantum wells with strongly asymmetric confinement (cubic Rashba terms), the spin Hall conductance has a quite universal value, of $\sigma_{\text{SH}} = Ne^2/(8\pi)$, where N is the number of times the spin-orbit field $B_{\text{SO}}(\mathbf{k})$ winds around a circle, as the momentum is moved once around the Fermi surface[Sch06].

Resonant Impurities

The effect of resonant impurities and of magnetic impurities on the SHC has not been studied yet in that detail[LX06, WLZ07a]. Especially, it is unclear how large its magnitude is, when the Fermi energy is in the vicinity of the resonant levels close to the metal-insulator transition, where it has been observed that the spin relaxation rate is minimal[DKK$^+$02], making it a potentially attractive regime for spintronic applications.

In the following we analyze the reduction of the SHC in a finite system with periodic boundary conditions in presence of non-magnetic impurities of binary type, i.e. on-site potential $V_i = p_i V$ where $p_i = 1$ for impurity sites and $p_i = 0$ otherwise. The lattice is assumed to be contaminated with 10% of impurities. To have a better understanding of how the SHC changes with the strength of impurities, V, we first calculate the DOS. The result is presented in Fig. 5.3. For small V one would expect the Van Hove singularity at half filling. Due to finite Rashba SOC it is split to finite energies $E = \pm(2t - \sqrt{4+\alpha_2^2}t)$, indicated in Fig. 5.1 for the energy below half filling. If the impurity strength is increased, a preformed impurity band is created. Using exact diagonalization[1] and applying the Kubo formalism, Eq. 5.22, we calculate the SHC. Exemplarily we show the result for $\sigma_{\,\text{SH}}(E)$ at $V = -2.8t$ in Fig. 5.4. The SHC is strongly reduced but shows an additional maximum at energy where the preformed impurity band is located, as can be seen in comparison with the DOS, Fig. 5.4(b).

To analyze the reduction of SHC for a given filling n, we vary the impurity strength up to $V = -5t$ and keep the concentration constant at 10%. Similar to the results in the case of block distribution of impurity strength, we see a monotone suppression at all fillings, even in the preformed impurity band, Fig. 5.5.

5.3.2 Kernel Polynomial Method

The numerical calculations presented in the previous section, which were based on exact diagonalization using LAPACK[LAP] routines, are limited to small system sizes. This leads to finite size effects like oscillations in the SHC, e.g. Fig. 5.4(b) above half filling. For further calculations concerning the role of the impurity band it is necessary to do a finite size scaling analysis and consider system-sizes beyond $L = 64$ which makes an exact treatment on current hardware impossible: for a D-dimensional matrix such a calculation requires memory of the order of D^2, and the LAPACK routine scales as D^3.

Another problem is the adjustment of the cutoff η, see Eq. (5.22), which has to be taken with care as analyzed e.g. by Nomura *et al.*, Ref. [NSSM05].

To overcome the limitation on small systems, there are different numerical order-D methods. One procedure is the time evolution projection method developed by Tanaka and Itoh[TI98], which was already used to calculate SHC[MMF08, MM07]. However, the algorithm requires both the choice of a sufficient number of time steps and an adjustment of cutoff η. A more effective method, which uses Chebyshev expansion based on Kernel Polynomial Method, will be presented in the following.

---

[1] using LAPACK[LAP] and OpenMP[OMP] in C++

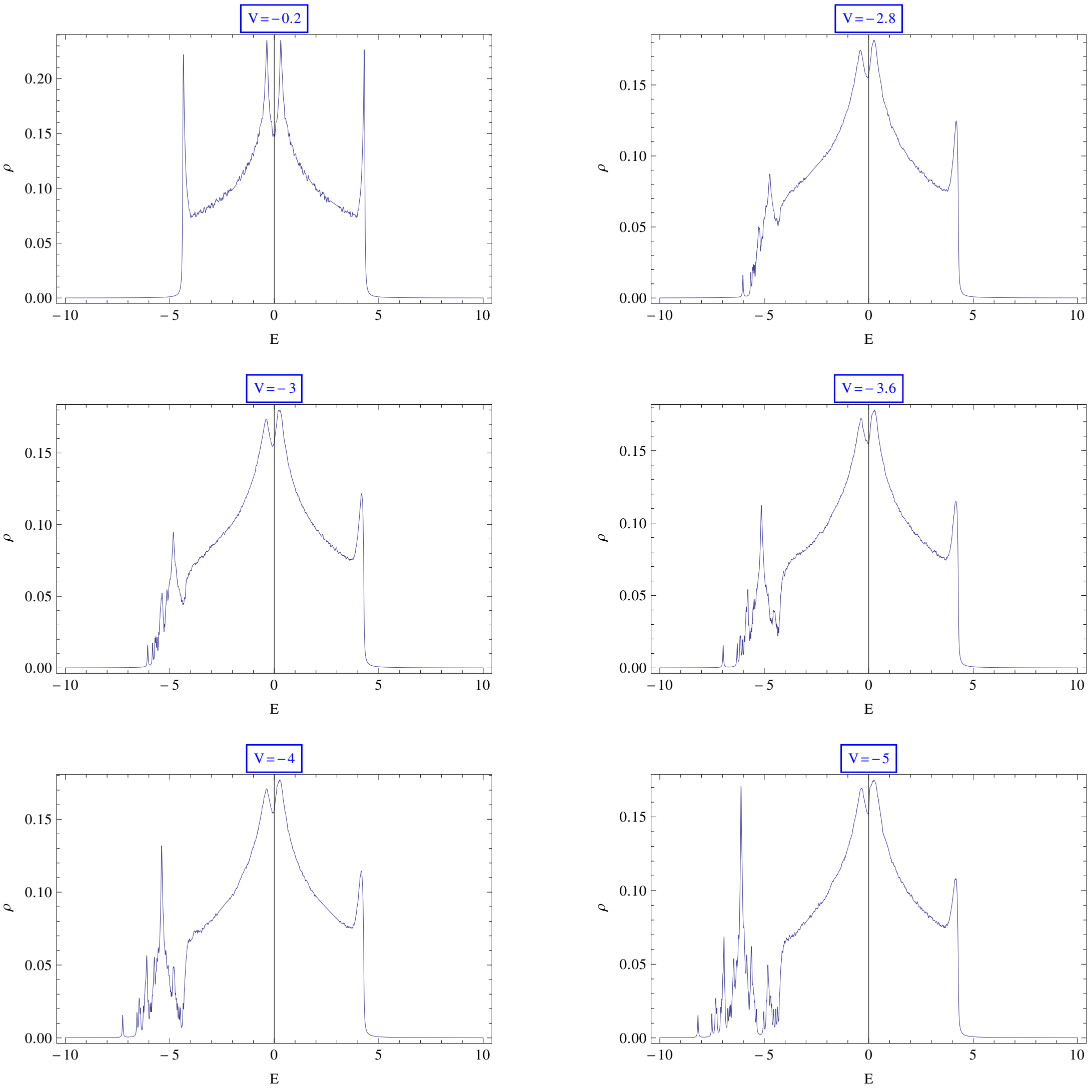

Figure 5.3: DOS, as a function of Fermi energy in units of t, in presence of impurities of binary type with a concentration of 10% calculated using exact diagonalization. The system size is $L^2 = 32^2$, and the SOC is Rashba type with $\alpha_2 = 1.2t$ with cutoff $\eta = 0.02t$.

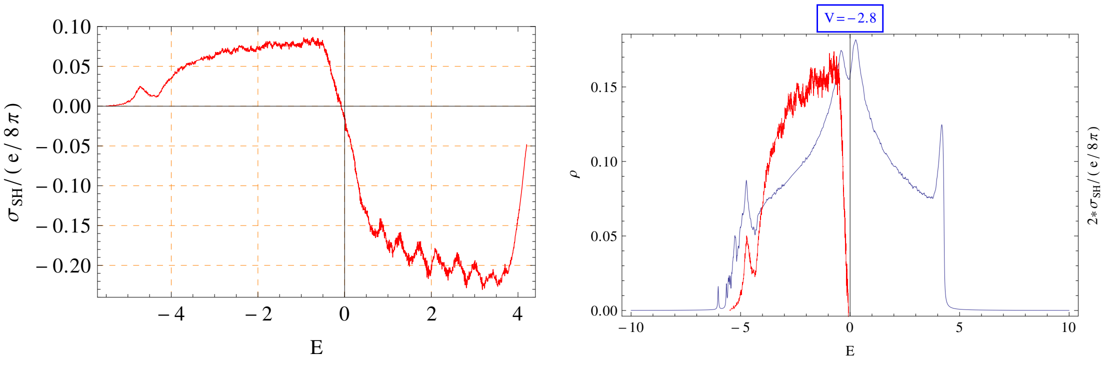

(a) (b)

Figure 5.4: (a) SHC, as a function of Fermi energy in units of t, in presence of impurities of binary type calculated using exact diagonalization. The impurity strength is $V = -2.8t$ with a concentration of 10%. The system size is $L^2 = 32^2$, and the SOC is Rashba type with $\alpha_2 = 1.2t$ with cutoff $\eta = 0.06$. (b) Comparison of a) with DOS (blue curve).

KPM in a Nutshell

The Kernel Polynomial Method (KPM) was first proposed by Silver *et al.*[SR94] to calculate DOS of large systems. It is a method to expand integrable functions defined on a finite interval $f : [a, b] \longrightarrow \mathbb{R}$ in terms of Chebyshev polynomials of the first,

$$T_n(x) = \cos(n \arccos(x)), \tag{5.31}$$

or second kind

$$U_n(x) = \frac{\sin((n+1)\arccos(x))}{\sin(\arccos(x))},$$

i.e., we can write for instance

$$f(x) = \frac{1}{\pi\sqrt{1-x^2}} \left[\mu_0 + 2 \sum_{n=1}^{\infty} \mu_n T_n(x) \right], \tag{5.32}$$

if we assume that the function f has been rescaled to $\tilde{f} : [-1, 1] \longrightarrow \mathbb{R}$ and can be expanded using the polynomials of the first kind, which are (as the one of the second kind) defined on the interval $[-1, 1]$. If so, the coefficients are given by

$$\mu_n = \int_{-1}^{1} \mathrm{d}x \, \tilde{f}(x) T_n(x). \tag{5.33}$$

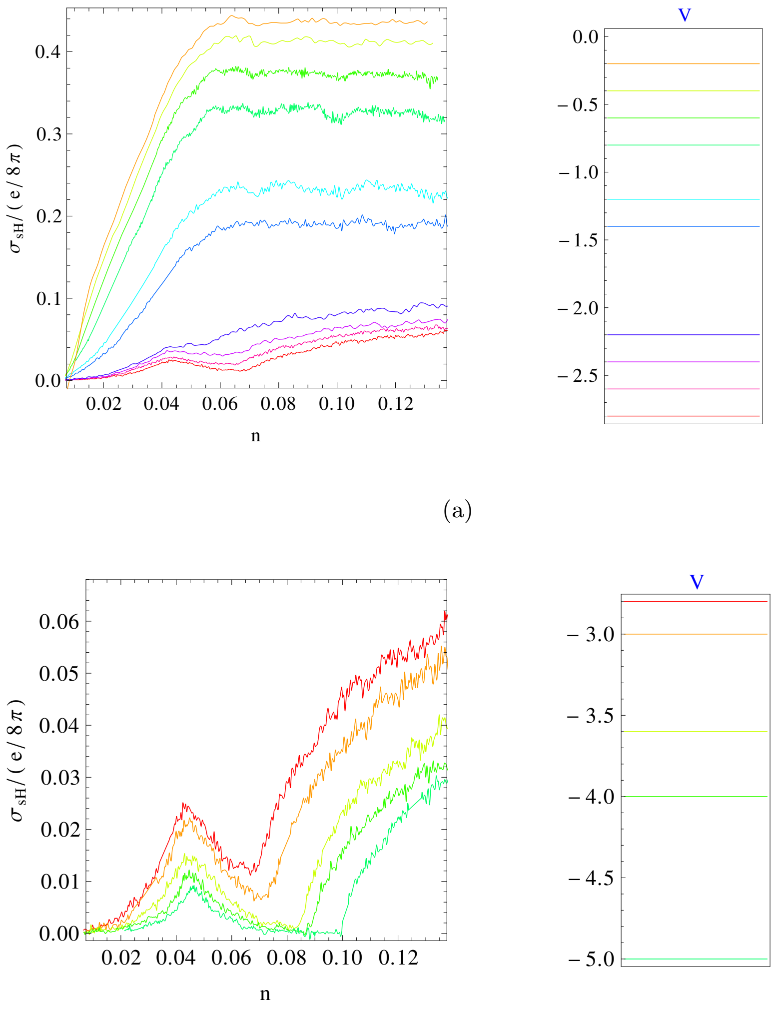

(a)

(b)

Figure 5.5: SHC σ_{SH} as function of filling n in presence of impurities of binary type calculated using exact diagonalization. The impurity concentration is set to 10% for all plots and the average is performed over 200 impurity configurations. The system size is $L^2 = 32^2$, and the SOC is Rashba type with $\alpha_2 = 1.2t$ with cutoff $\eta = 0.06$ (a) $V = -0.2t \ldots -2.8t$ (b) $V = -2.8t \ldots -5t$.

Using the recursion relations of the polynomials,

$$\begin{aligned} &T_0(x) = 1, \;\; T_{-1}(x) = T_1(x) = x, \\ &T_{m+1}(x) = 2xT_m(x) - T_{m-1}(x), \end{aligned} \tag{5.34}$$

and correspondingly for the polynomials of the second kind

$$\begin{aligned} &U_0(x) = 1, \;\; U_{-1}(x) = 0, \\ &U_{m+1}(x) = 2xU_m(x) - U_{m-1}(x), \end{aligned} \tag{5.35}$$

one can calculate the expansion coefficients μ_n iteratively. Replacing the variable x by the Hamiltonian one can calculate various spectral quantities. The simplest example is the calculation of the spectral density,

$$\rho(E) = \frac{1}{D} \sum_{k=0}^{D-1} \delta(E - E_k), \tag{5.36}$$

with the coefficients given by

$$\begin{aligned} \mu_n &= \int_{-1}^{1} \mathrm{d}x \, \rho(x) T_n[x] & (5.37) \\ &= \frac{1}{D} \mathrm{Tr}[T_n(\tilde{H})], & (5.38) \end{aligned}$$

where $\tilde{H}$ is the rescaled Hamiltonian with all D eigenvalues inside the interval $[-1, 1]$. The efficiency of the procedure is not yet evident. This changes if one realizes the following aspects:

- Self averaging properties allow for replacing the trace over the operator by a relatively small number $R \ll D$ of random vectors

  $$|r\rangle = \sum_{i=0}^{D-1} \zeta_{r_i} |i\rangle \,, \tag{5.39}$$

  where the amplitudes $\zeta_{r_i} = e^{i\phi}$ are random phases on site i. This makes the effort for the calculation of M coefficients μ_n *linear in D.*

- The most time consuming operation in this procedure is the matrix-vector multiplication (Appendix F). Due to the fact that the number of neighbors which a site has in the presented systems, the full multiplication can be replaced by sparse-matrix operations using a decomposition of the operators into a matrix which contains the connectivity information of the sites and a matrix where the hopping matrices according to the kind of hopping (e.g. with next nearest neighbor) are stored, as explained in more detail in Appendix F.

Adjusting the number of Moments in the KPM

Using exact diagonalization to calculate e.g. SHC as presented in Sec. 5.2 and Sec. 5.3.1, we were forced to adjust the cutoff η in the Kubo formula, Eq. (5.5) to get the 2D limit. Otherwise, we would be left with results which are highly oscillatory dependent on the Fermi energy. In the KPM the Hamiltonian is approximated by a finite polynomial, therefore the cutoff is implicitly set by choosing the number of moments M. Such a cutoff, which is inevitable in numerical calculations, leads i.g. to Gibbs oscillations, especially when the expanded function includes discontinuities or singularities. Therefore the expanded function is convoluted with a particular kernel (in our case the Jackson kernel) which damps this oscillations.

Exact Calculations on a finite lattice result in δ peaks in the DOS which are broadened due to the polynomial cutoff. The broadening can be approximated by Gauss curves of widths σ. To do finite-size analysis it is crucial to keep the same number of states within the kernel, i.e. within the distance of σ.[SSB$^+$10] Choosing a number of moments M in the KPM which is too large will lead to oscillations which are due to finite size of the system as can be seen in Fig. (5.6). On the other hand, a too small number will smear out features of the system which are independent of the size. This consideration leads to the condition $\sigma \overset{!}{>} \Delta$, with the averaged level spacing Δ. It is helpful to analyze the relation between M and the broadening σ. This can be done by a convolution of a δ-distribution with the mentioned kernel, which leads to[WWAF06]

$$M = \frac{\pi t}{\sigma}, \tag{5.40}$$

and at the boundaries

$$M = \left(\frac{\pi t}{\sigma}\right)^{2/3}.$$

This leads us to the following condition:

$$\sigma \overset{!}{>} \Delta \tag{5.41}$$

$$\frac{\pi t}{M} > \frac{D_B}{N} \tag{5.42}$$

$$M < \frac{\pi t N}{D_B}, \tag{5.43}$$

with the band width D_B, and the number of states N.
To get an impression of the relation between both the η cutoff in exact diagonalization and the finite number of moments in the KPM, we fix the system size, apply Rashba SOC, and calculate the DOS using the eigenvalues E_i calculated with exact diagonalization,

$$\rho_\eta(E) = \frac{1}{\pi} \sum_\lambda \Im \left[\frac{1}{E - E_\lambda + i\eta} \right]. \tag{5.44}$$

Now ρ can be calculated using KPM, and M is adjusted to fit best to $\rho_\eta(E)$. The relation between M and η is plotted in Fig. (5.6). Over a large interval of M we have $\eta \sim 1/M$. Only when the oscillations are too strong the differences between the Lorentz kernel, i.e. using Eq. (5.44), and the Jackson kernel appear.

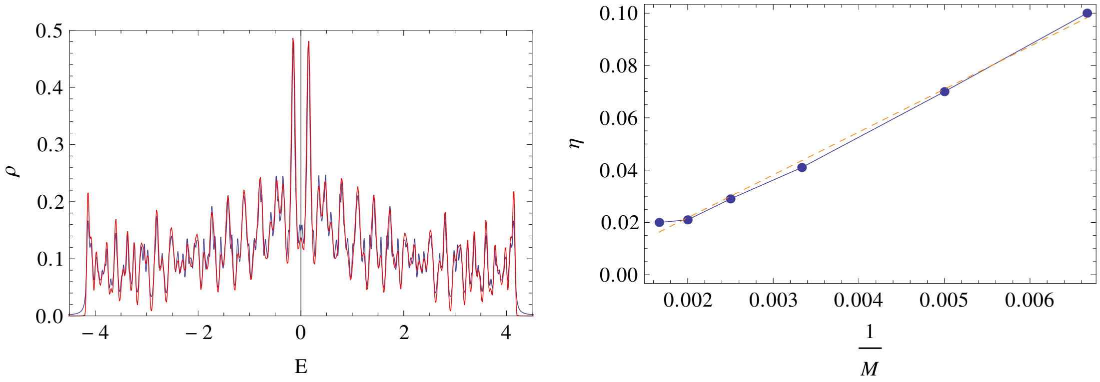

(a) (b)

Figure 5.6: (a) DOS of a system of size $L^2 = 40^2$ with Rashba SOC, $\alpha_2 = 0.8t$ calculated with exact diagonalization with cutoff $\eta = 0.0215$ (blue) and KPM with $M = 500$ moments. (b) Relation between number of moments M and cutoff η.

First application: Metal-Insulator Transition

To determine if a 2D system has a metal-insulator transition (MIT) it is important to analyze its symmetries: It is well known from the scaling theory of localization that in the case where time-reversal and spin-rotational symmetry are preserved, i.e. unitary and orthogonal universality class are present, the scaling function[AALR79]

$$\beta(g) = \frac{d\ln(g)}{d\ln(L)}, \tag{5.45}$$

where g is the dimensionless conductivity, L the side length of our system, scales like

$$\beta(g) \approx -\frac{1}{g} \tag{5.46}$$

for large g, which means that all macroscopic systems are insulators. Here we used the scaling parameter $g = E_{\text{Th}}/\Delta_{\text{LS}}$, where $E_{\text{Th}} = D_e/L^2$ is the Thouless energy and $\Delta_{\text{LS}} = 1/(\rho_{E_F} L^2)$ the typical energy level spacing. However, Hikami *et al.* could show in Ref. [HLN80] that if the universality class changes from orthogonal to symplectic, a MIT can appear in a 2D system. Because SOC breaks spin rotation symmetry one can show that SO interaction can enhance the localization length ξ drastically.[AT92, KKA10, SST05] Recalling results from transfer matrix calculations of the Anderson model in 2D with SOC, the critical disorder strength V_c for the MIT is for strong Rashba SOC $\alpha_2 = 1t$ given by $V_c \approx 6.3t$[SST05, And89] and for weaker SOC $\alpha_2 = 0.1t$ given by $V_c \approx 4.6t$[SST05]. As a first application of the KPM we use the typical DOS,

$$\rho_{\text{typ}}(E) = \exp[\langle\langle \log(\rho_i(E))\rangle\rangle], \tag{5.47}$$

in comparison to the local DOS

$$\rho_i(E) = \frac{1}{D}\sum_{k=0}^{D-1} |\langle i|k\rangle|^2 \delta(E - E_k), \tag{5.48}$$

as an indicator for the metallic or insulating regime. In contrast to the arithmetic mean of ρ_i, $\rho_{\text{avr}}(E) = \langle\langle \rho_i(E)\rangle\rangle$, the geometric mean is suppressed until it vanished for $V > V_c$: The impurity is added to the Hamiltonian by adding the term $H_{\text{imp}} = \sum_{i\sigma} \epsilon_i c^\dagger_{i\sigma} c_{i\sigma}$ where the ϵ_i are uniformly distributed between $[-V/2, V/2]$. In the following we consider the Fermi energy to be at half-filling. In the metallic regime we have $\rho = 1/(L^2\Delta_B)$ at all sites, therefore we expect $\exp[\langle\langle \log(\rho_i(E))\rangle\rangle]/\langle\rho\rangle = 1$.

In contrast, being deeply in the localized regime the states decay exponentially on the localization length ξ, $|\psi(\mathbf{x})|^2 \sim \exp(-x/\xi)$, which leads to

$$\frac{\rho_{\text{ typ}}}{\rho_{\text{ avr}}} = \frac{\exp\left[\frac{1}{\pi L^2}\int_0^L \mathrm{d}r\, r \int_0^{2\pi} \mathrm{d}\varphi \ln\left(\exp\left(-\frac{r}{\xi}\right)\rho_0\right)\right]}{\frac{1}{\pi L^2}\int_0^L \mathrm{d}r\, r\int_0^{2\pi}\mathrm{d}\varphi \exp\left[-\frac{r}{\xi}\right]\rho_0} \tag{5.49}$$

$$= -\frac{\exp\left[\frac{1}{3}\frac{L}{\xi}\right]L^2}{2\xi\left(L+\xi-\xi\exp\left[\frac{L}{\xi}\right]\right)} \tag{5.50}$$

$$= -\frac{\exp\left[\frac{1}{3}u\right]u^2}{2\left(u+1-\exp\left[u\right]\right)}, \tag{5.51}$$

with $u = L/\xi$. From the last equation we can conclude that

- this value vanishes in the thermodynamic limit, $\lim\limits_{L\to\infty}\frac{\rho_{\text{ typ}}}{\rho_{\text{ avr}}} = 0$,
- the fraction is a monotone function of the system length L (in contrast to e.g. the 1d case).

The explained difference between the averaged and typical DOS is plotted in Fig. 5.7: In (a) the averaged DOS is plotted for different impurity potentials V. The band edges are shifted to larger energies with larger V. In contrast, in (b) the typical DOS is plotted for different system sizes at impurity strength $V = 8t$. The product of local densities leads to a strong reduction with the size. This reduction is also significant at the band edges. Knowing the behavior of the typical DOS $\rho_{\text{ typ}}$, we carried out a finite size analysis for different impurity strengths V in a system with weak Rashba SOC strength $\alpha_2 = 0.5t$ to find the critical value V_c for the MIT. From Landauer-Bütiker calculations[SST05] it follows that at impurity strength $V = 8t$ we are already in the insulating regime. The typical DOS $\rho_{\text{ typ}}$ decays exponentially with L, as plotted in Fig. 5.8 (a), which confirms this assumption. If V is reduced the localization length ξ shows a strong increase, as shown in Fig. 5.8 (b), which, in turn, slows down the reduction of $\rho_{\text{ typ}}$, which comes along with increasing system size, significantly in case of large localization lengths. Adding the results from the calculation of $\rho_{\text{ typ}}/\rho_{\text{ avr}}$, which is plotted in Fig .5.9 as function of the inverse system size $1/L^2$ for $E_F = 0$, we can conclude that for $V \gtrsim 5t$ we are in the insulating regime. For a more precise analysis we have to go to larger systems due to the large localization lengths.

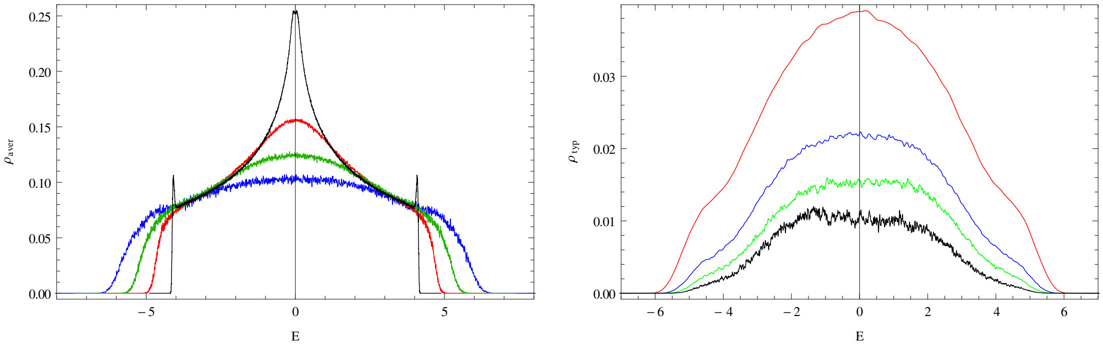

(a)

(b)

Figure 5.7: (a) Averaged DOS ρ_{avr} calculated with KPM (30 impurity configurations) for system size of $L^2 = 280^2$ with Rashba SOC $\alpha_2 = 0.5t$, for different impurity strengths: $V = 1t$(black), $V = 4t$(red), $V = 6t$(green), $V = 8t$(blue) (b) Monotoneous reduction of typical DOS ρ_{typ} with system size $L = 70$, 140, 200, 280, for impurity strength $V = 8t$.

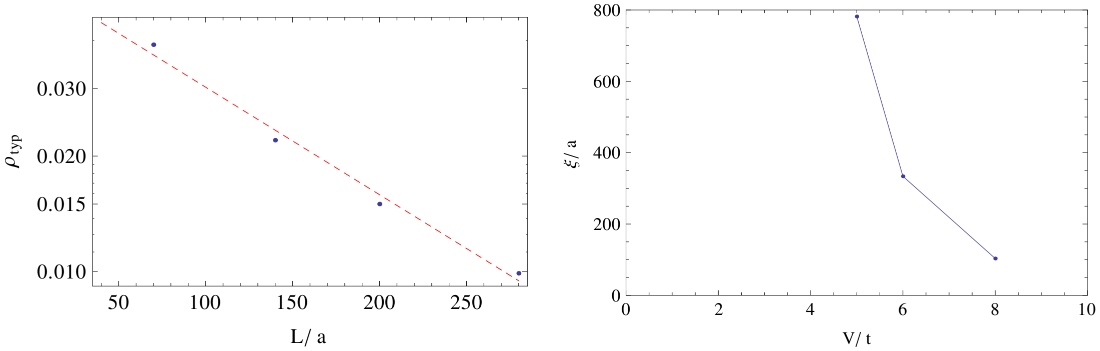

(a)

(b)

Figure 5.8: (a) Log-plot of typical DOS ρ_{typ} at $V = 8t$ for different system sizes L with Rashba SOC $\alpha_2 = 0.5t$ at half filling, calculated with KPM. The dashed line is a linear fit to the log-data which yields a localization length of $\xi \approx 100a$. (b) Localization length ξ at $E_F = 0$, plotted as a function of impurity strength V.

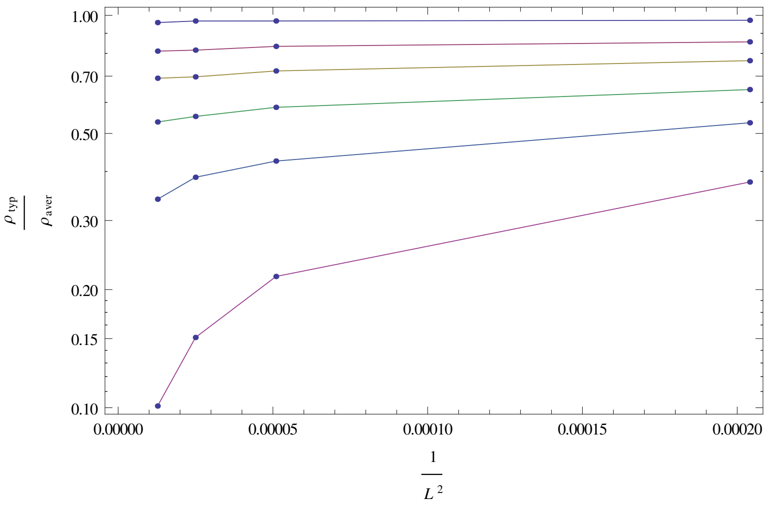

Figure 5.9: Finite size analysis of the typical DOS in relation to the averaged one, $\rho_{\text{typ}}/\rho_{\text{avr}}$, here plotted for $E_F = 0$: The system size has been changed with $L = 70$, 140, 200, 280. The impurity strength for the different curves is given by $V/t = 1, 3, 4, 5, 6, 8$ (monotone from top to bottom).

5.3.3 SHC calculation using KPM

In this section we are going to present calculation of SHC for much larger systems than with exact diagonalization analysis, using KPM. Also here we will use the Kubo formalism which is why we have to reformulate Eq. (5.5) to be applicable to this iterative method. In contrast to the calculation of the DOS, here we have to deal with a correlation of two operators. We will follow the approach presented in the KPM review by Weiße *et al.*[WWAF06].

We start with a KPM where we expand a function only in one dimension. Given a correlation function

$$\langle A; B\rangle_\omega = \left\langle 0 \middle| A \frac{1}{\omega + i\epsilon - H} B \middle| 0 \right\rangle , \tag{5.52}$$

the imaginary part of this function yields

$$-\frac{1}{\pi}\Im[\langle A; B\rangle]_\omega = \sum_{k=0}^{D-1} \langle 0\,|A|\,k\rangle \,\langle k\,|B|\,0\rangle \,\delta(\omega - E_k) \tag{5.53}$$

assuming that $\langle 0\,|A|\,k\rangle \,\langle k\,|B|\,0\rangle$ is real. To apply KPM, we have to rewrite this expression in terms of a trace. This can be done similar to a local DOS calculation according to

Eq. (5.37), which gives the coefficients

$$\mu_n = \frac{1}{D}\sum_{k=0}^{D-1} |\langle i\,|k\rangle|^2 T_n(\tilde{E}_k) \tag{5.54}$$

$$= \int_{-1}^{1} \mathrm{d}\tilde{\omega}\, \frac{1}{D}\sum_{k=0}^{D-1} \langle i\,|\mathbb{1}|\,k\rangle \langle k\,|\mathbb{1}|\,i\rangle\, \delta(\tilde{\omega}-\tilde{E}_k) T_n(\tilde{\omega}) \tag{5.55}$$

$$= \frac{1}{D}\left\langle i \left| T_n(\tilde{H}) \right| i\right\rangle . \tag{5.56}$$

Comparing directly the integrand of Eq. (5.55) with Eq. (5.53) it follows that the moments of the expansion of the imaginary part of the correlation function are given by

$$\mu_n = -\int_{-1}^{1} \mathrm{d}\tilde{\omega}\, \underbrace{\sum_{k=0}^{D-1} \langle 0\,|A|\,k\rangle \langle k\,|B|\,0\rangle\, \delta(\tilde{\omega}-\tilde{E}_k)}_{\equiv j(\tilde{\omega})}\, T_n(\tilde{\omega}) \tag{5.57}$$

$$= \left\langle 0 \left| A T_n(-\tilde{H}) B \right| 0\right\rangle . \tag{5.58}$$

Finally the reconstruction is done by using Eq. (5.32).

This scheme has to be adapted to calculate the SHC $\sigma_{\,\mathrm{SH}}$ in a finite system, as presented in Eq. (5.22),

$$\sigma_{\,\mathrm{SH}}(E_F) = 2\frac{e}{V} \sum_{E_m<E_F<E_n} \frac{\Im(\langle m|\, J_x^z\, |n\rangle \langle n|\, v_y\, |m\rangle)}{(E_n-E_m)^2+\eta^2}, \tag{5.59}$$

by finding the according matrix element density function j, Eq. (5.57), which now has to be a 2d function. Therefore, we rewrite $\sigma_{\,\mathrm{SH}}(E_F)$ in terms of δ-distributions:

$$\sigma_{\,\mathrm{SH}}(\tilde{E}_F) = \frac{e}{V}\int_{-1}^{1}\int_{-1}^{1} \mathrm{d}x\, \mathrm{d}y\, \frac{f(x)-f(y)}{(y-x)^2+\eta^2} \underbrace{\sum_{m,n} \Im[\langle m|\, J_x^z\, |n\rangle \langle n|\, v_y\, |m\rangle] \delta(x-\tilde{E}_m)\delta(y-\tilde{E}_n)}_{\equiv j(x,y)} . \tag{5.60}$$

As an example we plotted $j(x, y)$ for a clean system with 70×70 sites and pure Rashba SOC of strength $\alpha_2 = 1t$ using the analytical solution Eq. (5.20), Fig. 5.10. The δ-distributions have been approximated by Lorentzian functions with a scale parameter $\eta = 0.07$, i.e. we have to take approximately 200 moments in the calculation using KPM. The centrosymmetry in this plot is due to particle-hole symmetry.

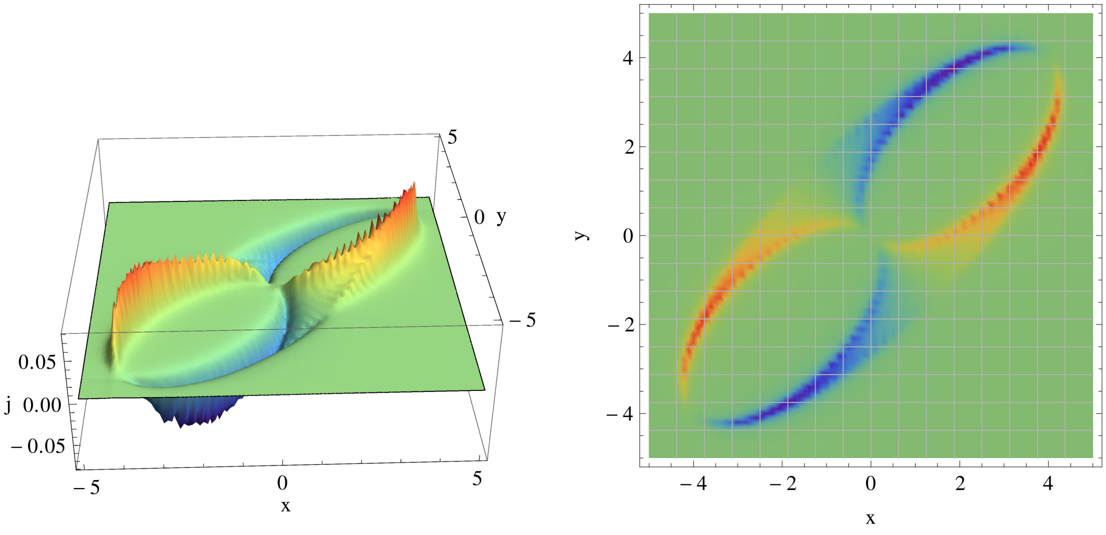

(a) (b)

Figure 5.10: a)+b) Matrix element density function $j(x,y)$ for a clean system with 70×70 sites and pure Rashba SOC of strength $\alpha_2 = 1t$ using the analytical solution Eq. (5.20).

The expansion is now evaluated in x and y and we have a matrix of moments, μ_{mn}. Extending Eq.(5.57) for this case we yield

$$
\begin{aligned}
\mu_{mn} &= \int_{-1}^{1}\int_{-1}^{1} \mathrm{d}x\,\mathrm{d}y\, j(x,y) T_m(x) T_n(y) && (5.61)\\
&= \sum_{k,q} \Im[\langle k| J_x^z |q\rangle \langle q| v_y |k\rangle]\delta(x-\tilde{E}_k)\delta(y-\tilde{E}_q) T_m(\tilde{E}_k) T_n(\tilde{E}_q) && (5.62)\\
&= \Im\left[\sum_k \left\langle k \left| T_m(\tilde{H}) J_x^z T_n(\tilde{H}) v_y \right| k \right\rangle\right] && (5.63)\\
&= \Im[\mathrm{Tr}[T_m(\tilde{H}) J_x^z T_n(\tilde{H}) v_y]]. && (5.64)
\end{aligned}
$$

As already mentioned, we can use the great benefit to replace the trace by an average over a number $R \ll D = 2 \times L^2$ (the two is due to spin degree of freedom) of random vectors, Eq.(5.39). Having the μ_{mn} calculated, we can reconstruct $j(x,y)$ according to Eq. (5.32),

$$
j(x,y) = \sum_{m,n=0}^{\infty} \frac{\mu_{mn} h_{mn} T_m(x) T_n(y)}{\pi^2 \sqrt{(1-x^2)(1-y^2)}}, \tag{5.65}
$$

where we added normalization functions

$$
h_{mn} = \frac{4}{(1+\delta_{m,0})(1+\delta_{n,0})}. \tag{5.66}
$$

On a computer we have to replace the infinite sum with a finite one where only M momenta are taken into account. To cure the mentioned appearance of Gibbs oscillations we use a convolution with a Jackson kernel, i.e. the coefficients μ_{mn} are replaced by $\mu_{mn} \rightarrow \mu_{mn} g_m(M) g_n(M)$, with kernel-damping factors[WWAF06]

$$g_n(M) = \frac{(M-n+1)\cos\left(\frac{\pi n}{M+1}\right) + \sin\left(\frac{\pi n}{M+1}\right)\cot\left(\frac{\pi}{M+1}\right)}{M+1}. \tag{5.67}$$

The function $j(x,y)$ for finite M is therefore given by

$$j_M(x,y) = \sum_{m,n=0}^{M-1} \frac{\mu_{mn} h_{mn} g_m(M) g_n(M) T_m(x) T_n(y)}{\pi^2\sqrt{(1-x^2)(1-y^2)}}. \tag{5.68}$$

Finally, we reconstruct $\sigma_{\,\mathrm{SH}}(E_F)$ with the calculated matrix element density function $j_M(x,y)$ using a finite number of moments,

$$\sigma_{\,\mathrm{SH}}(\tilde{E}_F, M) = \frac{e}{V}\int_{-1}^{1}\int_{-1}^{1} \mathrm{d}x\,\mathrm{d}y\,\frac{f(x)-f(y)}{(y-x)^2} j_M(x,y). \tag{5.69}$$

We set η to zero because now the divergent terms are damped by the fact that we use only a finite number of expansion terms M, which correspond to η as shown in Sec. 5.3.2. As a presentation of the KPM we chose the same system as used for Fig. 5.10. The Lorentzian function scale parameter was chosen as $\eta = 0.07$ which is why we choose $M = 200$ moments for the expansion, according to Fig. 5.11 (b). The resulting SHC $\sigma_{\,\mathrm{SH}}(E_F, M)$ is plotted in Fig. 5.11 (red curve) and for comparison the analytical solution (blue curve). The slight asymmetry is due to an asymmetric choice of discrete k-values in the arguments of the trigonometric functions. This asymmetry disappears for larger systems.

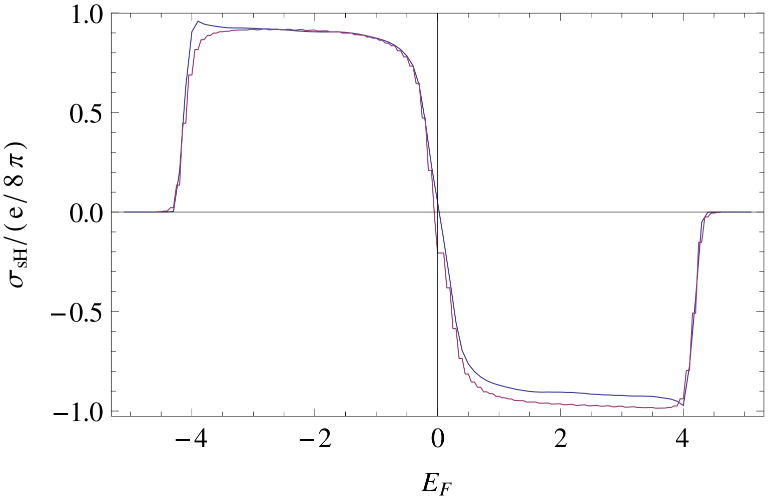

Figure 5.11: SHC $\sigma_{\mathrm{SH}}(E_F, M)$ calculated with KPM for a system with 70×70 sites, pure Rashba SOC of strength $\alpha_2 = 1t$ and $M = 200$ moments (blue curve). For comparison the analytical solution is plotted (red curve), corresponding to Fig. 5.10.

Chapter 6

Critical Discussion and Future Perspective

At first we address the topic of diffusive-ballistic crossover which was discussed in Sec. 4.5.1: The ansatz which was used to show a reduction of spin relaxation rate appearing due to cubic Dresselhaus SOC, was a discretization of angles when summing over momenta of the Cooperon. Although the constraint for the angles reduces the Cooperon eigenvalues significantly, this ansatz is still based on linear response. One consequence is that contributions appearing at low channel number and steaming from edge to edge skipping orbits, as shown in Ref. [BvH88b], are not included. Such orbits can lead to flux cancellation effects, which e.g. can weaken the magnetic field dependence of WL correction to the conductivity. However, in further work, we will show the reduction of spin relaxation rate dependence on the number of transverse channels in the framework of a nonperturbative theory based on the paper by S. Kettemann *et al.*, Ref. [KM02]. In latter work the magnetic phase-shifting rate $1/\tau_B$ has been identified with a correlation function of the magnetic vector potential. In turn, this correlation function is related to a term in the nonlinear σ-model which appears due to time-reversal symmetry breaking. Thus, in case of an effective magnetic field due to SOC, which brakes spin rotation symmetry, the respective term in the nonlinear σ-model has to be identified to yield a nonperturbative expression for the spin relaxation rate $1/\tau_s$. The last chapter of this work stands out from the rest by the fact that the focus is more on numerical calculations. The code was developed as general as possible by decomposing all matrix operations in connectivity and hopping matrices including magnetic field and different kinds of SOC. Having coded the KPM in a general form, one of the next steps will be the analysis of diluted magnetic semiconductors using the V-J $_{\mathrm{pd}}$ model developed by G. Bouzerar *et al.*[BBZ07]. Already analytical calculations show[WLZ07b] that in contrast to a lattice with only nonmagnetic impurities, the vertex correction corresponding to ladder diagrams, σ^L_{SH} does not cancel the one-loop part σ^0_{SH} which is equal to that derived by Sinova.[SCN$^+$04] This can be calculated now rigorously for large systems, i.e. also the clustering of Mn^{2+} can be included[CWBB12]. Numerical works like Ref. [LX06] show interesting change of sign of the SHC by changing the exchange interaction or the impurity density and strength. However the work was limited to smaller sizes, $L^2 = 20 \times 20$, and focused on energies away from the impurity band.

Due to the advantaged of the KPM concerning the obsolete cutoff η adjustment, we are able to go beyond calculations which extracted localization lengths using the computation of SHC by application of the time evolution projection method (see e.g. Ref. [MM07]).

Last but not least, due to the general structure of the KPM code, also the extension to the evaluation of other quantities like the anomalous Hall effect is possible.

List of Symbols

SOC	spin-orbit coupling	2
2DES	2D electron system	2
m_e	effective electron mass	3
λ_F	Fermi wavelength	3
WL	weak localization	4
WAL	weak antilocalization	4
m_{e0}	free electron mass	6
Δ_{SO}	Pauli splitting	7
γ_g	gyromagnetic ratio	8
τ	elastic scattering time	9
l_e	elastic mean free path	9
D_e	diffusion constant	9
υ_{F}	Fermi velocity	9
d_D	diffusion dimension of the electron system	9
ν	density of states per spin at E_F	9
DOS	density of states	9
L_D	diffusion length	10
a_z	thickness of the 2D electron system	11
γ_D	Dresselhaus-spin-orbit coefficient	11
α_1	linear Dresselhaus parameter	11
BIA	bulk inversion asymmetry	11
SIA	structural inversion asymmetryy	13
α_2	linear Rashba parameter	13
L_{SO}	spin precession length	14

τ_s	spin relaxation time	16
L_s	spin relaxation length	19
DP	D'yakonov-Perel'	19
E_F	Fermi energy	20
W	wire width	26
l_φ	phase coherence length	27
$\hat{C}$	Cooperon propagator	34
$\tilde{\alpha}_1$	reduced linear Dresselhaus parameter	36
l_B	magnetic length	37
τ_B	magnetic phase-shifting rate	37
Q_{SO}	spin precession wave vector equal to $2\pi/L_{\text{SO}}$	38
H_c	Cooperon Hamiltonian	38
H_{SD}	spin-diffusion Hamiltonian	39
B^*	effective external magnetic field	45
H_s	spin relaxation field	45
Δ_α	spin orbit splitting $2k_F\alpha_2$	53
LDES	low dimensional electron systems	83
SHE	spin Hall effect	84
KPM	Kernel Polynomial Method	84
SHC	spin Hall conductivity	85
$\mathbf{J}^z$	spin current	85
$\sigma^z_{xy} \equiv \sigma_{\text{SH}}$	spin hall conductivity	88
Δ_B	band width	98
MIT	metal-insulator transition	99
g	scaling parameter in scaling theory of localization	99
E_{Th}	Thouless energy	99
Δ_{LS}	typical energy level spacing	99

List of Figures

List of Tables

Bibliography

[AAKL82] B. L. Altshuler, A. G. Aronov, D. E. Khmelnitskii, and A. I. Larkin. Quantum Theory of Solids. Mir, Moscow, 1982.

[AALR79] E. Abrahams, P. W. Anderson, D. C. Licciardello, and T. V. Ramakrishnan. Scaling theory of localization: Absence of quantum diffusion in two dimensions. *Phys. Rev. Lett.*, 42(10):673–676, Mar 1979.

[AB59] Y. Aharonov and D. Bohm. Significance of electromagnetic potentials in the quantum theory. *Phys. Rev.*, 115(3):485–491, Aug 1959.

[ADK$^+$08] G. V. Astakhov, R. I. Dzhioev, K. V. Kavokin, V. L. Korenev, M. V. Lazarev, M. N. Tkachuk, Yu. G. Kusrayev, T. Kiessling, W. Ossau, and L. W. Molenkamp. Suppression of Electron Spin Relaxation in Mn-Doped GaAs. *Phys. Rev. Lett.*, 101(7):076602, 2008.

[AF01] I. L. Aleiner and Vladimir I. Fal'ko. Spin-Orbit Coupling Effects on Quantum Transport in Lateral Semiconductor Dots. *Phys. Rev. Lett.*, 87(25):256801, Nov 2001.

[AF07] David D Awschalom and Michael E Flatte. Challenges for semiconductor spintronics. *Nat Phys*, 3(3):153–159, Mar 2007.

[Ale06] I. L. Aleiner. privtate communication. 2006.

[And89] T. Ando. Numerical study of symmetry effects on localization in two dimensions. *Phys. Rev. B*, 40(8):5325–5339, Sep 1989.

[AOMO01] T. Adachi, Y. Ohno, F. Matsukura, and H. Ohno. Spin relaxation in n-modulation doped GaAs/AlGaAs (1 1 0) quantum wells. *Physica E: Low-dim. Sys. and Nanostr.*, 10(1-3):36–39, 2001.

[AT92] T. Ando and H. Tamura. Conductance fluctuations in quantum wires with spin-orbit and boundary-roughness scattering. *Phys. Rev. B*, 46(4):2332–2338, Jul 1992.

[BAP76] G. L. Bir, A. G. Aronov, and G. E. Pikus. Spin Relaxation of Electrons due to Scattering by Holes. *Sov. Phys.-JETP*, 42:705, 1976.

[BB04] A. A. Burkov and Leon Balents. Spin Relaxation in a Two-Dimensional Electron Gas in a Perpendicular Magnetic Field. *Phys. Rev. B*, 69(24):245312, Jun 2004.

[BBF$^+$88] M. Baibich, J. Broto, A. Fert, F. Van Dau, F. Petroff, P. Etienne, G. Creuzet, A. Friederich, and J. Chazelas. Giant Magnetoresistance of (001)Fe/(001)Cr Magnetic Superlattices. *Phys. Rev. Lett.*, 61(21):2472–2475, Nov 1988.

[BBZ07] R Bouzerar, G Bouzerar, and T Ziman. Non-perturbative V-Jpd model and ferromagnetism in dilute magnets. *EPL (Europhysics Letters)*, 78(6):67003, 2007.

[Ber84] Gerd Bergmann. Weak Localization in Thin Films : a Time-of-Flight Experiment with Conduction Electrons. *Physics Reports*, 107(1):1–58, 1984.

[BEW$^+$99] S. Brosig, K. Ensslin, R. J. Warburton, C. Nguyen, B. Brar, M. Thomas, and H. Kroemer. Zero-field Spin Splitting in InAs-AlSb Quantum Wells Revisited. *Phys. Rev. B*, 60(20):R13989–R13992, Nov 1999.

[BGSZ89] G. Binasch, P. Grünberg, F. Saurenbach, and W. Zinn. Enhanced magnetoresistance in layered magnetic structures with antiferromagnetic interlayer exchange. *Phys. Rev. B*, 39(7):4828–4830, Mar 1989.

[BNnM04] A. A. Burkov, Alvaro S. Núñez, and A. H. MacDonald. Theory of spin-charge-coupled transport in a two-dimensional electron gas with rashba spin-orbit interactions. *Phys. Rev. B*, 70(15):155308, Oct 2004.

[Bog80] P. Boguslawski. Electron-Electron Spin-Flip Scattering and Spin Relaxation in III-V and II-VI Semiconductors. *Solid State Commun.*, 33(3):389, jan 1980.

[BOZ06] B. Andrei Bernevig, J. Orenstein, and Shou-Cheng Zhang. Exact SU(2) Symmetry and Persistent Spin Helix in a Spin-Orbit Coupled System. *Phys. Rev. Lett.*, 97(23):236601, 2006.

[BPP48] N. Bloembergen, E. M. Purcell, and R. V. Pound. Relaxation Effects in Nuclear Magnetic Resonance Absorption. *Phys. Rev.*, 73(7):679–712, Apr 1948.

[BR84] Ya Bychkov and Ei Rashba. Properties of A 2d Electron-Gas With Lifted Spectral Degeneracy. *JETP Lett.*, 39(2):78–81, 1984.

[Bur08] Guido Burkard. Quantum information: positively spin coherent. *Nature materials*, 7(2):100–1, Feb 2008.

[BvH88a] C. W. J. Beenakker and H. van Houten. Flux-Cancellation Effect on Narrow-Channel Magnetoresistance Fluctuations. *Phys. Rev. B*, 37(11):6544–6546, Apr 1988.

[BvH88b] C. W. J. Beenakker and H. van Houten. Flux-cancellation effect on narrow-channel magnetoresistance fluctuations. *Phys. Rev. B*, 37(11):6544–6546, Apr 1988.

[Cha75] J. N. Chazalviel. Spin Relaxation of Conduction Electrons in n-Type Indium Antimonide at Low Temperature. *Phys. Rev. B*, 11(4):1555–1562, Feb 1975.

[CS86] Sudip Chakravarty and Albert Schmid. Weak Localization: The Quasiclassical Theory of Electrons in a Random Potential. *Physics Reports*, 140(4):193–236, 1986.

[CSS$^+$04] Dimitrie Culcer, Jairo Sinova, N. A. Sinitsyn, T. Jungwirth, A. H. MacDonald, and Q. Niu. Semiclassical spin transport in spin-orbit-coupled bands. *Phys. Rev. Lett.*, 93(4):046602, Jul 2004.

[CWBB12] Akash Chakraborty, Paul Wenk, Richard Bouzerar, and Georges Bouzerar. Spontaneous magnetization in the presence of nanoscale inhomogeneities in diluted magnetic systems. *Physical Review B*, 86(21), dec 2012. priv. communication, in preparation.

[CWd07] J. Cheng, M. Wu, and I. da Cunha Lima. Anisotropic spin transport in GaAs quantum wells in the presence of competing Dresselhaus and Rashba spin-orbit coupling. *Phys. Rev. B*, 75(20):205328, May 2007.

[DD90] Supriyo Datta and Biswajit Das. Electronic Analog of The Electro-Optic Modulator. *Appl. Phys. Lett.*, 56(7):665–667, 1990.

[DHR$^+$04] S. Döhrmann, D. Hägele, J. Rudolph, M. Bichler, D. Schuh, and M. Oestreich. Anomalous Spin Dephasing in (110) GaAs Quantum Wells: Anisotropy and Intersubband Effects. *Phys. Rev. Lett.*, 93(14), September 2004.

[DK84] V. K. Dugaev and D. E. Khmel'nitskii. Magnetoresistance of Metal Films with Low Impurity Concentrations in a Parallel Magnetic Field. *Soviet Physics - JETP*, 59(5):1038–1041, 1984.

[DKK$^+$02] R. I. Dzhioev, K. V. Kavokin, V. L. Korenev, M. V. Lazarev, B. Ya. Meltser, M. N. Stepanova, B. P. Zakharchenya, D. Gammon, and D. S. Katzer. Low-Temperature Spin Relaxation in n-Type GaAs. *Phys. Rev. B*, 66(24):245204, Dec 2002.

[DLS$^+$05] R. Dinter, S. Löhr, S. Schulz, Ch. Heyn, and W. Hansen. unpublished, 2005.

[DMD$^+$89] B. Das, D. C. Miller, S. Datta, R. Reifenberger, W. P. Hong, P. K. Bhattacharya, J. Singh, and M. Jaffe. Evidence for Spin Splitting in $\mathrm{In}_x\mathrm{Ga}_{1-x}\mathrm{As}/\mathrm{In}_{0.52}\mathrm{Al}_{0.48}\mathrm{As}$ Heterostructures as $B \to 0$. *Phys. Rev. B*, 39(2):1411–1414, jan 1989.

[DO79] G. Dolan and D. Osheroff. Nonmetallic Conduction in Thin Metal Films at Low Temperatures. *Phys. Rev. Lett.*, 43(10):721–724, Sep 1979.

[DP71a] M. I. D'yakonov and V. I. Perel'. Possibility of Orienting Electron Spins with Current . *JETP Lett.*, 13(11):467, 1971.

[DP71b] M I D'yakonov and V I Perel'. Spin Orientation of Electrons Associated with Interband Absorption of Light in Semiconductors. *Soviet Physics Jetp-Ussr*, 33(5):1053–&, 1971. [*Zh. Eksp. Teor. Fiz.*, 60:1954, 1971].

[DP71c] M. I. D'yakonov and V. I. Perel'. Spin Relaxation of Conduction Electrons in Noncentrosymmetric Semiconductors. *Fiz. Tverd. Tela*, 13:3581, 1971. [Sov. Phys. Solid State **13**, 3023-3026 (1972)].

[DP72] M I D'yakonov and V I Perel'. Spin Relaxation of Conduction Electrons in Noncentrosymmetric Semiconductors. *Sov. Phys. Solid State*, 13:3023–3026, 1972.

[DPWS92] P. D. Dresselhaus, C. M. A. Papavassiliou, R. G. Wheeler, and R. N. Sacks. Observation of Spin Precession in GaAs Inversion Layers Using Antilocalization. *Phys. Rev. Lett.*, 68(1):106–109, Jan 1992.

[DR93] T. Darnhofer and U. Rössler. Effects of Band Structure and Spin in Quantum Dots. *Phys. Rev. B*, 47(23):16020–16023, Jun 1993.

[DR04] A. Dyson and B. K. Ridley. Spin Relaxation in Cubic III-V Semiconductors via Interaction with Polar Optical Phonons. *Phys. Rev. B*, 69(12):125211, Mar 2004.

[Dre55] G. Dresselhaus. Spin-Orbit Coupling Effects in Zinc Blende Structures. *Phys. Rev.*, 100(2):580–586, Oct 1955.

[Dya04] M. I. Dyakonov. Spintronics? *eprint arXiv:cond-mat/0401369*, January 2004.

[Ell54] R. J. Elliott. Theory of the Effect of Spin-Orbit Coupling on Magnetic Resonance in Some Semiconductors. *Phys. Rev.*, 96(2):266–279, Oct 1954.

[ELSL97] G. Engels, J. Lange, Th. Schäpers, and H. Lüth. Experimental and Theoretical Approach to Spin Splitting in Modulation-Doped $\mathrm{In}_x\mathrm{Ga}_{1-x}\mathrm{As}$/InP Quantum Wells for $B \to 0$. *Phys. Rev. B*, 55(4):R1958–R1961, Jan 1997.

[ERH07] Hans-Andreas Engel, Emmanuel I. Rashba, and Bertrand I. Halperin. *MaterialsTheory of Spin Hall Effects in Semiconductors.* John Wiley & Sons, Ltd, Cambridge, MA, USA, December 2007.

[ESL05] Sigurdur I. Erlingsson, John Schliemann, and Daniel Loss. Spin susceptibilities, spin densities, and their connection to spin currents. *Phys. Rev. B*, 71(3):035319, Jan 2005.

[Fal03] V. L. Fal'ko. private communication. 2003.

[FMAE$^+$07] J. Fabian, A. Matos-Abiague, C. Ertler, P. Stano, and I. Zutic. Semiconductor Spintronics. *Acta Physica Slovaca*, 57:565, 2007.

[Fro01] V. A. Froltsov. Diffusion of inhomogeneous spin distribution in a magnetic field parallel to interfaces of a III-V semiconductor quantum well. *Phys. Rev. B*, 64(4):045311, Jun 2001.

[GF97] Claudio Grimaldi and Peter Fulde. Theory of screening of the phonon-modulated spin-orbit interaction in metals . *Phys. Rev. B*, 55(23):15523–15530, Jun 1997.

[GGB$^+$07] S. Giglberger, L. E. Golub, V. V. Bel'kov, S. N. Danilov, D. Schuh, C. Gerl, F. Rohlfing, J. Stahl, W. Wegscheider, D. Weiss, W. Prettl, and S. D. Ganichev. Rashba and dresselhaus spin splittings in semiconductor quantum wells measured by spin photocurrents. *Phys. Rev. B*, 75(3):035327, Jan 2007.

[GI02] M. M. Glazov and E. L. Ivchenko. Precession spin relaxation mechanism caused by frequent electron-electron collisions. *Jetp Lett.*, 75:403, 2002.

[GI04] M. M. Glazov and E. L. Ivchenko. Effect of electron-electron interaction on spin relaxation of charge carriers in semiconductors. *J. Exp. and Theoret. Phys.*, 99:1279, 2004.

[GKD04] Alexander O. Govorov, Alexander V. Kalameitsev, and John P. Dulka. Spin-dependent transport of electrons in the presence of a smooth lateral potential and spin-orbit interaction. *Phys. Rev. B*, 70(24):245310, Dec 2004.

[Gol05] L. E. Golub. Weak Antilocalization in High-Mobility Two-Dimensional Systems. *Phys. Rev. B*, 71(23):235310, 2005.

[Gru00] Dirk Grundler. Large Rashba Splitting in InAs Quantum Wells due to Electron Wave Function Penetration into the Barrier Layers. *Phys. Rev. Lett.*, 84(26):6074–6077, Jun 2000.

[HLN80] Shinobu Hikami, Anatoly I. Larkin, and Yosuke Nagaoka. Spin-Orbit Interaction and Magnetoresistance in the Two Dimensional Random System. *Prog. Theor. Phys.*, 63(2):707–710, 1980.

[HNA$^+$99] Can-Ming Hu, Junsaku Nitta, Tatsushi Akazaki, Hideaki Takayanagi, Jiro Osaka, P. Pfeffer, and W. Zawadzki. Zero-field spin splitting in an inverted $\mathrm{In_{0.53}Ga_{0.47}As/In_{0.52}Al_{0.48}As}$ heterostructure: Band nonparabolicity influence and the subband dependence. *Phys. Rev. B*, 60(11):7736–7739, Sep 1999.

[HPB$^+$97] T Hassenkam, S Pedersen, K Baklanov, A Kristensen, C B Sorensen, P E Lindelof, F G Pikus, and G E Pikus. Spin splitting and weak localization in (110) GaAs/AlxGa1-xAs quantum wells. *Phys. Rev. B*, 55(15):9298–9301, 1997.

[HSM$^+$06] A. W. Holleitner, V. Sih, R. C. Myers, A. C. Gossard, and D. D. Awschalom. Suppression of Spin Relaxation in Submicron InGaAs Wires. *Phys. Rev. Lett.*, 97(3):036805, 2006.

[HSM$^+$07] A W Holleitner, V Sih, R C Myers, A C Gossard, and D D Awschalom. Dimensionally constrained D'yakonov–Perel' spin relaxation in n-InGaAs channels: transition from 2D to 1D. *New Journal of Physics*, 9(9):342, 2007.

[HvWK$^+$98] J. P. Heida, B. J. van Wees, J. J. Kuipers, T. M. Klapwijk, and G. Borghs. Spin-orbit interaction in a two-dimensional electron gas in a InAs/AlSb quantum well with gate-controlled electron density. *Phys. Rev. B*, 57(19):11911–11914, May 1998.

[icvacFDS04] Igor Žutić, Jaroslav Fabian, and S. Das Sarma. Spintronics: Fundamentals and applications. *Rev. Mod. Phys.*, 76(2):323–410, Apr 2004.

[Ivc73] E. L. Ivchenko. Spin Relaxation of Free Carriers in a Noncentrosymmetric Semiconductor in a Longitudinal Magnetic Field. *Sov. Phys. Solid State*, 15:1048, 1973.

[JLS$^+$08] Minkyung Jung, Joon Sung Lee, Woon Song, Young Heon Kim, Sang Don Lee, Nam Kim, Jeunghee Park, Mahn-Soo Choi, Shingo Katsumoto, Hyoyoung Lee, and Jinhee Kim. Quantum Interference in Radial Heterostructure Nanowires. *Nano Letters*, 8(10):3189–3193, Sep 2008.

[JRA$^+$95] Bernard Jusserand, David Richards, Guy Allan, Catherine Priester, and Bernard Etienne. Spin orientation at semiconductor heterointerfaces. *Phys. Rev. B*, 51(7):4707–4710, Feb 1995.

[KCCC92] C Kurdak, A. M. Chang, A. Chin, and T. Y. Chang. Quantum Interference Effects and Spin-Orbit Interaction in Quasi-One-Dimensional Wires and Rings. *Phys. Rev. B*, 46(11):6846–6856, Sep 1992.

[Ket07] S. Kettemann. Dimensional Control of Antilocalization and Spin Relaxation in Quantum Wires. *Phys. Rev. Lett.*, 98(17):176808–4, April 2007.

[KH07] Jacob J. Krich and Bertrand I. Halperin. Cubic Dresselhaus Spin-Orbit Coupling in 2D Electron Quantum Dots. *Phys. Rev. Lett.*, 98(22):226802, 2007.

[KHG$^+$10] R L Kallaher, J J Heremans, N Goel, S J Chung, and M B Santos. Spin and phase coherence lengths in n-InSb quasi-one-dimensional wires. *Phys. Rev. B*, 81(3):35335, January 2010.

[KK00] A. A. Kiselev and K. W. Kim. Progressive Suppression of Spin Relaxation in Two-Dimensional Channels of Finite Width. *Phys. Rev. B*, 61(19):13115–13120, May 2000.

[KKA10] Tomoaki Kaneko, Mikito Koshino, and Tsuneya Ando. Symmetry crossover in quantum wires with spin-orbit interaction. *Phys. Rev. B*, 81(15):155310, Apr 2010.

[KKN09] Yoji Kunihashi, Makoto Kohda, and Junsaku Nitta. Enhancement of spin lifetime in gate-fitted InGaAs narrow wires. *Phys. Rev. Lett.*, 102(22):226601, 2009.

[KM02] Stefan Kettemann and Riccardo Mazzarello. Magnetolocalization in Disordered Quantum Wires. *Phys. Rev. B*, 65(8):085318, Feb 2002.

[KMGA04] Y K Kato, R C Myers, A C Gossard, and D D Awschalom. Observation of the spin Hall effect in semiconductors. *Science*, 306(5703):1910–3, December 2004.

[KRW03] J. Kainz, U. Rössler, and R. Winkler. Anisotropic spin-splitting and spin-relaxation in asymmetric zinc blende semiconductor quantum structures. *Phys. Rev. B*, 68(7), August 2003.

[KSZ$^+$96] W. Knap, C. Skierbiszewski, A. Zduniak, E. Litwin-Staszewska, D. Bertho, F. Kobbi, J. L. Robert, G. E. Pikus, F. G. Pikus, S. V. Iordanskii, V. Mosser, K. Zekentes, and Yu. B. Lyanda-Geller. Weak antilocalization and spin precession in quantum wells. *Phys. Rev. B*, 53(7):3912–3924, Feb 1996.

[KWO$^+$09] J D Koralek, C P Weber, J Orenstein, B A Bernevig, Shou-Cheng Zhang, S Mack, and D D Awschalom. Emergence of the persistent spin helix in semiconductor quantum wells. *Nature*, 458(7238):610–613, Apr 2009.

[LAP] Lapack linear algebra package. Available at: http://www.netlib.org/lapack/.

[LCCC06] Ming-Hao Liu, Kuo-Wei Chen, Son-Hsien Chen, and Ching-Ray Chang. Persistent spin helix in rashba-dresselhaus two-dimensional electron systems. *Phys. Rev. B*, 74(23):235322, 2006.

[LG98] Yuli Lyanda-Geller. Quantum Interference and Electron-Electron Interactions at Strong Spin-Orbit Coupling in Disordered Systems. *Phys. Rev. Lett.*, 80(19):4273–4276, May 1998.

[LLK$^+$10] J. Liu, T. Last, E. Koop, S. Denega, B. van Wees, and C. van der Wal. Spin-dephasing anisotropy for electrons in a diffusive quasi-1d gaas wire. *J. Supercond. Nov. Magn.*, 23(1):11–15, 2010.

[LMFS88] J. Luo, H. Munekata, F. F. Fang, and P. J. Stiles. Observation of the zero-field spin splitting of the ground electron subband in gasb-inas-gasb quantum wells. *Phys. Rev. B*, 38(14):10142–10145, Nov 1988.

[LSK$^+$07] P. Lehnen, T. Schapers, N. Kaluza, N. Thillosen, and H. Hardtdegen. Enhanced spin-orbit scattering length in narrow AlxGa1-xN/GaN wires. *Phys. Rev. B*, 76(20):205307, 2007.

[LX06] P. Liu and S.-J. Xiong. Spin-Hall transport in a two-dimensional electron system with magnetic impurities. *The European Physical Journal B*, 51(4):513–516, June 2006.

[MACR06] T. Micklitz, A. Altland, T. A. Costi, and A. Rosch. Universal Dephasing Rate due to Diluted Kondo Impurities. *Phys. Rev. Lett.*, 96(22):226601, 2006.

[Mah00] G. Mahan. *Many-Particle Physics, 3rd ed.* Plenum, New York, 2000.

[MC00] A. G. Mal'shukov and K. A. Chao. Waveguide Diffusion Modes and Slowdown of D'yakonov-Perel' Spin Relaxation in Narrow Two-Dimensional Semiconductor Channels. *Phys. Rev. B*, 61(4):R2413–R2416, Jan 2000.

[MCW97] A. G. Mal'shukov, K. A. Chao, and M. Willander. Magnetoresistance of a Weakly Disordered III-V Semiconductor Quantum Well in a Magnetic Field Parallel to Interfaces. *Phys. Rev. B*, 56(11):6436–6439, Sep 1997.

[Mei05] F. E. Meijer. private communication. 2005.

[MFA02] J S Meyer, V I Fal'ko, and B L Altshuler. *No Title*, volume 72 of *Nato Science Series II*, page 117. Kluwer Academic Publishers, Dordrecht, 2002.

[MHEZ71] Müller-Hartmann, E., and J. Zittartz. Kondo Effect in Superconductors. *Phys. Rev. Lett.*, 26(8):428–432, Feb 1971.

[MJM$^+$04] H. Malissa, W. Jantsch, M. Mühlberger, F. Schäffler, Z. Wilamowski, M. Draxler, and P. Bauer. Anisotropy of g-factor and electron spin resonance linewidth in modulation doped SiGe quantum wells. *Appl. Phys. Lett.*, 85(10):1739–1741, 2004.

[MKMM00] T. Matsuyama, R. Kürsten, C. Meißner, and U. Merkt. Rashba spin splitting in inversion layers on p-type bulk InAs. *Phys. Rev. B*, 61(23):15588–15591, Jun 2000.

[MM05] Cătălin Pa şcu Moca and D. C. Marinescu. Longitudinal and spin-hall conductance of a two-dimensional rashba system with arbitrary disorder. *Phys. Rev. B*, 72(16):165335, Oct 2005.

[MM07] C. P. Moca and D. C. Marinescu. Finite-size effects in a two-dimensional electron gas with rashba spin-orbit interaction. *Phys. Rev. B*, 75(3):035325, Jan 2007.

[MMF08] C. Moca, D. Marinescu, and S. Filip. Spin Hall effect in a symmetric quantum well by a random Rashba field. *Phys. Rev. B*, 77(19), may 2008.

[MST83] V. A. Marushchak, M. N. Stepanova, and A. N. Titkov. Spin Relaxation of Conduction Electrons in Moderately Doped Gallium arsenide crystals. *Soviet Physics - Solid State*, 25(12):2035–2038, 1983.

[MZM$^+$03] J. B. Miller, D. M. Zumbühl, C. M. Marcus, Y. B. Lyanda-Geller, D. Goldhaber-Gordon, K. Campman, and A. C. Gossard. Gate-Controlled Spin-Orbit Quantum Interference Effects in Lateral Transport. *Phys. Rev. Lett.*, 90(7):076807, Feb 2003.

[NATE97] J. Nitta, T. Akazaki, H. Takayanagi, and T. Enoki. Gate control of spin-orbit interaction in an inverted In(0.53)Ga(0.47)AS/In(0.52)Al(0.48)AS heterostructure. *Phys. Rev. Lett.*, 78(7):1335–1338, 1997.

[NATE98] Junsaku Nitta, Tatsushi Akazaki, Hideaki Takayanagi, and Takatomo Enoki. Gate control of spin-orbit interaction in an InAs-inserted $In_{0.53}Ga_{0.47}As/In_{0.52}Al_{0.48}As$ heterostructure. *Physica E: Low-dimensional Systems and Nanostructures*, 2(1-4):527–531, 1998.

[Nit06] J. Nitta. privtate communication of unpublished results. 2006.

[NSJ$^+$05] K. Nomura, Jairo Sinova, T. Jungwirth, Q. Niu, and A. H. MacDonald. Nonvanishing spin hall currents in disordered spin-orbit coupling systems. *Phys. Rev. B*, 71(4):041304, Jan 2005.

[NSJ$^+$06] K. Nomura, Jairo Sinova, T. Jungwirth, Q. Niu, and A. H. MacDonald. Erratum: Nonvanishing spin hall currents in disordered spin-orbit coupling systems [phys. rev. b71, 041304(r) (2005)]. *Phys. Rev. B*, 73(19):199901, may 2006.

[NSSM05] K. Nomura, Jairo Sinova, N. Sinitsyn, and A. MacDonald. Dependence of the intrinsic spin-Hall effect on spin-orbit interaction character. *Phys. Rev. B*, 72(16), October 2005.

[OMP] Openmp.org. Available at: http://openmp.org/wp/.

[OMP$^+$92] H. Ohno, H. Munekata, T. Penney, S. von Molnár, and L. Chang. Magnetotransport properties of p-type (In,Mn)As diluted magnetic III-V semiconductors. *Phys. Rev. Lett.*, 68(17):2664–2667, Apr 1992.

[OTA$^+$99] Y. Ohno, R. Terauchi, T. Adachi, F. Matsukura, and H. Ohno. Spin Relaxation in GaAs(110) Quantum Wells. *Phys. Rev. Lett.*, 83(20):4196–4199, Nov 1999.

[OW53] Overhauser and Albert W. Paramagnetic Relaxation in Metals. *Phys. Rev.*, 89(4):689–700, Feb 1953.

[Pei33] R. Peierls. Zur Theorie des Diamagnetismus von Leitungselektronen. *Zeitschrift für Physik*, 80(11-12):763–791, November 1933.

[PF06] Alexander Punnoose and Alexander M. Finkel'stein. Spin Relaxation in the Presence of Electron-Electron Interactions. *Phys. Rev. Lett.*, 96(5):057202–4, February 2006.

[PHC$^+$09] G. Petersen, S. Estévez Hernández, R. Calarco, N. Demarina, and Th. Schäpers. Spin-orbit coupling and phase-coherent transport in InN nanowires. *Phys. Rev. B*, 80(12):125321, 2009.

[PMT88] G. E. Pikus, V. A. Marushchak, and A. N. Titkov. Spin splitting of energy bands and spin relaxation of carriers in cubic III-V crystals (Review). *Soviet Physics - Semiconductors*, 22(2):115–124, 1988.

[PP95] F. G. Pikus and G. E. Pikus. Conduction-band spin splitting and negative magnetoresistance in a_3b_5 heterostructures. *Phys. Rev. B*, 51(23):16928–16935, Jun 1995.

[PT84] G. E. Pikus and A. N. Titkov. Spin Relaxation under Optical Orientation in Semiconductors. In F. Meier and B. P. Zakharchenya, editors, *Optical Orientation*, volume 8 of *Modern Problems in Condensed Matter Sciences*, chapter 3, pages 73–131. North-Holland, Amsterdam, 1984.

[Ram82] J. Rammer. *Quantum Transport Theory.* Frontiers in Physics. Perseus Books, 1982.

[Ras60] EI Rashba. Properties of Semiconductors with an Extremum Loop .1. Cyclotron and Combinational Resonance in a Magnetic Field Perpendicular to the Plane of the Loop. *Sov. Phys.-Solid State*, 2(6):1109–1122, 1960.

[Ras04] Emmanuel Rashba. Sum rules for spin Hall conductivity cancellation. *Phys. Rev. B*, 70(20), November 2004.

[RJA$^+$96] D. Richards, B. Jusserand, G. Allan, C. Priester, and B. Etienne. Electron spin-flip Raman scattering in asymmetric quantum wells: Spin orientation. *Solid-State Electronics*, 40(1-8):127–131, 1996. Proceedings of the Seventh International Conference on Modulated Semiconductor Structures.

[RS05] Roberto Raimondi and Peter Schwab. Spin-hall effect in a disordered two-dimensional electron system. *Phys. Rev. B*, 71(3):033311, Jan 2005.

[Sak67] J. J. Sakurai. *Advanced Quantum Mechanic.* Addison-Wesley Pub Co Inc, 1967.

[SANR09] Matthias Scheid, Inanc Adagideli, J Nitta, and Klaus Richter. Anisotropic universal conductance fluctuations in disordered quantum wires with Rashba and Dresselhaus spin-orbit interaction and applied in-plane magnetic field. *Semicond. Sci. and Technol.*, 24(6):64005, 2009.

[SAYI99] S. Sasa, K. Anjiki, T. Yamaguchi, and M. Inoue. Electron transport in a large spin-splitting 2DEG in InAs/AlGaSb heterostructures. *Physica B: Condensed Matter*, 272(1-4):149–152, 1999.

[SBK$^+$10] K. Sato, L. Bergqvist, J. Kudrnovský, P. H. Dederichs, O. Eriksson, I. Turek, B. Sanyal, G. Bouzerar, H. Katayama-Yoshida, V. A. Dinh, T. Fukushima, H. Kizaki, and R. Zeller. First-principles theory of dilute magnetic semiconductors. *Rev. Mod. Phys.*, 82(2):1633–1690, May 2010.

[Sch06] John Schliemann. Spin Hall Effect. *International Journal of Modern Physics B*, 20(9):1015–1036, apr 2006.

[SCN⁺04] J Sinova, D Culcer, Q Niu, N A Sinitsyn, T Jungwirth, and A H MacDonald. Universal intrinsic spin Hall effect. *Phys. Rev. Lett.*, 92(12), 2004.

[SDGR06] Peter Schwab, Michael Dzierzawa, Cosimo Gorini, and Roberto Raimondi. Spin Relaxation in Narrow Wires of a Two-Dimensional Electron Gas. *Phys. Rev. B*, 74(15):155316, October 2006.

[SEL03] John Schliemann, J. Egues, and Daniel Loss. Nonballistic Spin-Field-Effect Transistor. *Phys. Rev. Lett.*, 90(14):146801, April 2003.

[SGB⁺09] Th Schäpers, V A Guzenko, A Bringer, M Akabori, M Hagedorn, and H Hardtdegen. Spin-orbit coupling in $\mathrm{Ga}_x\mathrm{In}_{1-x}\mathrm{As}$/InP two-dimensional electron gases and quantum wire structures. *Semicond. Sci. and Technol.*, 24(6):64001, 2009.

[SGP⁺06] Th. Schäpers, V. A. Guzenko, M. G. Pala, U. Zülicke, M. Governale, J. Knobbe, and H. Hardtdegen. Suppression of Weak Antilocalization in $\mathrm{Ga}_x\mathrm{In}_{1-x}\mathrm{As}$/InP Narrow Quantum Wires. *Phys. Rev. B*, 74(8):081301(R), 2006.

[She04] Shun-Qing Shen. Spin hall effect and berry phase in two-dimensional electron gas. *Phys. Rev. B*, 70(8):081311, Aug 2004.

[SKK⁺08] Matthias Scheid, Makoto Kohda, Yoji Kunihashi, Klaus Richter, and Junsaku Nitta. All-Electrical Detection of the Relative Strength of Rashba and Dresselhaus Spin-Orbit Interaction in Quantum Wires. *Phys. Rev. Lett.*, 101(26):266401 – 266401–4, dec 2008.

[SR94] R.N. Silver and H. Röder. Densities of States of Mega-Dimensional Hamiltonian Matrices. *International Journal of Modern Physics C*, 05(04):735–753, aug 1994.

[SSB⁺10] Gerald Schubert, Jens Schleede, Krzysztof Byczuk, Holger Fehske, and Dieter Vollhardt. Distribution of the local density of states as a criterion for anderson localization: Numerically exact results for various lattices in two and three dimensions. *Phys. Rev. B*, 81(15):155106, Apr 2010.

[SST05] L. Sheng, D. N. Sheng, and C. S. Ting. Spin-hall effect in two-dimensional electron systems with rashba spin-orbit coupling and disorder. *Phys. Rev. Lett.*, 94(1):016602, Jan 2005.

[SZXN06] Junren Shi, Ping Zhang, Di Xiao, and Qian Niu. Proper definition of spin current in spin-orbit coupled systems. *Phys. Rev. Lett.*, 96(7):076604, Feb 2006.

[TI98] Hiroshi Tanaka and Masaki Itoh. Ab initio calculation of the hall conductivity: Positive hall coefficient of liquid fe. *Phys. Rev. Lett.*, 81(17):3727–3730, Oct 1998.

[Tor56] H. C. Torrey. Bloch Equations with Diffusion Terms. *Phys. Rev.*, 104(3):563–565, Nov 1956.

[VMRM01] I. Vurgaftman, J. R. Meyer, and L. R. Ram-Mohan. Band parameters for III–V compound semiconductors and their alloys. *Journal of Applied Physics*, 89(11):5815–5875, 2001.

[Wen07] P. Wenk. Spin-Orbit Coupling in Quantum Wires. Master's thesis, Universität Hamburg (Germany), 2007.

[WGZ$^+$06] A. Wirthmann, Y.S. Gui, C. Zehnder, D. Heitmann, C.-M. Hu, and S. Kettemann. Weak Antilocalization in InAs Quantum Wires. *Physica E: Low-dimensional Systems and Nanostructures*, 34(1-2):493–496, 2006. Proceedings of the 16th International Conference on Electronic Properties of Two-Dimensional Systems (EP2DS-16).

[Win03] R. Winkler. *Spin-Orbit Coupling Effects in Two-Dimensional Electron and Hole Systems*, volume 191 of *Springer Tracts in Modern Physics*. Springer-Verlag, Berlin, 2003.

[Win04a] R. Winkler. Rashba spin splitting and Ehrenfest's theorem. *Physica E: Low-dimensional Systems and Nanostructures*, 22(1-3):450–454, 2004.

[Win04b] R. Winkler. Spin orientation and spin precession in inversion-asymmetric quasi-two-dimensional electron systems. *Phys. Rev. B*, 69(4):045317, Jan 2004.

[WJW10] M. W. Wu, J. H. Jiang, and M. Q. Weng. Spin dynamics in semiconductors. *Physics Reports*, 493(2-4):61–236, August 2010.

[WK] P. Wenk and S. Kettemann. in preparation.

[WKSJ05] J. Wunderlich, B. Kaestner, J. Sinova, and T. Jungwirth. Experimental observation of the spin-hall effect in a two-dimensional spin-orbit coupled semiconductor system. *Phys. Rev. Lett.*, 94(4):047204, Feb 2005.

[WLZ07a] Pei Wang, You-Quan Li, and Xuean Zhao. Nonvanishing spin Hall currents in the presence of magnetic impurities. *Phys. Rev. B*, 75(7), 2007.

[WLZ07b] Pei Wang, You-Quan Li, and Xuean Zhao. Nonvanishing spin hall currents in the presence of magnetic impurities. *Phys. Rev. B*, 75(7):075326, Feb 2007.

[WOB$^+$07] C. P. Weber, J. Orenstein, B. Andrei Bernevig, Shou-Cheng Zhang, Jason Stephens, and D. D. Awschalom. Nondiffusive Spin Dynamics in a Two-Dimensional Electron Gas. *Phys. Rev. Lett.*, 98(7):076604, 2007.

[WWAF06] Alexander Weiße, Gerhard Wellein, Andreas Alvermann, and Holger Fehske. The kernel polynomial method. *Rev. Mod. Phys.*, 78(1):275–306, Mar 2006.

[Yaf63] Y. Yafet. g factors and spin-lattice relaxation of conduction electrons. In F. Seitz and D. Turnbull, editors, *Solid State Physics*, volume 14, pages 1–98. Elsevier, 1963.

[YDKO06] M Yamamoto, K Dittmer, B Kramer, and T Ohtsuki. Spin-polarization induced by Rashba spin–orbit coupling in three-terminal devices. *Physica E: Low-dimensional Systems and Nanostructures*, 32(1-2):462–465, Mai 2006.

[ZBvDA04] Gergely Zaránd, László Borda, Jan von Delft, and Natan Andrei. Theory of Inelastic Scattering from Magnetic Impurities. *Phys. Rev. Lett.*, 93(10):107204, Sep 2004.

[ZFD04] Igor Zutic, Jaroslav Fabian, and Sarma S. Das. Spintronics: Fundamentals and Applications. *Rev. Mod. Phys.*, 76(2):323, 2004.

Appendix A

SOC Strength in the Experiment

System	Spin splitting at E_F (meV)	α_2 (meV Å)	Reference
AlSb/InAs/AlSb	3.2 - 4.5	60	[HvWK+98]
AlSb/InAs/AlSb	0	0	[BEW+99]
AlSb/InAs/AlSb	0	0	[SAYI99]
AlGaAs/GaAs/AlGaAs	-	6.9 ± 0.4	[JRA+95]
2DEG GaAs/AlGaAs	-	5 ± 1	[MZM+03]
AlGaSb/InAs/AlSb	5.6 - 13	120 - 280	[SAYI99]
InAlAs/InGaAs/InAlAs	1.5	40	[DMD+89]
InAlAs/InGaAs/InAlAs	4.9 - 5.9	63 - 93	[NATE97]
InAlAs/InGaAs/InAlAs	-	50 - 100	[HNA+99]
InGaAs/InAs/InGaAs	5.1 - 6.8	60 - 110	[NATE98]
InGaAs/InAs/InGaAs	9 - 15	200 - 400	[Gru00]
InGaAs/InP/InGaAs	-	63 - 153	[ELSL97]
GaSb/InAs/GaSb	3.7	90	[LMFS88]
Si/SiGe QW	-	0.03 - 0.12	[MJM+04]
SiO2/InAs/	5.5 - 23	100 - 300	[MKMM00]
n-$In_{0.2}Ga_{0.8}As$/GaAs QW		50-70	[HSM+06]

Table A.1: Values of Rashba parameter α_2 measured in experiments [QW=quantum wire]. (List extracted from[FMAE+07].)

Parameter	AlAs	AlP	AlSb	GaAs	GaP	GaSb	InAs	InP	InSb
m_e	0.15	0.22	0.14	0.067	0.13	0.039	0.026	0.0795	0.0135

Table A.2: Experimental values of m_e[VMRM01]

System	γ_D (eV Å^3)	Reference
GaAs	24.5	[MST83]
GaAs	17.4 - 26	[PMT88]
GaAs	26.1 ± 0.9	[DPWS92]
GaAs	16.5 ± 3	[JRA+95]
GaAs	11	[RJA+96]
GaAs	9	[KH07]
GaAs	28 ± 4	[MZM+03]
InGaAs	24	[KSZ+96]

Table A.3: Values of Dresselhaus parameter γ_D measured in experiments. (List extracted from[FMAE+07].)

material	QW width Å	spacer 1 Å	spacer 2 Å	mobility (cm^2/Vs)	density cm^{-2}	α_2/α_1 SGE	α'_2/α'_1 CPGE
InAs/AlGaSb	150			3.0×10^5	8×10^{11}	2.1	2.3
InAs/AlGaSb	150			2.0×10^5	1.4×10^{12}		1.8
InAs/InAlAs	60		75	1.1×10^5	7.7×10^{11}		1.6
GaAs/AlGaAs	∞	700		3.5×10^6	1.1×10^{11}	7.6	7.6
GaAs/AlGaAs	82	50	50	2.6×10^6	9.3×10^{11}	-4.5	-4.2
GaAs/AlGaAs	150	600	300	1.0×10^5	6.6×10^{11}		-3.8
GaAs/AlGaAs	150	400	500	2.6×10^5	5.3×10^{11}		-2.4
GaAs/AlGaAs	300	700		3.2×10^6	1.3×10^{11}		2.8
GaAs/AlGaAs	300	700	1000	3.4×10^6	1.8×10^{11}		1.5

Table A.4: Measured α_2/α_1 ratios with spin-galvanic effect (SGE) and Circular photogalvanic effect (CPGE) with the according parameters at $4.2K$ [QW=quantum wire].[GGB$^+$07]

Appendix B

Linear Response

Applying linear response to first order with a perturbation $W(t)$ we get for the time dependent expectation value of an operator $\hat{A}$

$$\left\langle \hat{A} \right\rangle_t = \mathrm{Tr}\left[\rho_0 \hat{A}\right] - i \int_{-\infty}^{\infty} dt'\, \theta(t-t') \left\langle [\hat{A}_D(t), \hat{W}_D(t')] \right\rangle_0 , \tag{B.1}$$

where the index D indicates the Dirac picture. The source of the perturbation is an electric field $\mathbf{E}(t) = \mathbf{E}_0 e^{-i(\omega+i\eta)t}$ with η being an infinitesimally small positive value. The perturbation is then given by $W(t) = -\hat{\mathbf{P}} \cdot \mathbf{E}(t)$, with the dipole operator $\hat{\mathbf{P}} = \sum_i q_i \hat{\mathbf{r}}_i$ and the charge q_i at the positions $\mathbf{r}_i$.

The response to the applied electric field is a current $J_\mu = \sigma_{\mu\nu} E_\nu$. For the next steps we keep the definition of the current general. Later on we can relate it to the spin Hall current $J_x^z = -\sigma_{xy}^z E_y$, with the spin Hall conductivity $\sigma_{xy}^z \equiv \sigma_{\,\mathrm{SH}}$.

$$\langle J_\mu \rangle_t = i \sum_\nu \int_{-\infty}^{\infty} dt\, \theta(t-t') \left\langle [J_{\mu D}(0), P_{\nu D}(t'-t)] \right\rangle e^{i(\omega+i\eta)(t'-t)} \underbrace{E_{0\nu} e^{-i(\omega+i\eta)t}}_{E_{\nu(t)}} \tag{B.2}$$

the spin Hall conductivity (in the following the subscript D will be left out)

$$\sigma_{\mu\nu}(\omega) = i \int_{-\infty}^{\infty} dt\, \theta(-t) \left\langle [J_\mu(0), P_{\nu D}(t)] \right\rangle e^{-i(\omega+i\eta)t} \tag{B.3}$$

In the next step we want to replace $\hat{P}$ by its time derivative. This can be accomplished by applying the Kubo identity

$$[A(t), \rho_0] = -i\rho_0 \int_0^\beta \mathrm{d}x\, \dot{A}(t-ix) \tag{B.4}$$

in combination with $\langle [J,P]\rangle = \mathrm{Tr}([P,\rho_0]J)$. We get

$$\sigma_{\mu\nu}(\omega) = V\int_0^\beta \mathrm{d}x \int_0^\infty \mathrm{d}t\, \mathrm{Tr}(\rho_0 J_\nu(0)J_\mu(t+ix))e^{i(\omega+i\eta)t}, \tag{B.5}$$

using $(1/V)\dot{\mathbf{P}} = \mathbf{J}$, with the system volume V, $\beta = 1/k_BT$ and the density matrix

$$\rho_0 = \frac{e^{-\beta H_0}}{\mathrm{Tr}(e^{-\beta H_0})}. \tag{B.6}$$

Extracting the time dependency of the current operator $J_{\mu_D}(t+ix) = e^{i(t+ix)H_0}J_\mu e^{-i(t+ix)H_0}$ and using the eigenvector basis $\{|i\rangle\}$ we can write the conductivity tensor in the following way

$$\sigma_{\mu\nu}(\omega) = V\int_0^\beta \mathrm{d}x \int_0^\infty \mathrm{d}t \sum_{m,n} \langle m\,|J_\nu(0)|\,n\rangle \left\langle n\left| e^{i(t+ix)E_n}J_\mu e^{-i(t+ix)E_m}\right| m\right\rangle e^{i(\omega+i\eta)t}. \tag{B.7}$$

$$\cdot\, \mathrm{Tr}(\rho_0 a_m^\dagger a_n a_p^\dagger a_q). \tag{B.8}$$

We used $H = \sum_m E_m a_m^\dagger a_m$. For the next step we need the identity

$$\mathrm{Tr}(\rho_0 a_m^\dagger a_n a_p^\dagger a_q) = \delta_{mq}\delta_{np} f(E_m)(1-f(E_n)), \tag{B.9}$$

where $f(E)$ is the Fermi distribution function.

Proof. The factor $\delta_{mq}\delta_{np}$ is due to momentum conservation. The second part is yield by commutator relation

$$\begin{aligned}
\mathrm{Tr}(\rho_0 a_m^\dagger a_n a_p^\dagger a_q) &= \mathrm{Tr}(\rho_0 a_m^\dagger a_n(\delta_{nm} - a_m a_n^\dagger)) && \text{(B.10)}\\
&= \mathrm{Tr}(\rho_0(a_m^\dagger a_n\delta_{nm} - a_m^\dagger a_n a_m a_n^\dagger)) && \text{(B.11)}\\
&= \mathrm{Tr}(\rho_0(a_m^\dagger a_n\delta_{nm} - a_m^\dagger a_m a_n a_n^\dagger)) && \text{(B.12)}\\
&= \mathrm{Tr}(\rho_0(a_m^\dagger a_n\delta_{nm} - a_m^\dagger a_m(1 - a_n^\dagger a_n)) && \text{(B.13)}\\
&= \mathrm{Tr}(\rho_0(a_m^\dagger a_n\delta_{nm} - n_m(1-n_n)). && \text{(B.14)}
\end{aligned}$$

□

Applying Eq.(B.9) to Eq.(B.7) and evaluating the integral over x we get

$$\sigma_{\mu\nu}(\omega) = V\int_0^\infty \mathrm{d}t \sum_{m,n} \underbrace{f(E_m)(1-f(E_n))\frac{1-e^{-\beta(E_n-E_m)}}{(E_n-E_m)}}_{\frac{f(E_m)-f(E_n)}{E_n-E_m}} \langle m\,|J_\nu|\,n\rangle \langle n\,|J_\mu|\,m\rangle$$

$$\cdot\, e^{it(\omega+i\eta+E_n-E_m)}. \tag{B.15}$$

Finally we perform the t-integration and rewrite the formula for currents j:

$$= \frac{i}{V}\sum_{m,n} \frac{(f(E_m)-f(E_n))}{E_n-E_m}\,\frac{\langle m\,|j_\nu|\,n\rangle\,\langle n\,|j_\mu|\,m\rangle}{E_n-E_m+\omega+i\eta}. \tag{B.16}$$

B.1 Kubo Formula for Weak Disorder

In the following we are interested in the real part of Eq.(B.16) for the longitudinal conductivity at zero frequency. We rewrite the real part to a form which is suitable for the diagrammatic perturbation. The first step is (factor 2 due to spin degeneracy)

$$\begin{aligned}
\sigma_{x,x}(\omega=0) &= \lim_{\omega\to 0}\frac{2\pi}{V}\frac{e^2}{m_e^2}\sum_{m,n}\frac{f(E_m)-f(E_n)}{E_n-E_m}\,\langle m\,|p_x|\,n\rangle\,\langle n\,|p_x|\,m\rangle\,\delta(E_m-E_n+\omega) \quad \text{(B.17)}\\
&= \frac{2\pi}{V}\frac{e^2}{m_e^2}\int_0^\infty \mathrm{d}E\left(-\frac{\partial f(E)}{\partial E}\right)\langle m\,|p_x|\,n\rangle\,\langle n\,|p_x|\,m\rangle\,\delta(E-E_m)\delta(E-E_n). \quad \text{(B.18)}
\end{aligned}$$

Including impurities we average over all configurations, writing the sum as a trace

$$\sigma_{\text{imp}x,x}(0) = \frac{2\pi}{V}\frac{e^2}{m_e^2}\int_0^\infty \mathrm{d}E\left(-\frac{\partial f(E)}{\partial E}\right)\left\langle \mathrm{Tr}\left[\delta(E-H_0)p_x\delta(E-H_0)p_x\right]\right\rangle_{\text{imp}},$$

Now we chose the basis in momentum space $\{|\mathbf{k}\rangle\}$. After applying orthogonality relation we get

$$\begin{aligned}
\sigma_{\text{imp}x,x}(0) &= \frac{1}{2\pi V}\frac{e^2}{m_e^2}\int_0^\infty \mathrm{d}E\sum_{\mathbf{k},\mathbf{k}'}k_xk'_x\left\langle \mathbf{k}\left|\frac{1}{E-H_0-i\eta}-\frac{1}{E-H_0+i\eta}\right|\mathbf{k}'\right\rangle\cdot\\
&\quad\cdot\left\langle \mathbf{k}'\left|\frac{1}{E-H_0-i\eta}-\frac{1}{E-H_0+i\eta}\right|\mathbf{k}\right\rangle \quad \text{(B.19)}\\
&= \frac{1}{2\pi V}\frac{e^2}{m_e^2}\int_0^\infty \mathrm{d}E\sum_{\mathbf{k},\mathbf{k}'}k_xk'_x\cdot\\
&\quad\cdot\left\langle 2G_E^R(\mathbf{k},\mathbf{k}')G_E^A(\mathbf{k}',\mathbf{k})-G_E^R(\mathbf{k},\mathbf{k}')G_E^R(\mathbf{k}'\mathbf{k})-G_E^A(\mathbf{k},\mathbf{k}')G_E^A(\mathbf{k}',\mathbf{k})\right\rangle_{\text{imp}} \quad \text{(B.20)}
\end{aligned}$$

with the definition

$$G_E^{R/A}(\mathbf{k}',\mathbf{k}) = \left\langle \mathbf{k}'\left|\frac{1}{E-H_0\mp i\eta}\right|\mathbf{k}\right\rangle. \tag{B.21}$$

This can be simplified by noticing that the averages $\left\langle G^RG^R\right\rangle_{\text{imp}}$ and $\left\langle G^AG^A\right\rangle_{\text{imp}}$ are small compared with the other terms

Proof. We start by writing down the Green's function with finite complex self-energy Σ

$$G^{\,\mathrm{R/A}}(E) = \frac{1}{E - (H_0 - \mu + \Sigma^{\,\mathrm{R/A}})} \tag{B.22}$$

$$= \frac{x \mp iI}{x^2 + I^2} \tag{B.23}$$

with $x = E - (H_0 - \mu + \Re\Sigma)$ and $\mp I = \Im\Sigma^{\,\mathrm{R/A}}$, where μ is the chemical potential. To calculate $G^{\,\mathrm{R}}(E)G^{\,\mathrm{R}}(E)$, and accordingly for the pair of advanced Green's functions, we write the expression in terms of x, I and the spectral function

$$S = \frac{1}{\pi}\frac{I}{x^2 + I^2}. \tag{B.24}$$

This yields

$$G^R G^R = \frac{(x - iI)^2}{(x^2 + I^2)^2} \tag{B.25}$$

$$= \frac{1}{(x^2 + I^2)} - \frac{2iIx}{(x^2 + I^2)^2} - \frac{2I^2}{(x^2 + I^2)^2} \tag{B.26}$$

$$= \pi\frac{S}{I} - 2\pi^2 i\frac{S^2}{I}x - 2\pi^2 S^2. \tag{B.27}$$

Assuming the weak disorder limit, i.e. the impurity density $n_{\,\mathrm{imp}} \to 0$, it follows that due to $\tau \propto n^{-1}_{\,\mathrm{imp}}$, with $\tau^{-1} \equiv -2\Im\Sigma^R$, the spectral function becomes a delta distribution. Using[Mah00]

$$\lim_{I\to 0}\left(\frac{S}{I} - 2\pi S^2\right) = 0 \tag{B.28}$$

we end up with

$$G^R G^R = \lim_{I\to 0} -2\pi^2 i\frac{S^2}{I}x \tag{B.29}$$

$$= -\,i\pi\frac{1}{I^2}x\delta(x) \tag{B.30}$$

$$= 0. \tag{B.31}$$

In the last step we applied again Eq. (B.28).

In contrast to this result we get for the retarded-advanced-pair of Green's functions in the weak disorder limit

$$G^R G^A = \lim_{I\to 0}\frac{1}{x^2 + I^2} \tag{B.32}$$

$$= \lim_{I\to 0}\pi\frac{S}{I}, \tag{B.33}$$

which is divergent and therefore significant. □

Furthermore, we assume low temperature which is why the derivative of the Fermi function fixes the energy of the Green's functions to the Fermi energy,

$$-\frac{\partial f_{T=0}}{\partial E} = \delta(E - E_F). \tag{B.34}$$

We end up with

$$\sigma_{\text{ imp}x,x}(0) = \frac{1}{\pi V}\frac{e^2}{m_e^2}\sum_{\mathbf{k},\mathbf{k}'} k_x k'_x \left\langle G^R_E(\mathbf{k},\mathbf{k}')G^A_E(\mathbf{k}',\mathbf{k})\right\rangle_{\text{ imp}}. \tag{B.35}$$

Appendix C

Cooperon and Spin Relaxation

C.1 Sum Formula for the Cooperon

Writing the Cooperon (Eq. 3.43)

$$\hat{C}(\mathbf{Q}) = \frac{1}{D_e(\mathbf{Q} + 2e\mathbf{A} + 2e\mathbf{A_S})^2 + H_{\gamma_D}}. \tag{C.1}$$

in singlet, $|S=0;m=0\rangle = (|\uparrow\downarrow\rangle - |\downarrow\uparrow\rangle)/\sqrt{2} \equiv |\rightleftarrows\rangle$ and triplet $|S=1;m=0\rangle = (|\uparrow\downarrow\rangle + |\downarrow\uparrow\rangle)/\sqrt{2} \equiv |\rightrightarrows\rangle, |S=1;m=1\rangle \equiv |\upuparrows\rangle, |S=1;m=-1\rangle \equiv |\downdownarrows\rangle$ representation, without magnetic field the singlet sector is decoupled from the triplet one. To sum over $C_{\alpha\beta\beta\alpha}$ in the case of a finite magnetic field and having calculated the eigenvectors $|i\rangle$ and eigenvalue λ_i for the Cooperon Hamiltonian, we can use the following simplification:

$$\sum_{\alpha\beta} C_{\alpha\beta\beta\alpha} = \sum_{\alpha\beta} \sum_{\substack{mS \\ m'S'}} \langle \alpha\beta \,| mS \rangle \langle m'S' \,| \beta\alpha \rangle \langle mS \,| C |\, m'S' \rangle . \tag{C.2}$$

Only several of the prefactors $\langle \alpha\beta \,| mS \rangle \langle m'S' \,| \beta\alpha \rangle$ are non-zero:

For $\alpha\beta = \upuparrows$

$$\langle \upuparrows | \upuparrows \rangle \langle \upuparrows | \upuparrows \rangle = 1, \tag{C.3}$$

For $\alpha\beta = \downdownarrows$

$$\langle \downdownarrows | \downdownarrows \rangle \langle \downdownarrows | \downdownarrows \rangle = 1, \tag{C.4}$$

For $\alpha\beta = \uparrow\downarrow$

$$\langle \uparrow\downarrow | \rightleftarrows \rangle \langle \rightleftarrows | \downarrow\uparrow \rangle = -\frac{1}{2}, \tag{C.5}$$

$$\langle \uparrow\downarrow | \rightleftarrows \rangle \langle \rightrightarrows | \downarrow\uparrow \rangle = +\frac{1}{2}, \tag{C.6}$$

$$\langle \uparrow\downarrow | \rightrightarrows \rangle \langle \rightleftarrows | \downarrow\uparrow \rangle = -\frac{1}{2}, \tag{C.7}$$

$$\langle \uparrow\downarrow | \rightrightarrows \rangle \langle \rightrightarrows | \downarrow\uparrow \rangle = +\frac{1}{2}, \tag{C.8}$$

For $\alpha\beta = \downarrow\uparrow$

$$\langle \downarrow\uparrow | \rightleftarrows \rangle \langle \rightleftarrows | \uparrow\downarrow \rangle = -\frac{1}{2}, \tag{C.9}$$

$$\langle \downarrow\uparrow | \rightleftarrows \rangle \langle \rightrightarrows | \uparrow\downarrow \rangle = -\frac{1}{2}, \tag{C.10}$$

$$\langle \downarrow\uparrow | \rightrightarrows \rangle \langle \rightleftarrows | \uparrow\downarrow \rangle = +\frac{1}{2}, \tag{C.11}$$

$$\langle \downarrow\uparrow | \rightrightarrows \rangle \langle \rightrightarrows | \uparrow\downarrow \rangle = +\frac{1}{2}. \tag{C.12}$$

Inserting the eigenvectors,

$$\sum_{\alpha\beta} C_{\alpha\beta\beta\alpha} = \sum_{\alpha\beta} \sum_{\substack{mS \\ m'S'}} \sum_{i} \langle \alpha\beta | mS \rangle \left\langle m'S' | \beta\alpha \right\rangle \langle mS | i \rangle \left\langle i | C | m'S' \right\rangle, \tag{C.13}$$

we end up with

$$= \sum_{i} (\langle \upuparrows | i \rangle \langle i | \upuparrows \rangle + \langle \rightrightarrows | i \rangle \langle i | \rightrightarrows \rangle + \langle \downdownarrows | i \rangle \langle i | \downdownarrows \rangle - \langle \rightleftarrows | i \rangle \langle i | \rightleftarrows \rangle) \lambda_i^{-1}. \tag{C.14}$$

Writing

$$\sum_{\alpha\beta} C_{\alpha\beta\beta\alpha} = C_{\uparrow\uparrow,\uparrow\uparrow} + C_{\uparrow\downarrow,\downarrow\uparrow} + C_{\downarrow\uparrow,\uparrow\downarrow} + C_{\downarrow\downarrow,\downarrow\downarrow} \tag{C.15}$$

$$= \mathrm{Tr}\left[\begin{pmatrix} 1 & 0 & 0 & 0 \\ 0 & 0 & 1 & 0 \\ 0 & 1 & 0 & 0 \\ 0 & 0 & 0 & 1 \end{pmatrix} C \right] \tag{C.16}$$

$$\equiv \mathrm{Tr}[\Lambda C] \tag{C.17}$$

in singlet-triplet representation by using the transformation U_{ST},

$$U_{ST} \equiv \begin{pmatrix} |\upuparrows\rangle \\ |\uparrow\downarrow\rangle \\ |\downarrow\uparrow\rangle \\ |\downdownarrows\rangle \end{pmatrix} \otimes \begin{pmatrix} |\rightleftarrows\rangle \\ |\upuparrows\rangle \\ |\rightrightarrows\rangle \\ |\downdownarrows\rangle \end{pmatrix} = \begin{pmatrix} 0 & \frac{1}{\sqrt{2}} & -\frac{1}{\sqrt{2}} & 0 \\ 1 & 0 & 0 & 0 \\ 0 & \frac{1}{\sqrt{2}} & \frac{1}{\sqrt{2}} & 0 \\ 0 & 0 & 0 & 1 \end{pmatrix}, \tag{C.18}$$

it can be seen that the singlet term has positive contribution to the conductivity in contrast to the triplet terms which have a different sign: Transforming Λ using U_{ST} we get

$$U_{ST} \Lambda U_{ST}^{-1} = \begin{pmatrix} -1 & 0 & 0 & 0 \\ 0 & 1 & 0 & 0 \\ 0 & 0 & 1 & 0 \\ 0 & 0 & 0 & 1 \end{pmatrix}, \tag{C.19}$$

where we can immediately extract the signs.

C.2 Spin-Conserving Boundary

In the following we set $\gamma_g = 1$. In order to generate a finite system, we need to specify the boundary conditions. These can be different for the spin and charge current. Here we derive the spin-conserving boundary conditions. Let us first recall the diffusion current density $\mathbf{j}$ at position $\mathbf{r}$ as derived from a classical picture in Sec. 2.3.4, which is given by

$$\mathbf{j}_{s_i}(\mathbf{r}, t) = \langle \mathbf{v} s_i^{\mathbf{k}}(\mathbf{r}, t) \rangle - D_e \nabla s_i(\mathbf{r}, t), \tag{C.20}$$

where $s_i^{\mathbf{k}}$ is the part of the spin-density which evolved from the spin-density at $\mathbf{r} - \Delta\mathbf{x}$ moving with velocity $\mathbf{v}$ and momentum $\mathbf{k}$. Using the Bloch equation

$$\frac{\partial \hat{\mathbf{s}}}{\partial t} = \hat{\mathbf{s}} \times \mathbf{B}_{\text{SO}}(\mathbf{k}) - \frac{1}{\hat{\tau}_s} \hat{\mathbf{s}}, \tag{C.21}$$

we rewrite the first term in Eq. (C.20) yielding the total spin-diffusion current as

$$\mathbf{j}_{s_i} = -\tau \langle \mathbf{v}_F \left[\mathbf{B}_{\text{SO}}(\mathbf{k}) \times \mathbf{S} \right]_i \rangle - D_e \nabla s_i. \tag{C.22}$$

In Sec. 3.4.1 we consider specular scattering from the boundary with the condition that the spin is conserved, so that the spin current density normal to the boundary must vanish

$$\mathbf{n} \cdot \mathbf{j}_{s_i}|_{\pm W/2} = 0, \tag{C.23}$$

where $\mathbf{n}$ is the vector normal to the boundary. Noting the relation between the spin-diffusion equation in the s_i representation and the triplet components of the Cooperon density $\tilde{s}_i$ ($\{|\upuparrows\rangle, |\rightrightarrows\rangle, |\downdownarrows\rangle\}$), Eq. (3.60),

$$U_{\rm CD}(\epsilon_{ijk}B_{{\rm SO},j})_{i=1..3,k=1..3}U^{\dagger}_{\rm CD} = -i(\langle\tilde{s}_i|\,\mathbf{B}_{\rm SO}\cdot\mathbf{S}\,|\tilde{s}_k\rangle)_{i=1..3,k=1..3}, \tag{C.24}$$

where the matrix $U_{\rm CD}$ is given by Eq. (3.61), we can thereby transform the boundary condition for the spin-diffusion current, Eq. (C.23), to the triplet components of the Cooperon density $\tilde{s}_i$,

$$0 = \mathbf{n}\cdot\mathbf{j}_{\tilde{s}_i}|_{y=\pm W/2}. \tag{C.25}$$

Requiring also that the charge density is vanishing normal to the transverse boundaries, which transforms into the condition $-i\partial_{\mathbf{n}}\tilde{\rho}|_{\rm Surface} = 0$ for the singlet component of the Cooperon density $\tilde{\rho}$, we finally get the boundary conditions for the Cooperon without external magnetic field, Eq. (3.70),

$$\left(-\frac{\tau}{D_e}\mathbf{n}\cdot\langle\mathbf{v}_F[\mathbf{B}_{\rm SO}(\mathbf{k})\cdot\mathbf{S}]\rangle - i\partial_{\mathbf{n}}\right)C|_{\rm Surface} = 0. \tag{C.26}$$

The last expression can be rewritten using the effective vector potential $\mathbf{A_S}$, Eq. (3.43),

$$(\mathbf{n}\cdot 2e\mathbf{A_S} - i\partial_{\mathbf{n}})\,C|_{\rm Surface} = 0. \tag{C.27}$$

In the case of Rashba and linear and cubic Dresselhaus SO coupling in (001) systems, we get

$$\begin{aligned}\frac{D_e}{\tau}2e\mathbf{A_S} &= -\langle\mathbf{v}_F(\mathbf{B}_{\rm SO}(\mathbf{k})\cdot\mathbf{S})\rangle \\ &= v_F^2 m_e\begin{pmatrix} -(\alpha_1 - \frac{\gamma_D(m_e v_F)^2}{4}) & -\alpha_2 \\ \alpha_2 & \alpha_1 - \frac{\gamma_D(m_e v_F)^2}{4}\end{pmatrix}.\mathbf{S}.\end{aligned} \tag{C.28}$$

C.3 Relaxation Tensor

To connect the effective vector potential $\mathbf{A_S}$ with the spin relaxation tensor, we notice that $\hat{\tau}$ can be rewritten in the following way:

$$\frac{1}{\hat{\tau}_s} = \tau(\langle\mathbf{B}_{\rm SO}(\mathbf{k})^2\rangle\delta_{ij} - \langle B_{\rm SO}(\mathbf{k})_i B_{\rm SO}(\mathbf{k})_j\rangle)_{i=1..3,j=1..3} \tag{C.29}$$

using $U_{\rm CD}$, Eq. (3.60),

$$
\begin{aligned}
&= \tau U^{\dagger}_{\rm CD}\{\langle B_{\rm SO}(\mathbf{k})_x\rangle S_x^2 + \langle B_{\rm SO}(\mathbf{k})_y\rangle S_y^2 \\
&\quad + \langle B_{\rm SO}(\mathbf{k})_x B_{\rm SO}(\mathbf{k})_y\rangle (S_x S_y + S_y S_x)\} U_{\rm CD} && \text{(C.30)}\\
&= \tau U^{\dagger}_{\rm CD}\langle(\mathbf{B}_{\rm SO}(\mathbf{k}).\mathbf{S})^2\rangle U_{\rm CD} && \text{(C.31)}\\
&= \frac{\tau}{v_F^2} U^{\dagger}_{\rm CD}\langle(\mathbf{v}_F \mathbf{B}_{\rm SO}(\mathbf{k}).\mathbf{S})^2\rangle U_{\rm CD}. && \text{(C.32)}
\end{aligned}
$$

Because

$$\frac{\tau}{v_F^2}\langle(\mathbf{v}_F[\mathbf{B}_{\rm SO}(\mathbf{k}).\mathbf{S}])^2\rangle = \frac{2\tau}{v_F^2}\langle(\mathbf{v}_F[\mathbf{B}_{\rm SO}(\mathbf{k}).\mathbf{S}])\rangle^2 \tag{C.33}$$

is true for linear Rashba and linear Dresselhaus SO coupling but, in general, false if cubic-in-k terms are included in the SO field, we have to write

$$\tau\langle(\mathbf{B}_{\rm SO}(\mathbf{k}).\mathbf{S})^2\rangle = \frac{2\tau}{v_F^2}\langle(\mathbf{v}_F \mathbf{B}_{\rm SO}(\mathbf{k}).\mathbf{S})\rangle^2 + \mathrm{ct} \tag{C.34}$$

so that we conclude

$$\frac{1}{\hat{\tau}_s} = U^{\dagger}_{\rm CD}(D_e(2e\mathbf{A}_{\mathbf{S}})^2 + ct)U_{\rm CD} \tag{C.35}$$

with the separated cubic part $ct = D_e m_e^2 E_F^2 \gamma_D^2 (S_x^2 + S_y^2)$. This reflects nothing but the fact that the effective SO Zeeman term in Eq. (3.32) can only be rewritten as a vector potential $\mathbf{A}_{\mathbf{S}}$ when the SO coupling is linear in momentum.

As an example we assume a very general Cooperon that means the growth direction of the material and the SO coupling should be very general. We set

$$(2e\mathbf{A}_S)^2 + H_\gamma = (\alpha_{11}S_x + \alpha_{21}S_y + \alpha_{31}S_z)^2 + (\alpha_{12}S_x + \alpha_{22}S_y + \alpha_{32}S_z)^2 + \alpha_4 S_z^2 \tag{C.36}$$

After the transformation we get

$$\frac{1}{\hat{\tau}} = \begin{pmatrix} \alpha_{21}^2 + \alpha_{22}^2 + \alpha_{31}^2 + \alpha_{32}^2 + \alpha_4 & -\alpha_{11}\alpha_{21} - \alpha_{12}\alpha_{22} & -\alpha_{11}\alpha_{31} - \alpha_{12}\alpha_{32} \\ -\alpha_{11}\alpha_{21} - \alpha_{12}\alpha_{22} & \alpha_{11}^2 + \alpha_{12}^2 + \alpha_{31}^2 + \alpha_{32}^2 + \alpha_4 & -\alpha_{21}\alpha_{31} - \alpha_{22}\alpha_{32} \\ -\alpha_{11}\alpha_{31} - \alpha_{12}\alpha_{32} & -\alpha_{21}\alpha_{31} - \alpha_{22}\alpha_{32} & \alpha_{11}^2 + \alpha_{12}^2 + \alpha_{21}^2 + \alpha_{22}^2 \end{pmatrix}. \tag{C.37}$$

C.4 Weak Localization Correction in 2D

In contrast to the case where we have a wire with a finite width, we can calculate the weak localization correction to the conductivity analytically in the 2D case. The cutoffs due to dephasing $c_1 = 1/D_e Q_{\text{SO}}^2 \tau_\varphi$ and elastic scattering $c_2 = 1/D_e Q_{\text{SO}}^2 \tau$ determine whether we have a positive or negative correction. Integrating over all possible wave vectors $K = k/Q_{\text{SO}}$ in the case without boundaries yields

$$\begin{aligned}
\Delta\sigma \quad = \quad & -\frac{2e^2}{2\pi}\frac{1}{(2\pi)^2}\int_0^{\sqrt{c_2}} \mathrm{d}K\,(2\pi K)\Bigg(-\frac{1}{E_S(Q_{\text{SO}}K)/Q_{\text{SO}}^2 + c_1} + \frac{1}{E_{T_0}(Q_{\text{SO}}K)/Q_{\text{SO}}^2 + c_1} \\
& + \frac{1}{E_{T_+}(Q_{\text{SO}}K)/Q_{\text{SO}}^2 + c_1} + \frac{1}{E_{T_-}(Q_{\text{SO}}K)/Q_{\text{SO}}^2 + c_1}\Bigg) \qquad \text{(C.38)}
\end{aligned}$$

$$\begin{aligned}
= \quad & -\frac{2e^2}{2\pi}\Bigg(-\frac{1}{2}\ln\left(1+\frac{c_2}{c_1}\right) + \frac{1}{2}\ln\left(1+\frac{c_2}{1+c_1}\right) \\
& + \left\{\frac{\arctan\left(\frac{5}{4}\frac{1}{\sqrt{\frac{7}{16}+c_1}}\right) - \arctan\left(\frac{\sqrt{\frac{1}{16}+c_2}+1}{\sqrt{\frac{7}{16}+c_1}}\right)}{\sqrt{\frac{7}{16}+c_1}} - \frac{1}{2}\ln\left(\frac{2+c_1}{\frac{3}{2}+c_1+c_2+2\sqrt{\frac{1}{16}+c_2}}\right)\right\} \\
& + \left\{\frac{\arctan\left(\frac{3}{4}\frac{1}{\sqrt{\frac{7}{16}+c_1}}\right) + \arctan\left(\frac{\sqrt{\frac{1}{16}+c_2}-1}{\sqrt{\frac{7}{16}+c_1}}\right)}{\sqrt{\frac{7}{16}+c_1}} - \frac{1}{2}\ln\left(\frac{1+c_1}{\frac{3}{2}+c_1+c_2-2\sqrt{\frac{1}{16}+c_2}}\right)\right\} \\
& \Bigg)\,. \qquad \text{(C.39)}
\end{aligned}$$

As an example, we choose parameters which have been used in the case of boundaries, $1/D_e Q_{\text{SO}}^2 \tau_\varphi = 0.08, 1/D_e Q_{\text{SO}}^2 \tau = 4$: $\Delta\sigma/(2e^2/2\pi) = -0.29$. The exact calculation of wide wires ($Q_{\text{SO}} W > 1$) approaches this limit as can be seen in Fig. 3.11. The weak localization correction in 2D as function of these parameters is plotted in Fig. C.1.

C.5 Exact Diagonalization

We write the inverse Cooperon propagator, the Hamiltonian $\tilde{H}_c$, in the representation of the longitudinal momentum Q_x, the quantized transverse momentum with quantum number $n \in \mathbb{N}$, and in the representation of singlet and triplet states with quantum numbers S, m, where we note that $\tilde{H}_c$ is diagonal in Q_x,

$$\langle Q_x, n, S, m \mid \tilde{H}_c \mid Q_x, n', S', m' \rangle. \qquad \text{(C.40)}$$

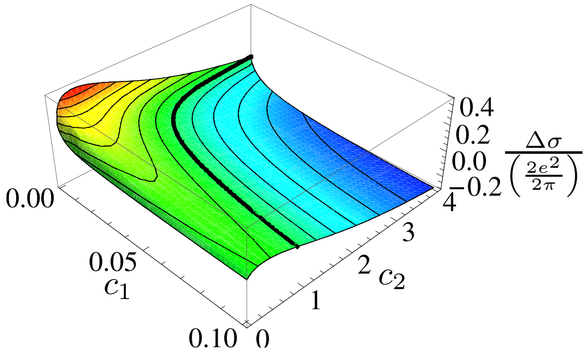

Figure C.1: Weak localization correction in 2D in units of $(2e^2/2\pi)$. The parameters are $c_1 = 1/D_e Q^2_{\text{SO}} \tau_\varphi$ and $c_2 = 1/D_e Q^2_{\text{SO}} \tau$. Thick line indicates $\Delta\sigma = 0$.

The spin subspace is thus represented by 4×4 matrices, which we order starting with the singlet $S = 0$ and then $S = 1, m = 1$, $m = 0$, and $m = -1$. Thus, we get

$$\langle Q_x, n \mid \tilde{H}_c \mid Q_x, n \rangle = Q^2_{\text{SO}} \begin{pmatrix} A_n & 0 & 0 & 0 \\ 0 & B_n & iF_n & D_n \\ 0 & -iF_n & C_n & iF_n \\ 0 & D_n & -iF_n & B_n \end{pmatrix}. \tag{C.41}$$

The calculation of the matrix elements yields (we set $P = Q_{\text{SO}} W/\pi$)

$$A_0 = K_x^2, \tag{C.42}$$

$$B_0 = \frac{3}{4} + K_x^2 - \frac{1}{4}\frac{\sin(P\pi)}{P\pi}, \tag{C.43}$$

$$C_0 = \frac{1}{2} + K_x^2 + \frac{1}{2}\frac{\sin(P\pi)}{P\pi}, \tag{C.44}$$

$$D_0 = -\frac{1}{4} \quad - \frac{1}{4}\frac{\sin(P\pi)}{P\pi}, \tag{C.45}$$

$$F_0 = \sqrt{2} K_x \frac{\sin(\frac{P\pi}{2})}{\frac{P\pi}{2}}, \tag{C.46}$$

and for $n > 0$:

$$A_n = K_x^2 + \left(\frac{n}{P}\right)^2, \tag{C.47}$$

$$B_n = \frac{3}{4} + K_x^2 + \left(\frac{n}{P}\right)^2 + \frac{2P^2 - n^2}{4(n+P)(n-P)}\frac{\sin(P\pi)}{P\pi}, \tag{C.48}$$

$$C_n = \frac{1}{2} + K_x^2 + \left(\frac{n}{P}\right)^2 - \frac{2P^2 - n^2}{2(n+P)(n-P)} \frac{\sin(P\pi)}{P\pi}, \tag{C.49}$$

$$D_n = -\frac{1}{4} - \frac{n^2 - 2P^2}{4(n-P)(n+P)} \frac{\sin(P\pi)}{P\pi}, \tag{C.50}$$

$$F_n = \frac{\sqrt{2}(2n^2 - P^2)}{2\left(n - \frac{P}{2}\right)\left(n + \frac{P}{2}\right)} \frac{\sin(\frac{P\pi}{2})}{\frac{P\pi}{2}}. \tag{C.51}$$

For $n \neq n'$, the spin matrices have the form

$$\langle Q_x, n \mid \tilde{H}_c \mid Q_x, n' \rangle = \frac{Q_{\mathrm{SO}}^2}{\pi} P \begin{pmatrix} 0 & 0 & 0 & 0 \\ 0 & a & ig & d \\ 0 & -ig & b & if \\ 0 & d & -if & c \end{pmatrix}. \tag{C.52}$$

Calculating the matrix elements for $n = 0, n' > 0$, we get

$$a = \frac{1}{\sqrt{2}} \left(\frac{\left(1 + (-1)^{n'}\right)\sin(P\pi)}{(n' - 2P)(n' + 2P)} - \frac{4\left(-1 + (-1)^{n'}\right) K_x \cos\left(\frac{P\pi}{2}\right)}{(n' - P)(n' + P)} \right), \tag{C.53}$$

$$b = -\frac{\sqrt{2}\left(1 + (-1)^{n'}\right)\sin(P\pi)}{(n' - 2P)(n' + 2P)}, \tag{C.54}$$

$$c = \frac{1}{\sqrt{2}} \left(\frac{4\left(-1 + (-1)^{n'}\right) K_x \cos\left(\frac{P\pi}{2}\right)}{(n' - P)(n' + P)} + \frac{\left(1 + (-1)^{n'}\right)\sin(P\pi)}{(n' - 2P)(n' + 2P)} \right), \tag{C.55}$$

$$d = \frac{\left(1 + (-1)^{n'}\right)\sin(P\pi)}{\sqrt{2}(n' - 2P)(n' + 2P)}, \tag{C.56}$$

$$f = 2 \left(\frac{\left(-1 + (-1)^{n'}\right)\cos(P\pi)}{2(n' - 2P)(n' + 2P)} - \frac{\left(1 + (-1)^{n'}\right) K_x \sin\left(\frac{P\pi}{2}\right)}{(n' - P)(n' + P)} \right), \tag{C.57}$$

$$g = -2 \left(\frac{\left(-1 + (-1)^{n'}\right)\cos(P\pi)}{2(n' - 2P)(n' + 2P)} + \frac{\left(1 + (-1)^{n'}\right) K_x \sin\left(\frac{P\pi}{2}\right)}{(n' - P)(n' + P)} \right). \tag{C.58}$$

And for $n > 0, n' > 0$, we get

$$\begin{aligned} a &= R_{\{2,+\}} \sin(P\pi) + 4K_x R_{\{1,-\}} \cos\left(\frac{P\pi}{2}\right), && \text{(C.59)} \\ b &= -2R_{\{2,+\}} \sin(P\pi), && \text{(C.60)} \\ c &= R_{\{2,+\}} \sin(P\pi) - 4K_x R_{\{1,-\}} \cos\left(\frac{P\pi}{2}\right), && \text{(C.61)} \\ d &= R_{\{2,+\}} \sin(P\pi), && \text{(C.62)} \\ f &= -\sqrt{2}\left(R_{\{2,-\}} \cos(P\pi) + 2K_x R_{\{1,+\}} \sin\left(\frac{P\pi}{2}\right)\right), && \text{(C.63)} \\ g &= \sqrt{2}\left(R_{\{2,-\}} \cos(P\pi) - 2K_x R_{\{1,+\}} \sin\left(\frac{P\pi}{2}\right)\right), && \text{(C.64)} \end{aligned}$$

with the functions

$$\begin{aligned} R_{\{1,\pm\}} &= \frac{\left(1 \pm (-1)^{n+n'}\right)(n^2 + n'^2 - P^2)}{((n-n') - P)((n+n') - P)((n-n') + P)((n+n') + P)}, && \text{(C.65)} \\ R_{\{2,\pm\}} &= \frac{\left(1 \pm (-1)^{n+n'}\right)(n^2 + n'^2 - (2P)^2)}{((n-n') - 2P)((n+n') - 2P)((n-n') + 2P)((n+n') + 2P)}. && \text{(C.66)} \end{aligned}$$

Appendix D

Hamiltonian in [110] growth direction

The Cooperon Hamiltonian in the 0-mode approximation is given as follows

$$H_{c,0} = \begin{pmatrix} A & B & C \\ B^* & D & E \\ C^* & E^* & F \end{pmatrix} + M_{q3}, \tag{D.1}$$

with

$$\begin{aligned} A = \frac{1}{4q_2W}&\left(q_2\left(4k_x^2 + 3\left(\tilde{q}_1^2 + q_2^2\right)\right)W \right. \\ &\left. - 16k_x\tilde{q}_1 \sin\left(\frac{q_2W}{2}\right) + \left(\tilde{q}_1^2 - q_2^2\right)\sin(q_2W)\right), \end{aligned} \tag{D.2}$$

$$B = \frac{i\left(4k_x \sin\left(\frac{q_2W}{2}\right) - \tilde{q}_1 \sin(q_2W)\right)}{\sqrt{2}W}, \tag{D.3}$$

$$C = -\frac{q_2\left(\tilde{q}_1^2 + q_2^2\right)W + \left(q_2^2 - \tilde{q}_1^2\right)\sin(q_2W)}{4q_2W}, \tag{D.4}$$

$$D = \frac{q_2\left(2k_x^2 + \tilde{q}_1^2 + q_2^2\right)W + \left(q_2^2 - \tilde{q}_1^2\right)\sin(q_2W)}{2q_2W}, \tag{D.5}$$

$$E = \frac{i\left(4k_x \sin\left(\frac{q_2W}{2}\right) + \tilde{q}_1 \sin(q_2W)\right)}{\sqrt{2}W}, \tag{D.6}$$

$$\begin{aligned} F = \frac{1}{4q_2W}&\left(q_2\left(4k_x^2 + 3\left(\tilde{q}_1^2 + q_2^2\right)\right)W \right. \\ &\left. + 16k_x\tilde{q}_1 \sin\left(\frac{q_2W}{2}\right) + \left(\tilde{q}_1^2 - q_2^2\right)\sin(q_2W)\right) \end{aligned} \tag{D.7}$$

and the term due to cubic Dresselhaus SOC

$$M_{q3} = \\ q_3 \begin{pmatrix} \frac{1}{4}\operatorname{sinc}(q_2 W) + \frac{3}{4} & 0 & \frac{1}{4}\operatorname{sinc}(q_2 W) - \frac{1}{4} \\ 0 & \frac{1}{2} - \frac{1}{2}\operatorname{sinc}(q_2 W) & 0 \\ \frac{1}{4}\operatorname{sinc}(q_2 W) - \frac{1}{4} & 0 & \frac{1}{4}\operatorname{sinc}(q_2 W) + \frac{3}{4} \end{pmatrix}. \tag{D.8}$$

Appendix E

Summation over the Fermi Surface

The Cooperon Hamiltonian in the 2D case is given by

$$\begin{aligned}H_c = \tau v^2 \{ &\langle \cos^2(\varphi)\rangle (\mathbf{Q} + 2m_e \mathbf{a}.\mathbf{S})_x^2 \\ &+ \langle \sin^2(\varphi)\rangle (\mathbf{Q} + 2m_e \mathbf{a}.\mathbf{S})_y^2 \\ &+ 4m_e^2 \gamma_D v^2 \langle \cos^2(\varphi)\sin^2(\varphi)\rangle (\mathbf{Q} + 2m_e \mathbf{a}.\mathbf{S})_x . S_x \\ &- 4m_e^2 \gamma_D v^2 \langle \sin^2(\varphi)\cos^2(\varphi)\rangle (\mathbf{Q} + 2m_e \mathbf{a}.\mathbf{S})_y . S_y \\ &+ (2m_e^3 \gamma_D v^2)^2 (\langle \cos^2(\varphi)\sin^4(\varphi)\rangle S_x^2 \\ &+ \langle \sin^2(\varphi)\cos^4(\varphi)\rangle S_y^2)\},\end{aligned} \tag{E.1}$$

with wave vector $\mathbf{Q}$. We set

$$m_e \equiv 1, \tag{E.2}$$

$$f_1 := \langle \sin^2(\varphi)\rangle, \tag{E.3}$$

$$f_2 := \langle \cos^2(\varphi)\rangle, \tag{E.4}$$

$$f_3 := \langle \sin^2(\varphi)\cos^2(\varphi)\rangle, \tag{E.5}$$

$$f_4 := \langle \sin^4(\varphi)\cos^2(\varphi)\rangle, \tag{E.6}$$

$$f_5 := \langle \sin^2(\varphi)\cos^4(\varphi)\rangle. \tag{E.7}$$

Using the Matsubara trick we write

$$\int_0^{2\pi} \frac{\mathrm{d}\varphi}{2\pi} = \frac{2}{\pi N} \sum_{s=1}^{N} \frac{1}{\sqrt{1 - \left(\frac{s}{N}\right)^2}}. \tag{E.8}$$

This gives us

$$f_1 = \frac{2}{\pi N} \sum_{s=1}^{N-1} \frac{s^2}{N^2 \sqrt{1 - \left(\frac{s}{N}\right)^2}}, \tag{E.9}$$

$$f_2 = \frac{2}{\pi N} \sum_{s=1}^{N} \sqrt{1 - \left(\frac{s}{N}\right)^2}, \tag{E.10}$$

$$f_3 = \frac{2}{\pi N} \sum_{s=1}^{N} \left(\frac{s}{N}\right)^2 \sqrt{1 - \left(\frac{s}{N}\right)^2}, \tag{E.11}$$

$$f_4 = \frac{2}{\pi N} \sum_{s=1}^{N} \left(\frac{s}{N}\right)^4 \sqrt{1 - \left(\frac{s}{N}\right)^2}, \tag{E.12}$$

$$f_5 = \frac{2}{\pi N} \sum_{s=1}^{N} \left(\frac{s}{N}\right)^2 \left(1 - \left(\frac{s}{N}\right)^2\right)^{\frac{3}{2}}. \tag{E.13}$$

Writing Eq. (E.1) in a compact way gives us Eq. (4.49).

Appendix F

KPM

The recursion relations of the polynomials of first and second kind, Eq. (5.34) and Eq. (5.35), allow for a simple iteration procedure: The core of KPM is the iterative construction of the states $|\alpha_n\rangle = T_n(\tilde{H})\,|\alpha\rangle$, described by the following steps[WWAF06],

$$|\alpha_0\rangle = |\alpha\rangle\,, \tag{F.1}$$

$$|\alpha_1\rangle = \tilde{H}\,|\alpha_0\rangle\,, \tag{F.2}$$

$$|\alpha_{n+1}\rangle = 2\tilde{H}\,|\alpha_n\rangle - |\alpha_{n-1}\rangle\,, \tag{F.3}$$

where $|\alpha\rangle$ is the starting vector. For instance, to calculate the local DOS at site i, our starting vector would be the site-occupation vector $|i\rangle$. Then the coefficients for the $T_n(E)$ polynomial are given by $\mu_n = \langle i\,|i_n\rangle$ and $\rho_i(E)$ is reconstructed by using Eq. (5.32). Consequently, the most time consuming part is the matrix-vector multiplication $H\,|\alpha_n\rangle$. Because H is sparse in our case, a very efficient multiplication is done by decomposing the operator

- in a matrix A which contains the information about connected sites, which comprises their site number and the type of hopping between them
- and a matrix SOH which contains all hopping matrices which are two-dimensional due to SOC.

The type of hopping is coded in a number h_{ij}, e.g. $h_{ij} = 0$ can be defined as "hopping from i to j $\Longleftrightarrow$ hopping in the positive x-direction". To give an example: The site i is connected with site $j = A[i][2*k]$[1] and the type of hopping is $h_{ij} = A[i][2*k+1]$, with k being an

---

[1] we use C-type of writing matrices

integer running from 0 up to the number of neighbors. The hopping matrix $\mathbf{t}(i,j)$, which includes the SOC, is then given by

$$\mathbf{t}(i,j) = \begin{pmatrix} \mathrm{SOH}[h_{ij}][0][0] & \mathrm{SOH}[h_{ij}][0][1] \\ \mathrm{SOH}[h_{ij}][1][0] & \mathrm{SOH}[h_{ij}][1][1] \end{pmatrix}. \tag{F.4}$$

This leads finally to the following algorithm for the operation $H.v = v_{\text{out}}$:

Listing F.1: Optimized matrix-vector multiplication

```
for ( m=0; m<siteNum; m++ )
{
    temp_up = temp_down=0.;
    Msize_m = A[m].size()/2;
    for ( j=0; j<Msize_m; j++ )
    {
        m2 = A[m][2*j+1];
        m1 = A[m][2*j];
        temp_up    += SOH[m2][0][0]*v[2*m1]+SOH[m2][0][1]*v[2*m1+1];
        temp_down  += SOH[m2][1][0]*v[2*m1]+SOH[m2][1][1]*v[2*m1+1];
    }

    v_out[2*m]= temp_up;
    v_out[2*m+1]=temp_down;

}
```

where Msize_m is the number of neighbors a site m has and siteNum is the number of sites.